Computer Simulations of a Chromatographic Column used in the Separation of Platinum Group Metal Chlorinated Complexes

Thesis submitted to the University of Cape Town in fulfillment of the requirements for the MSc degree in Chemistry

Nengwekhulu Thizwilondi Michael

BSc. (Hons) (UCT)

Supervisors:

Prof. K. J. Naidoo

Dr. G. Venter

10 February 2012

Declaration

I declare that Computer Simulations of a Chromatographic Column used in the Separation of Platinum Group Metal Chlorinated Complexes, is my own work and that all sources that I have used or quoted have been indicated and acknowledged.

Nengwekhulu Michael Thizwilondi

Acknowledgements

I would like to thank the following people for their contributions and help in the preparation of this thesis:

My supervisors Professor Kevin J. Naidoo and Dr Gerhard A. Venter for their encouragement and undying support through the whole process.

The SCRU group members for all the help in the preparation of the simulations, the analysis of the results and their general camaraderie.

I would also like to thank UCT, NRF for funding and CHPC for providing their resources to run the simulations.

And finally my family for their continued support.

Dedications

I am dedicating this thesis to the love of my heart whom I dearly miss, my mom. I will always miss you mom. Thanks for the life you have given to me, the guidance, the unconditional love and for making me the person I am today. This day wouldn't be possible if it was not of your hardwork and perseverance. You might be gone but you will always remain close to my heart. RIP.

List of the Abbreviations Used

CHARMM	Chemistry At Harvard For Molecular Mechanics
D	Diffusion Coefficient
FEP	Free Energy of Perturbation
MD	Molecular Dynamics
MM	Molecular Mechanics
MSD	Mean Square Displacement
PBC	Periodic Boundary Condition
PGM	Platinum Group Metal (and contextually PGMs for the plural)
RDF	Radial Distribution Function
RMSD	Root Mean Square Deviation
TIP3P	TIP3P
TSM	Thermodynamic Simulation Method

Table of Contents

Chapter 1

Abstract

The PGMs, which are comprised of Ru, Pt, Rh, Ir, Os and Pd, are highly regarded as technologically important precious metals. They have a wide range of applications and are used predominantly as catalysts. These metals are found collectively in nature and hence have similar chemical properties. This makes their separation from contaminants and each other a cumbersome process that requires the most technologically sophisticated refinery processes in metallurgical extraction. An efficient method in which these metal complexes are separated is based on gel chromatography. This uses a concentrated aqueous acidic medium, predominantly hydrochloric acid, and their separation is achieved through differentiation of their different elution orders. However, the similarity in their chemistry makes their separation via current experimental methods difficult.

In this project we investigated ways in which the development of potential organic polymer stationary phases can be guided by rational design to produce efficient, clean separation of PGM anionic chloro-complexes in aqueous solution. We made use of a molecular mechanics (MM) description to run classical molecular dynamics (MD) simulations that mimic the column chromatographic separation process. In order to accurately simulate the chromatographic process, calculation of diffusion coefficients that correspond to experimental retention time (elution order) is necessary. Diffusion coefficients of anionic PGM chloro complexes, both in pure aqueous medium and in the presence of a representative organic dextran, were calculated. These results were found to correspond well with experimental elution order in similar media. The trend of diffusion reproduced from the computational calculations corresponds well with the experimental measurements.

In expanding the investigation, calculation of PGM interaction energy profiles with an organic polymer; their solvation structure and free energy of solvation and binding were also investigated. The interaction energy of PGM chloro complexes was not clearly categorised and correlated with the diffusion. However, the trends in which these complexes interact with the polymer in a solution still obey the rule based on this order: $MCl_6^{3-} < MCl_4^{2-} < MCl_6^{2-}$. Their sophisticated interacting behaviour in the solution shows why their separation is difficult to understand.

Nevertheless, their solvation structure is well studied and their trend in solvation is understood based on their charges and effective radii. The order: $MCl_6^{3-} > MCl_4^{2-} > MCl_6^{2-}$ is

consistently retained, from the most solvated to the least solvated. It has been found that their solvation is crucial when looking at the interaction with the polymer. Therefore, if successful separation is to be achieved, the organic polymer will have to disrupt their solvation structure; this is also discussed.

The free energy of solvation was found to correlate with the diffusion order in water. For the free energy of binding to the polymer, results are less consistent, however some correlation is shown with the expected interaction energies. Overall however, free energy of binding rankings does not match the diffusion rate order.

Chapter 1

Introduction

1.1. Platinum Group Metals (PGMs)

Beneficiation of precious metals from their raw-ore concentrates into pure processed valuable products presents immense challenges for their metallurgical extraction. Platinum group metals (PGMs) are highly regarded as technologically important precious metals. However, their separation requires highly sophisticated industrial extraction and refining to access the pure metal product.[1,2] PGMs are commercially important and are used in products ranging from ornamental to critical components in heavy industry. Principally they are exploited for their catalytic properties, the most recognizable of these products are found in the automobile industries for automotive emission control catalysts.[2-4] The uses of PGMs as chemical catalysts are numerous. Examples where these catalysts are used include reforming reactions for gasoline refining, upgrading the content of octane gasoline petroleum, the hydrogenation and dehydrogenation reaction in pharmaceutical industry for drug manufacturing process, for organic reactions such as the Wacker process and inorganic oxidation reactions such as the Ostwald and Brauer process. High value materials take advantage of the special chemical properties of PGMs where they are used in the formation of dental alloys, electronic components and computer hard discs, fuel cells for power generation, glassmaking equipment, investment coinage, jewellery, medicines, etc.[2-4] The high costs of research and development and production invested by mining houses to separate and produce pure metals are offset by the many important commercial applications of this class of transition metals.

The difficulties in separating these precious metals are a result of their very similar chemical properties. They are similar in size and charge and have similar variations in oxidation states. Developing a chemical separation method based on their chemical properties requires a thoroughly sophisticated understanding of their solution and binding properties. The complex and challenging problem of understanding the chemical and physical properties of these precious metals upon binding to large organic macromolecules (i.e. a chromatographic stationary gel phase) in aqueous solution lies at the heart of this thesis.

The industrial separation of PGMs involves dissolving the PGM ore concentrates in concentrated hydrochloric acid to form PGM chloro complex anions. It is thus the chloro

species that need to be extracted via a column chromatographic process with the use of organic polymers as an extractant.

1.1.1 Refinery Process

As mentioned above, the current method of separating PGMs are based on forming the chloro species by dissolving the ore concentrate into hydrochloric acid. Up until the mid-seventies, separation of PGMs was mainly achieved by using a series of precipitation reactions.[3,5] There has however, been a variety of other efficient methods developed which were successful and conveniently used for the separation and refining of PGM tetrachlorometallates and hexachlorometallates. Such methods include ion-exchange and solvent extraction and chromatography.[3,5,6,7] The implementation of these methods has lead to substantial improvement in the number of factors such as improved selectivity, increased percentage yield, reduced lengthy refining time due to elimination of multi recycle streams [3,5] and easy labour work and more compliance to environmental safety.

Regardless of this advancement by the newly implemented methods, there are still concerns that the purity of the metal is not entirely obtained with the use of these methods. This has a direct consequence on the economic trade value. The purity of the metal is of particular interest as this is directly associated with some desired functionality in which these precious metals are applied. The cause of this is mainly attributed to the fact that little is understood about the chemistry of these metals in aqueous solutions and the mechanism in which they are separated. As a result of these, there is on-going extensive research aimed at understanding the mechanism involved in separation and to develop potential models in which clean, pure, green separation can be achieved. Current industrial separation of PGMs uses gel permeation column chromatography in which organic polymers are used as the stationary phase and aqueous solutions, most preferable containing hydrochloric acid and sodium chloride, are used as the mobile phase. The schematic flow chat showing classical separation and refinery process of PGMs ore concentrates is presented on figure 1.1 below. In this study we investigate potential stationary phases that can be uses to separate PGMs in aqueous solution.

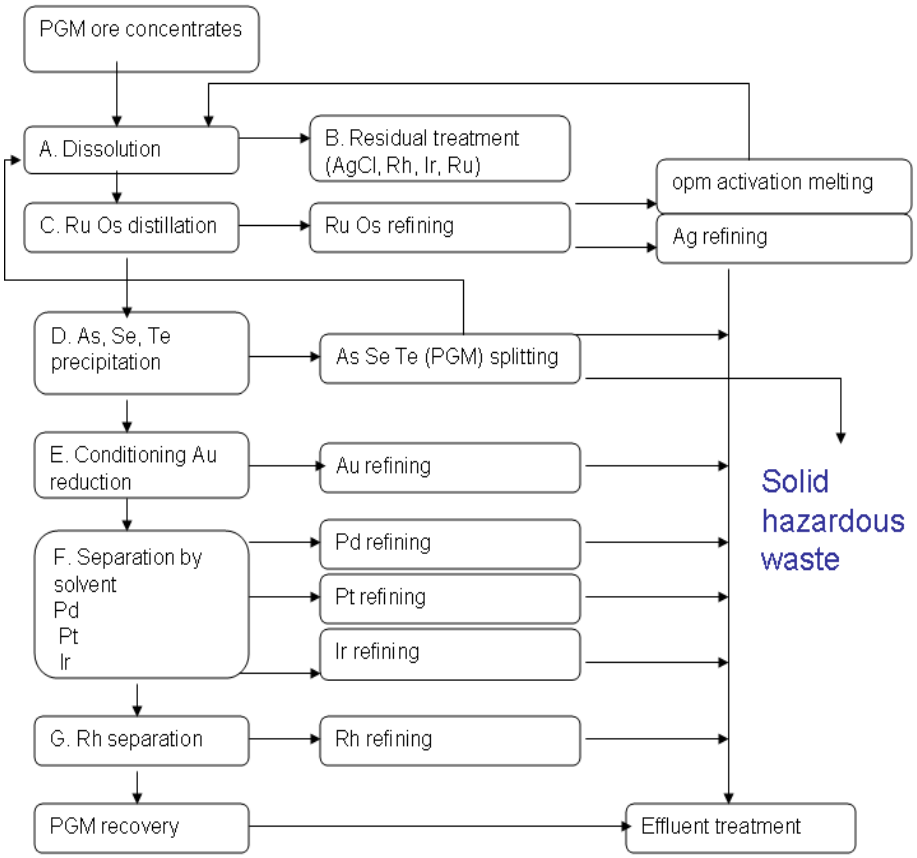

Figure 1.1 Schematic flow diagram of the classical separation and refinery process of the PGM ore concentrates. Adapted from the paper of Bernardis *et. al.*[1]

1.1.2. Separation Techniques and Principles

Gel permeation column chromatography is the most preferred industrial method used for the extraction of PGMs chloro complex anions. Gel permeation should be differentiated from gel filtration in that in gel permeation the organic solvent is used as the mobile phase while in gel filtration water is used as the mobile phase. In gel permeation chromatography particles are separated based on their sizes. Typical gel permeation column chromatography illustration for the separation of PGMs chloro complex anions is showed on figure 1.2 below.

The elution time of the different metals in a column is controlled by the strength of the electrostatic interactions between the extractant gel and the metal chloro complex anion, and the ability of the extractant gel to form hydrogen bonding with the chlorine ligand of the chlorometallates. The separation process as explained in the patent by Schmuckler et al., occurs via the adsorption of the dissolved noble metal components onto the gel.[8-12] Different metals are then separated based on their interaction with the gel and their sizes. PGM complexes are known to form hydrogen bonds with the gels, in contrast to their counterpart

base metals.[8-12] The mechanism in which these metals are recovered also involves liquid chromatography, ion-exchange and size exclusion.[1,6, 8-12]

One of the disadvantages of gel permeation chromatography in the extraction of PGMs is the lifetime of the gel in concentrated acidic solution. The result of this is poor separation which might result in low purity of the metals. Most gels that are used are based on the hydroxyl group and amine/amide groups or containing both amine and alcohol groups, which are amino alcohols structures.[8-12] The most common known gels used in gel permeation are sephadex gels and Biogels, reported in a US patent by Schmuckler et al.[8,9] Another preferable gel is from the Toyopearl range of chromatographic media.[8,9] Different solvents are used as the mobile phase, and the most common as mentioned above are concentrated hydrochloric acid and aqueous sodium chloride. Water is also used as the mobile phase all these properties makes this process an ideal system to study for molecular design using computer aided techniques.

The outcome of the classical separation process of gel permeation is determined by diffusion, which relies on the electrostatics interactions in the solution and is based on sizes of the separated molecules.

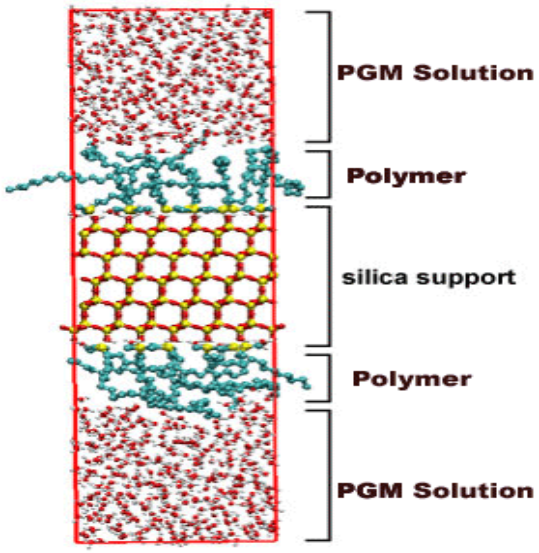

Figure 1.2 Schematic representation diagram of the classical gel chromatographic column setup for the separation of PGMs chloro complex anions. Adapted from the paper of Bernardis *at. el.*[1]

1.2. Classical Chromatography Separation Methods and Techniques

1.2.1 What is Column Chromatography?

Column chromatography is the separation technique in which the stationary phase, a solid adsorbent, is placed into the vertical tube column and the mobile phase, a liquid, is added from the top. The mobile phase then flows down through the column either by gravity or external forces. Column chromatography is mainly used for the purification of chemical compounds from their mixtures. The column is packed either by the solid stationary phase and the liquid solvent completely filling the whole inside volume of the tube or an open tubular where the column is concentrated along the inside wall of the tube leaving an open, unrestricted path in the middle of the tube for the mobile phase. For most column chromatography separations, a packed column is the preferred method. The column chromatography as mentioned above is separated into two ways. Firstly, if the solvent is allowed to flow by gravity the process is called gravity column chromatography. Secondly, if the solvent is force down the column by air pressure it is called flash chromatography. The latter method is the one most often used currently in organic chemistry laboratories.

1.2.2 Historical Background on the development of Chromatography Methods

The first chromatography method was invented by the Russian botanist M. S. Tswett in 1903.[13,14] In his experiment, Tswett used a column of powdered calcium carbonate to separate green leaf plants into a series of coloured bands by allowing solvent to be absorbed into the column bed.[14] He also came up with the name chromatography where he combined two Greek words: *chroma* meaning colour and *graphein* to describe the process.[13,14] However, Tswett's column liquid chromatography was not an ultimate success as the standard laboratory techniques. From then on, further development took place. Amongst others, the major contribution came from A. Tiselius of Sweden in 1948 and to A. J .P. Martin and R. L. M. Synge of Great Britain in 1952 whom were eventually awarded a Nobel Prize in Chemistry. Martin and Synge's award was for the invention of partition chromatography. In the same year, 1952, A. J .P. Martin and A. T. James introduced a technique for gas-liquid chromatography.[13,14] A full chain of the historical evolution of chromatography is summarised in table 1.1 below.

Table 1.1. Summary of the timeline in the developments of modern chromatography.

Continued on the next page

Date	Associated development
1903	Original description of column liquid chromatography by M. S Tswett.
1931	Colum liquid chromatography development by Lederer and co workers as a standard laboratory method.
1938	Introduction of ion-exchange column chromatography.
1941	Introduction of column liquid-liquid partition chromatography.
1944	Paper chromatography was introduced based on partition chromatography.
Mid-1940s	Gel electrophoresis was developed for the separation of charged analytes in a stabilizing gel matrix.
Early-1950s	Thin-layer chromatography was popularised as a faster and more convenient method than column liquid chromatography.
1952	Gas-liquid chromatography was described by James and Martin.
1958	Column liquid size-exclusion chromatography using contolled porosity dextran gel was introduced by Flodin and Porath.
Mid-1960s	The technique of field flow fractioning for the separation of particles was introduced by Giddings.
1967	Affinity chromatography for the isolation of biological polymers based on the specificity of their interaction with appropriate immobilized ligands was introduced by Porath and co-workers
Late -1960s	The introduction of pellicular sorbents catalysed the development of high pressure liquid chromatography
1970	Everaerts and co-workers introduced capillary isotachophoresis for the concentration and separation of ions
1970s	Ito and co-workers commenced a number of advances in counter current chromatography using centrifugal and planetary motion for liquid-liquid separations
Mid-1970s	Small and co-workers introduced ion chromatography based on the integration of ion exchange chromatography with conductivity detection for the analysis of ion.
Early-1980s	Jorgenson and co-workers popularized the use of zone electrophores in capillary columns for the fast and efficient separation of ions and biopolymer

1984	Terabe introduced the method of micellar electrokinetic chromatography (MEKC) using surfactant-containing buffers in a capillary electrophoresis apparatus
Late-1980s	Rediscovery of capillary electrochromatography. Pioneering work by Knox leads to the evolutionary development of this technique during the 1990s.

Continued from previous page

1.2.3 Overview of Chromatography and its Methods

Chromatography is a universal and versatile technique.[13] Its applications extend in all areas of chemistry, biochemistry, biology, quality control, research, analysis, preparative-scale separations and physiochemical measurements. Industrially, this technique is used in the purification of such diverse materials such as cane sugar, pharmaceuticals, and rare earths.[14] There are diverse multitudes of chromatography separation methods available. Each of these methods is used for different applications depending on the nature of particles being analysed or separated and/or purified. To discuss all of them here is beyond the scope of this dissertation. Instead, the focus will be on those methods that are of interest to this study.

There are many definitions for chromatography. This can be attributed to rapid advancement in the principles of chromatographic methods and techniques since its first development by the Russian botanist M. S. Tswett. As a result, many definitions have been formulated when new techniques are developed. The universal definition of chromatography was first given by IUPAC.[13] "This refers to chromatography as the process in which the components of the chemical mixtures are analysed, identified, separated and purified from their impurities using a range of physical methods where the components of mixtures are distributed between two phases, the stationary phase and the mobile phase".[13,14] The principle is to dissolve the mixtures into the mobile phase (solvent) and then pass it through the stationary phase (stationary bed, mostly gels of different particle grades), which then separates the analyte. However, by virtue of this definition it suggests that the separation should occur in two phases, stationary and mobile. This does not recognise that the separation can be a single phase system. An example of this is capillary electrophoresis where separation occurs by differential migration of a single phase system.[14] It is therefore not always necessary that one phase is stationary.[14] This definition also neglects the possibilities of using supercritical fluids as the mobile phase.[13] Due to this lack of recognition, a

generalised definition of chromatography is required, which should globalise the term chromatography to all methods and principles associated with it. The universal definition of chromatography can be defined as the group of separation methods that are undergoing continuous development and refinement. [13] Nevertheless, all these definitions are found to be relevant and are both going to be used in this dissertation when reference is made to chromatography.

The common thread in the definitions given above is an unequal distribution of components of a mixture between a stationary and mobile phase.[15] The prerequisite for an unequal distribution is the affinity of single components for both phases or the unequal possibility of diffusion into them.[15]

Chromatography methods are categorised into gas, supercritical and liquid chromatography. Only liquid chromatography methods and principles are discussed here. Liquid chromatographic separation methods are divided into liquid-liquid chromatography, liquid-solid chromatography and micellar electrokinetic chromatography.[13,14] The central topic of this work is mainly based on liquid-solid chromatography principles as well as the analysis and purification methods associated with it. The liquid-solid chromatographic analysis and purification methods are adsorption, size-exclusion, ion exchange, affinity, reversed-phase chromatography and capillary electrochromatography.[13,14] The description of some of these methods and their principle are discussed in section 1.3 below.

Before going into details on the methods and principles mentioned above, in this section we give different chromatographic technique and provide a further detailed description of only column chromatography method which is of special interest in this thesis. In addition to column chromatograph there are other varieties of techniques such as thin layer chromatography, paper chromatography, etc. We will only limit our discussion to column chromatography. The section below gives a description of what column chromatography is.

1.2.4. How Column Chromatography Separation is Prepared

The column chromatography separation is prepared by first filling the column with the solid stationary phase or adsorbent. Then the mixture that contains the analyte to be separated is fed to the top of the vertical tube column. The mobile phase eluent solvent is passed through the column either by gravity or air pressure. This liquid is then distributed into the adsorbent and equilibrium is reached between the solid stationary phase and the eluent flowing down

the column. The different components of the mixture are expected to interact differently with the stationary phase and mobile phase. The separation is reached after which the eluent is collected at the bottom of the column outlet. This method of preparing a column is referred to as the dry method, where the stationary phase is filled first into the column and then the mobile phase is passed through. The other way of preparing the column would be to use the wet method. Here the mobile phase, and the stationary phase is mixed together before the mixture is fed into the column and then added carefully into the vertical tube column.

1.2.5. Commonly Used Stationary Phases and Choice of Solvent

The common stationary phases used in column chromatography are silica gel and alumina. The chemical formulas for these adsorbents are SiO_2 and Al_2O_3, respectively.[13] Silica gel is the most commonly used adsorbent of the two. One application of this in metallurgical industrial processes involves leaching of metal salts from ores. Different adsorbents with differently sized pores are used, depending on the type of molecules that are being separated. If the particle size of the adsorbent is too small this usually affects the flow of the molecules in the column, depending on their size, and as a result flash chromatography methods are used. On the other hand, if the particle size of the absorbent is larger than the molecules being separated, gravity column chromatography is used.

In addition to this, the choice of the solvent is very important. The polar molecule will interact with polar solvents and compete with the adsorbent. The polarity of the solvents directly affects the speed of the molecules through the column. In a case where the solvent is too polar, the molecules will move too fast and separation might not occur. On the other hand, if the solvent it is non-polar, the molecules will get stuck in the column and not move through.

1.2.6. Advantages and Disadvantages of Column Chromatography

Column chromatography has the advantage that it can be used both as a preparative and an analytical tool. Components of the mixtures can be separated and purified. The obvious disadvantage of column chromatography is that it requires more attention; constant supervision from the beginning when one starts running the column until the analyte is

recovered. The mobile phase should be constantly refilled to maintain the same level as it runs out. This makes the whole process of running a column time consuming and laborious.

1.3 Extraction methods

Extraction is the process of withdrawing or pulling an active agent or waste substance from a solid or liquid mixture with a solvent. A common example of extraction is that of a hydrometallic process, where it involves leaching of metal salts from ore. Another example of extraction is that of brewing tea or making coffee. Extraction methods are categorised into different types depending on the phase, namely liquid-liquid chromatography and liquid-solid chromatography. Another extraction method is gas-liquid chromatography or adsorption. In this section though, a detailed explanation of solid-liquid extraction is given.

1.3.1 Liquid-Solid Extraction

Liquid chromatography refers to separation techniques with a single common feature, that of a liquid mobile phase.[14] One of the examples of liquid chromatography that is of interest in this dissertation is liquid-solid extraction. However, the terms liquid-solid extraction and liquid-solid chromatography are used interchangeable in this work.

Liquid-solid extraction is the most common extraction method used in the hydrometallic process/leaching. It refers to the removal of chemical components from solid with solvent. Liquid-solid chromatography is also referred to as normal phase or straight phase adsorption chromatography. It is the oldest chromatographic separation method to date.[13-15]

Separation in liquid-solid chromatography is achieved by using a polar or relatively less polar stationary phase and a non-aqueous mobile phase.[14] Retention is due to interaction of polar functional groups on the solute with the discrete sites on the stationary phase surface.[13] The selectivity of the separation depends on the relative strength of this polar interaction with different solutes. The extent to which the solute can be accommodated on the stationary phase depends on its spatial configuration and its ability to form hydrogen bonds with the adsorbent.[13]

Appropriate stationary phase materials used in adsorption chromatography include inorganic oxides and polar chemically bound phases.[14] Common stationary phases include

sucrose, cellulose, starch, silica gel, florisil, charcoal, magnesium oxide, hydroxylapatite and alumina.[13,14] In actual fact, all adsorption chromatography is performed on silica gel and alumina, with silica gel being the most preferred of the two. Silica gel has the advantage over alumina in that it allows sample loading and is less likely to catalyse the decomposition of any sample, whereas alumina has been known to catalytically decompose many organic compounds.[13]

It is well known that a molecule's polarity is based on its ability to interact through nonbonding interaction. The total interaction can be seen as the result of four interactions: dispersion, interaction of dipoles and/or higher order multipoles, hydrogen bonding and electrostatics.[13] A solvent molecule interacting with a sample compound in most of these ways is regarded as polar. Hence, polar solvents preferentially attract and dissolve polar compounds. In a similar fashion, the chromatography strength in a normal-phase system is related directly to its polarity.[13]

1.4. Column Liquid-Solid Chromatography - Purification Methods

1.4.1. Ion-exchange chromatography

Ion-exchange chromatography (IEC) is used for the separation of ions and easily ionized substances that form ions by pH manipulation or complex formation.[14] Ion exchangers are insoluble solid materials that carry an exchangeable cation and/or anion.[16] The exchangeable cation carriers are called cation exchangers and the exchangeable anion carriers are called anion exchangers. In addition, there are those materials that are capable of undergoing both cation and anion exchange.

Most ion-exchange operations in both laboratory or in plant-scale processes, are carried out in columns.[16]

Ions with a large charge have a greater affinity for the exchanger than do ions with a small charge.[15] Ion exchange chromatography of components of a mixture will depend on the difference in the charges of the components.[15]

1.4.2. Size exclusion chromatography

Size-exclusion chromatography is the chromatography method in which the component mixture of the material is separated based on the size of its particles. Modern size-exclusion chromatography commonly uses cross-linked polydextran and polysaccharide gels for the size separation of water-soluble biopolymers and polystyrene gels to separate organic polymers.[14] The separation of water-soluble biopolymers is known as gel-filtration chromatography while the use of organic solvent for the separation of organic polymer is known as gel permeation chromatography.[14] The common behaviour is that the method is size-dependant with the distribution of samples molecules between a mobile phase and a porous stationary phase.

To emphasise, separation in size-exclusion is based on the differences in size, which has no direct correlation with the molecular weight. The size of macromolecular molecules in solution is said to be a function of its intrinsic structure and solvent interaction.[14] Like in other chromatography methods, the separation order depends on the physical nature of the stationary phase and its ability to intentionally differentiate between particles of relatively similar size. Most importantly, the separation depends on the relative polarity of the solvent.

1.5. Descriptions of Common Stationary Phases used for Separation

This section provides a detailed description of the Sephadex LH-20 polymer and its derivative structures used for the separation of PGM chloro complex anion. It also provides a full explanation of the force fields used and the parameterisation procedure followed for building the functional groups in the molecular structure of this polymer(s). Furthermore, the practical application of the sephadex gel for the separation of PGM chloro complex anions is looked at.

1.5.1. Physical and Chemical Structural Description of Sephadex LH-20

Sephadex LH-20 is a gel based on hydroxypropylated dextran that is cross-linked to yield a polysaccharide network and is commonly used for gel filtration columns.[17] The molecular structure of Sephadex LH-20 is given on figure 1.3 below. Gel filtration and the chromatographic columns are composed of macroscopic beads synthetically derived from the polysaccharide.[17,18] The organic chains are cross-linked to give three dimensional networks

having functional ionic groups attached by ether linkages to glucose units of the polysaccharide chains.

Sephadex LH-20 is prepared by hydroxypropylation of Sephadex G-25.[18] It is specifically designed for the separation and purification of natural products that require the presence of organic solvents to maintain their solubility, including molecules such as steroids, terpenoids, lipids and low molecular weight peptides.[17,18] Sephadex LH-20 shows both hydrophilic and lipophilic characteristics, with the combination of these offering unique chromatography selectivity for certain applications.[17] The ether linkage of the glucose units of the polysaccharide chain and the propyl group is believed to have improved the hydrophilicity of Sephadex LH-20.[17] It is generally very stable at the pH range of 2-13, for a pH of below 2 its stability is relatively low.[18] Its operational temperature is recommended within the range of 4-40 degrees celcius.[17]

The main component of Sephadex gel is a dextran that is cross-linked together by alpha 1-6 glycosidic bonds. The branched chains are linked together by alpha 1-3 and 1-4 glycosidic bonds. Koo *et al.,* in his studies of the conformation and dimensions of dextran gels, describes the gel that forms the main constituent in Sephadex having the structure of a linear polysaccharides composed exclusively of the monomeric unit, α–D glucopyranose, linked mainly by alpha 1-6 glycosidic bonds.[19] The polymer used in this study is based on the chemical features of this structure.

Sephadex gel is available in different particles sizes (or grades) and each grade has unique chromatographic beads with different efficiencies and operating pressures. The grades with highest efficiency and operating pressure are those with superfine grades. The superfine grades are suitable for thin layer gel filtration. Some known Sephadex gel according to their grades and size particles are Sephadex G-10, Sephadex G-15, Sephadex G-25, and Sephadex G-50. These are recommended for the separation of peptides and other small biological molecules. Other types are Sephadex G-70, Sephadex G-100, Sephadex G-150 and Sephadex G-200; these are useful for proteins and other macromolecules.[20] The numbers occurring in these names represent the size of the pores of the gel.

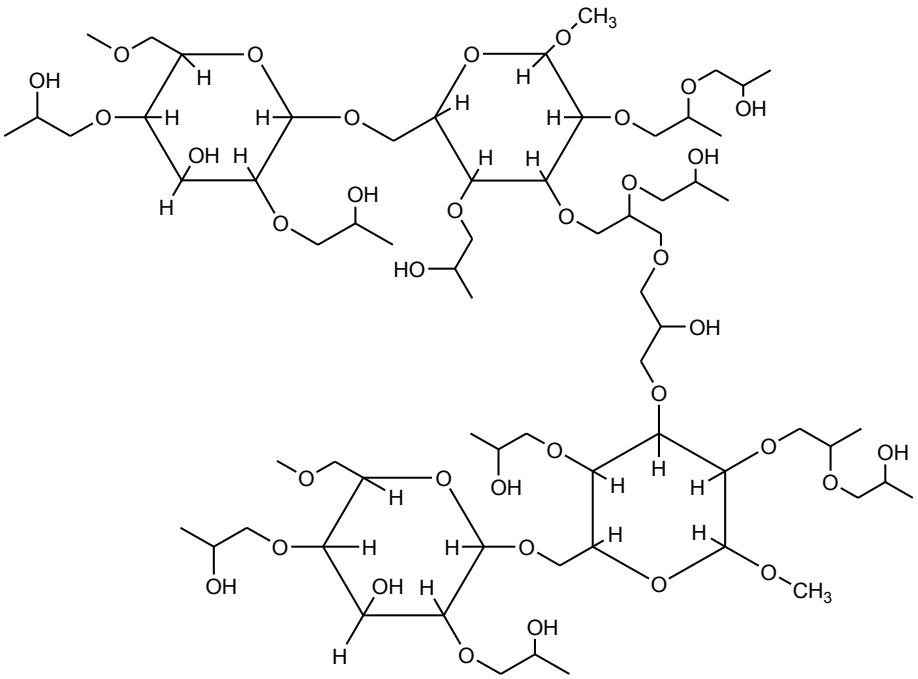

Figure1.3 Partial structure of sephadex LH-20.[17] The polymer is primarily made up of building blocks of sugars linked together via glycosidic bonds with the replacement of an OH by a propanol chain at the C1, C2, C3, C4 and C5 positions. The structure is composed of repetitive monomers of these blocks linked together via alpha 1-6- glycosidic linkages forming a polysaccharide chain.

1.5.2 Sephadex LH-20 Extended Molecular Structures – Stationary Phase

The industrial separation of PGM chloro complex anions is carried out on different stationary phases depending on their properties. The stock solution is allowed to pass through the stationary phase, which is then adsorbed into the gel pores allowing it to interact with the gel. The gel fills the column interior dimensions to allow the stock solution to pass through more efficiently. Therefore, it is one of the aims of this study to choose the polymer to be sufficiently large to make sure that during the entire simulation the complexes are interacting with a polymer segment that is representative of the true gel structure. In the case of the Sephadex LH-20 partial structure, it is also clear that an increase in the size of the polymer increases the number of polar groups present due to the repeated hydroxyl group occurring in the structure. This is one of the chemical and physical features of the polymer that will be exploited in this study. Since the polymer is dominated by hydroxyl groups, which are characterised by highly polarised O-H and C-O bonds, this offers increased hydrophilicity characteristics on both the sugar back bone and the hydroxypropyl chain, making the entire

polymer equally polarised on all sites. The OH groups of the hydroxypropyl chains are expected to be the main target sites and of particular interest due their interaction with the PGM hexachloro and tetrachloro complex anions.

The section below gives a detailed explanation of the polymer structure used for the separation as well as the naming scheme employed in this study.

1.5.3. Choice of the Polymer: Structure of the Polymer One and Two.

The choice for this polymer was guided by several reasons. Firstly, the structure of the polymer used here was derived based on the Sephadex LH-20 structure, figure 1.3, since Sephadex gel polymers have been implemented in a series of PGM chloro complex anions separations in aqueous solution.[8,9] Secondly, the presence of the O-H functional group in the structure offers higher bond polarity and this suited the targeted H••• Cl interaction. The selective separation of base metals using a extractant based on the imine and amido functional group has been described by Tasker *et al.*[12] Such reagents results in interaction between N-H and C-H groups and tetrachlorometallates in an outer coordination sphere mechanism.[21,22] A similar approach has been shown for the recovery of $PtCl_6^{2-}$ by the same authors.[12]

The two systems were run to compare which would best represent the PGM complex interaction with the organic system, and to test the effect of chain length on the results.

Polymer one

This polymer is referred to as polymer one. The polymer structure was built through addition of the sugar ring, repeatedly connected through the ether linkages of the branched hydroxypropylated chain of the disaccharides and via the 1-6 glycosidic bonds of the glucose ring, similar to the partial structure of sephadex LH-20 figure 1.3 above. The complete structure is composed of four trisaccharide chains that are repeatedly connected together via the repeated ether linkage of the branched hydroxypropylated chain. The sugar backbone ring has been increased from two rings, as in the Sephadex LH-20 partial structure, to three, figure 1.4. The polymer was allowed to retain its flexibility, which stems from the ether linkages of the branched hydroxypropylated chain.

This structure is characterised by the presence of H-O and C-O bonds, which offers high bond polarity across the entire structure, a feature that is expected to offer better chromatographic separation.

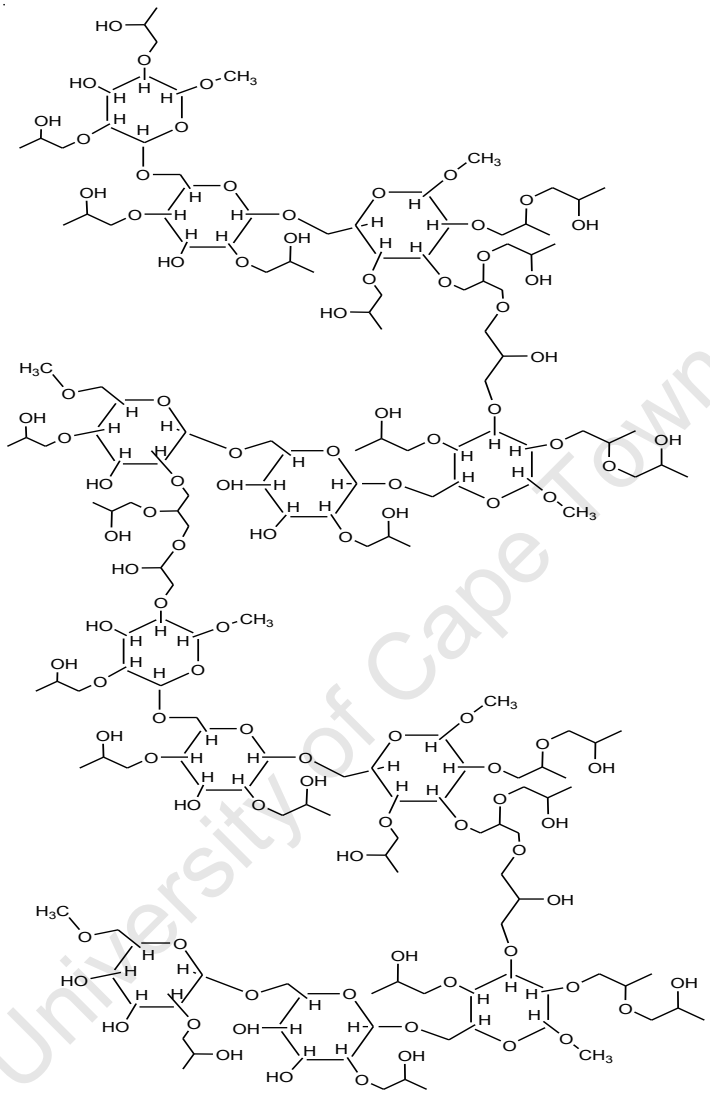

Figure 1.4 Extended molecular structure of Sephadex LH-20 – identified polymer one . This polymer is extended with twelve sugar rings forming linear chains which are repeated via 1-6 glycosidic bond linkage.

Polymer Two

Polymer two, figure 1.5 below, is in fact composed of two smaller, separate strands. Instead of extending to twelve rings in total, this system is composed of two six-ring strands, each containing 1-6 linkages to form the three-ring subunit, with two of these subunits connected through the extended ether chains. The two structures are similar except that structure 1.5 (a)

contain three propanol-chain linked to OH group on the glucose ring at the one end, whereas structure 1.5 (b) contain two propanol-chain linked to OH group at the same glucose ring.

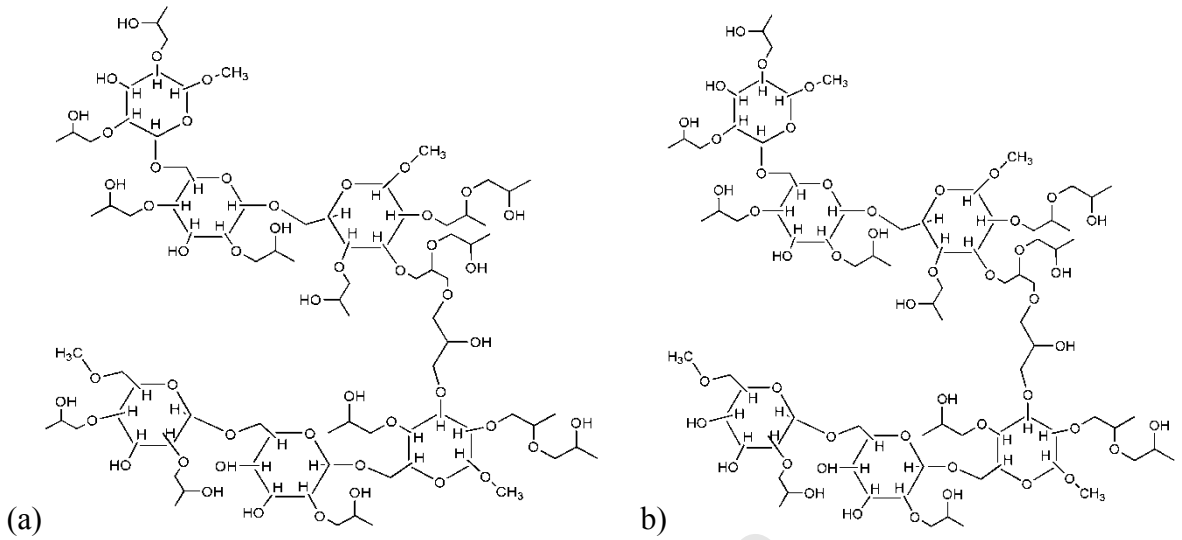

(a) b)

Figure 1.5 Structures (a) and (b) are the extended molecular structure of sephadex LH-20 – named polymer two. Both these structures are extended with six sugar rings forming linear chains repeated via 1-6 glycosidic bond linkages. These structures were simulated together in the same system with PGMs anionic hexa-chloro-complexes and tetra-chloro complexes in water.

1.5.4. Application of Sephadex Gel for the separation of PGM complexes.

PGM separation requires efficient and robust separation techniques in order to meet the enormous growth and scale of global demand, which is constantly influenced by the growth in the number of applications of PGMs in the many various chemical industries. Current effective methods available for the separation of PGMs include ion-exchange, solvent extraction and chromatographic separation methods.[1,7] The latter is the main focus of interest and is at the center of this study.

As mentioned earlier, the industrial process of the chromatographic separation of these systems is carried out by passing the PGM halide stock solution through a chromatographic medium using HCl as an eluent.[8,9] Chromatographic media that are used are based on strong bases, which are supported in acidic solution, and the neutral chromatographic media that are not well supported in acid due to their relatively low speed of protonation by the acid.[1]

The first category includes the glycol methacrylate chromatographic medium. The mechanism by which PGMs are separated by this chromatographic medium involves genuine ion exchange.[1] Glycol methacrylate is a co-polymer of ethylene glycol and methacrylic acid, for example a medium from the MACRO-PREP range of chromatographic media, a trademark of Bio-Rad Laboratories, or a co-polymer of oligo(ethylene glycol), glycidylmethacrylate and pentaerythrol-dimethacrylate, for example a medium from the Toyopearl range, a trademark of TosoHaas and previously known as Fractogel.[8,9] The presence of the ether linkage in the polymer and the hydroxyl groups confer a highly hydrophilic nature to both the outer and internal surfaces of the gel particles. This chromatographic medium has an advantage over Sephadex and Biogel due to their improved lifetime in acidic media and the fact that high pressure can be applied, permitting the use of a high flow rate.

The second category includes chromatographic media Sephadex and Biogel.[1,8,9] Sephadex is a polysaccharide gel, a trademark of Pharmacia Biotech, and Biogel is a polyacrylamide gel, a trademark of Bio-Rad Laboratories.[8,9] The separation between the noble metals is quite unexpected in view of the weak bonding of Pt to Sephadex gel.[8] The inventor explains the unexpected separation using the polarisability of the metal halide bonds, which influence the hydrogen bonds in the gel and allows for separation of the noble metals.[8]

In the case of Biogel the separation is based on the electrostatic interactions of the PGM complexes with the charged amide groups of the gel, where electrostatic interaction strengths are charge-dependent. In Sephadex the interactions of the PGM complexes are of bipolar type, being weaker than those of the electrostatic type but more selective.[8] There are however, disadvantages to this method: there is no clean separation of the PGM complexes, and the chromatographic medium denatures over a period of time resulting in a steady decline in the separating of the PGMs. Consequently the media have limited effective lifetimes.[7]

1.6 Objectives and Outline

1.6.1 Objectives

The purpose of this research is to investigate ways in which the development of potential polymer stationary phases can be guided by rational design to achieve the efficient separation of PGM chloro complex anions in aqueous solution, figure 1.6. We make use of a classical

mechanics (i.e. molecular mechanics) description of the molecular complexes. The dynamic performance of the complexes in water is achieved through molecular dynamics (MD) computer simulations. Together these mimic the column chromatographic separation process. The simulations are validated by calculating the diffusion coefficients, which correspond to experimental elution times. Diffusion coefficients of PGM chloro complex anions in solution, both in pure aqueous medium and in the presence of a representative organic dextran, are calculated. Free energy perturbation (FEP) calculations are used to determine the preferential binding patterns of the PGM chloro complex anions to the polymer and their solvation free energy in water. From the combined diffusion and free energy calculations a rationale for observed elution times are sought. The goal and objective of this project is thus to use computer simulation calculations to understand and predict trends of the PGM chloro complex anions in aqueous solution in the presence of an organic polymer.

Two systems are considered for the simulations of the complexes. Firstly, aqueous solutions are simulated using a periodic cell in the presence of ammonium cations that are counter-ions to neutralize the system. Secondly, the complexes are simulated in water and in the presence of the organic polymer, again with ammonium counter-ions and periodic boundary conditions.

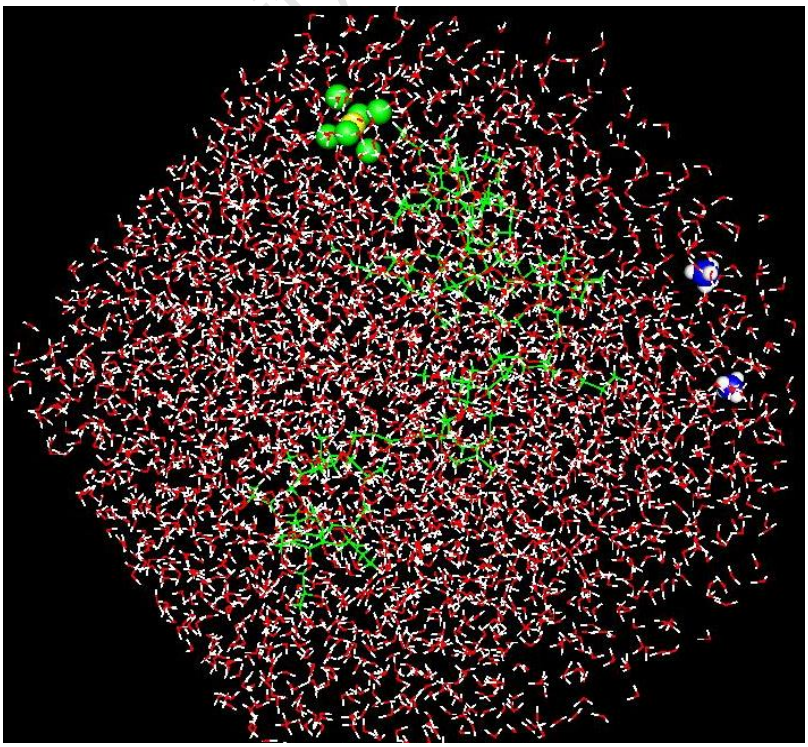

Figure 1.6 An illustration of the computer setup model of simulated truncated octahedron periodic cell mimicking the gel chromatographic separation of PGMs chloro complex anions in aqueous solution. The system is made up of water, extractant polymer, represented in green long chain of sticks, PGMs chloro complex anions, represented in green (chlorine ligands) and yellow (metal center) spheres and ammonium cations (represented in blue and white spheres). This snapshot was extracted from the initial setup of the model.

1.6.2 Outline

In Chapter 2 the details of the simulation conditions and the procedure followed in setting up the system to run molecular dynamics (MD) is discussed. This comprises an explanation of the molecular mechanics (MM) force fields used to construct the model, the MD simulation steps, which includes heating, equilibration and production and the choice and availability of all the MD simulations methods such as the integration methods, statistical collection methods and the usage of the Ewald-summation method, periodic boundary conditions (PBC) and the minimum image conversion.

In Chapter 3, all the analytical methods used to analyse the simulations trajectory are provided and discussed. Calculations that are key tools in this study include the determination of transport properties (calculating of the diffusion coefficient, D), energetic properties (determining the free energy of solvation and binding using free energy perturbation (FEP) methods), structural properties such as the radial distribution function (RDFs) and the root mean square displacement (RMSD) for monitoring the convergence of the system during dynamics.

Finally, in Chapter 4 the results are presented. This includes calculation of the average size of the PGM complexes and their charge density to compare that with their solvation structure and diffusion in water. Furthermore, the interaction energy computed between the complexes and polymer, their RDFs, diffusion coefficients, D, water and in aqueous solution in the presence of polymer, and free energy of solvation and binding is presented. Comparison is made between the interaction energy, RDF and diffusion of PGMs to identify and attempt to establish a pattern in the behaviour of these metal complexes. In addition, the diffusion trend is compared with the experimental retention times. Another comparison is made between the free energy of solvation and binding with the diffusion in water and in solution in the presence of polymer.

References

1. Francesco L. Bernardis, Richard A. Grant and David C. Sherrington, Reactive and Functional polymer, 2005, *65*, 205-217.

2. Platinum-Group Metals. Richard J. Seymour and Julia I. O'farrelly. Kirk-Othmer Encyclopedia of Chemical Technology. Johnson Matthey Public Limited Company, 2001, John Wiley & sons.

3. Platinum-Group Metals—World Supply and Demand *By* David R. Wilburn and Donald I. Bleiwas, U.S. Geological Survey Open-File Report 2004-1224.

4. Platinum Group Metals, Johnson Matthey, Londong, Uk, Publishing annually since 1985

5. P. Charlesworth, Platinum Metals Rev., 1981, 25 (3), 106-112.

6. William M. MacNevin and Warren B. Crummett, Behaviour of Platinum Group Metals Toward Ion Exchange Resins, Vol. 25, (11), Nov. 1953, 6th Annual Summer Symposium – Less Familiar Elements.

7. Platinum-Group Metals; Assembly of life sciences (U.S). Committee on Medical and Biologic Effects of Environmental Pollutants. Subcommittee on Platinum-Group Metals.

8. Gabriella Schmuckler, U.S. Patent, 4885143, 1989.

9. Richard A. Grant and Yvonne Taylor, U.S. Patent, 5879644, 1999.

10. Moine et al., U.S. Patent, 7354517 B2, 2008.

11. G. Levitin, G. Schmuckler / Reactive & Functional Polymers 54 (2003) 149–154.

12. Katherine J. Bell, Arjan N. Westra, Rebecca J. Warr, Jy Chartres, Ross Ellis, Christine C. Tong, Alexander J. Blake, Peter A. Tasker, and Martin Schroder, Angew. Chem. Int. Ed. 2008, 47, 1745-1748.

13. Keving Robards, Paul R. Haddad, Peter E. Jackson, Principles and Practice of Modern Chromatographic Methods, Elsevier Academic Press, 2004.

14. Colin F. Poole,The Essence of Chromatography, Elsevier Science B.V., 2003.

15. Laboratory Handbook of Chromatography and Allied Methods, Ellis Horwood Series in Analytical Chemistry, Ellis Horwood Limited, 1979.

16. Friedrich Helfferich, Ion Exchange, McGraw-Hill Book Company, Inc., 1962.

17. Amersham biosciences, Sephadex® LH-20, 18-1107-22.

18. GE Healthcare, 561199097AD.pdf. 03/2006 Gel filtration.

19. Yoon-Mo Koo, and Philip C Wankart. Korean Biochem. J. (1998), Vol. 21, No 1. pp 22-3.

20. http://www.scribd.com/doc/6941835/gel-filtration.

21. Peter A. Tasker, Christine C. Tong, Arjan N. Westra, Coordination Chemistry Reviews, 251 (2007), 1868-1877.

22. Ross J. Ellis,Jy Chartres, Kathyyn C. Sole Timothy G. Simmance, Christine C. Tong, Fraser J. White Martin Schroder and Peter A. Tasker, ChemComm, 2008, DOI: 10.1039/b815895a.

Chapter 2

Computational Method

Introduction

The separation process was investigated using atomistic MD simulations. In this chapter the details of the MD methods and simulation conditions are given. The generic steps followed in running MD, using the CHARMM program, are shown in figure 2.1 below.

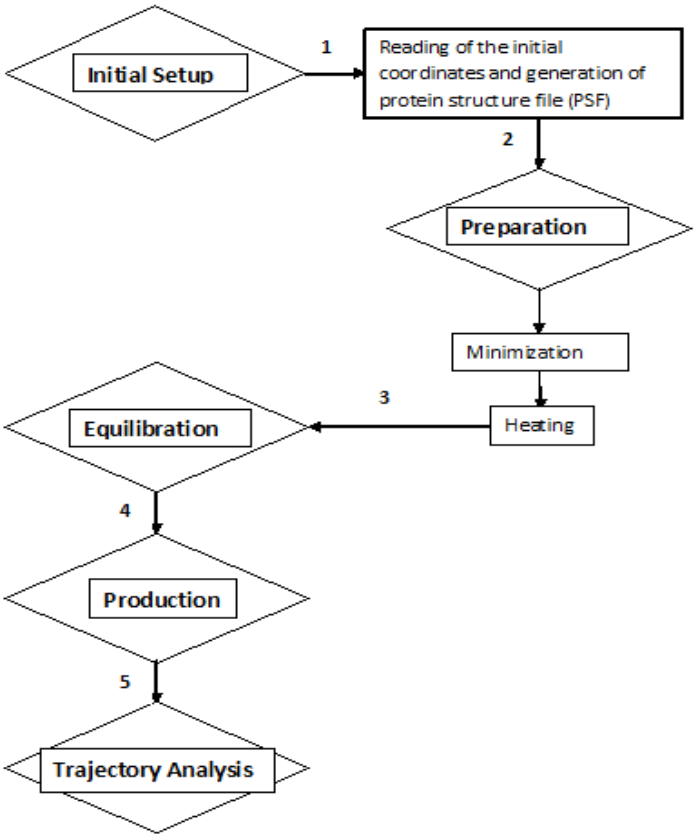

Figure 2.1 Schematic flow diagram of the generic steps of running MD simulations using CHARMM.

The MD method as used here produces a time evolution of the atomic and molecular constituents of the chemical system being simulated using numerical methods to solve Newton's equation of motion. Atoms and molecules will be referred to as particles to facilitate the flow of the discussion. The forces and potential energy between the particles are

calculated using MM force fields and Newton's equations of motion. The MM method is a classical mechanics interpretation of the molecular structure and atomic interactions using the principles of electrostatics and statics. The generated atomic behaviour results of MD simulation can be used to determine the thermodynamic properties. This chapter further provides background on the statistical methods available and where they are applied in an attempt to provide answers to the question raised in this study. In addition, free energy methods have been used to identify the binding pattern of different metal complexes to the polymer. The free energy perturbation method and its application is explained in detail in this chapter.

2.1 Descriptions of Computational Methods and Theory

2.1.1 Empirical Force Fields: Molecular Mechanics (MM) Method

Born-Oppenheimer Approximation

The classical mechanics or MM equations that relate variables describing key components (bonds, angles, torsions etc.) in molecules along with the unique parameters that are specific to each functional group or bond is referred to as a *force field*. More precisely, force fields hold information about the connectivity of atoms within the molecules and the parameters derived from various sources, such as force constants, equilibrium geometries from *ab initio* simulations, van der Waals radii from crystallographic data, thermodynamic data obtained from solution chemistry and other energy parameter values that describe the forces and energies of the molecules. Force fields are used extensively in MD and Monte Carlo simulations. MM methods allow the energy of a system to be calculated as a parametric function of the nuclear coordinates.[2] A major advantage of these force fields is their ability to uniquely treat molecules composed of structurally similar units and describe their relative energies.[2] Various force fields have been developed and are widely used with high accessibility.[2] Popular force fields used in computer simulations of molecular systems include MM2, MM3, AMBER, GROMOS and CHARMM.[3] Principally, the electronic motion in a system is significantly ignored and the energies are computed as a function of the nuclear positions.[1] MM methods allow calculations in a multi-atomic system to be performed with as high accuracy as that of the highest level of quantum mechanics calculation.[1] However, molecular mechanics methods are limited to provide properties that are not dependent on

electronic structure.[1] The Born-Oppenheimer approximation validates the calculation of energy as a function of nuclear coordinates[1,7] and introduces the concept of a potential energy surfaces defined over all nuclear coordinates.[7] This approximation further makes the concepts of equilibrium and transition state geometries possible as these are defined as critical points on the potential surface energy.[7] The origin of the Born-Oppenheimer approximation lies in quantum mechanics. The assumption is made that the electronic motion and the nuclear motion can be separated in solving the Schrodinger wave equation. The Schrodinger wave equation is given below.[1,7]

$$H\Psi = E\Psi \tag{2.1}$$

$$\frac{-h^2}{8\pi^2}\nabla^2\Psi(nuclear, electron) + U(nuclear, electron)\Psi(nuclear, electron) = E\Psi(nuclear, electron) \tag{2.2}$$

Equation [2.1] is the generalised Schrodinger wave equation in operator form where H is the Hamiltonian operator, E is the energy eigenvalue of the system and Ψ is the wave function. Equation [2.2] gives this equation where Planck's constant is given by h, ∇ is the del operator and the square of it is given by $\nabla^2 \equiv \frac{\partial^2}{\partial x^2} + \frac{\partial^2}{\partial y^2} + \frac{\partial^2}{\partial z^2}$ in 3 dimensional coordinates, $U(nuclear, electron)$ is the potential energy and $\Psi(nuclear, electron)$ is the wave function for the nuclei and electrons motion. For free particles, the potential energy is zero.[7]

There are several assumptions involved in which the above theory is valid. Firstly, the Born-Oppenheimer approximation assumes that the electronic wave function depends on nuclear positions but not upon their velocities.[1,7] The second assumption states that nuclear motion sees a smeared out potential from the speedy electrons.[1,7] The Born-Oppenheimer approximation expression of the wave function for the energy contributions of the molecule is given as the product of the wave function of the electronic motion with respect to nuclear positions and the wave function of the nuclear position. The resultant separable expression is given as follows:[7]

$$\Psi_{total}(electrons, nuclear) = \Psi_{electrons}(electrons)\,\Psi_{nuclear}(nuclear) \tag{2.3}$$

Molecular Mechanics (MM) Force Fields

Molecular Mechanics (MM) force fields are defined by intra- and inter molecular terms.[1] In MM chemical systems, atoms are represented as balls and bonds are modelled as springs.[2] The total energy, E_{total}, of a system is calculated as the sum of each energy function and is given by the following equation:[1]

$$U_{total}(r^N) = \sum_{i=1}^{bonds} \frac{k_i}{2}(l_i - l_{i,0})^2 + \sum_{i=1}^{angles} \frac{k_i}{2}(\theta_i - \theta_{i,0})^2 + \sum_{i=1}^{torsions} \frac{V_n}{2}(1 + \cos(nw - \gamma)) + \sum_{ij=1}^{atoms} \frac{q_i q_j}{4\pi\varepsilon_0 r_{ij}} + \sum_{ij=1}^{atoms} 4\varepsilon_{ij}\left(\frac{A_{ij}}{r_{ij}^{12}} - \frac{B_{ij}}{r_{ij}^{6}}\right) \quad (2.4)$$

$U_{total}(r^N)$ is the potential energy of the system and a function of the position vectors, r, N is the number of atoms.[1] The first terms as they appear in equation [2.4] above are the bond potential energy, bond angle potential energy, torsional potential energy and are classified as intramolecular forces. The last two are electrostatic energy and van der Waals energy and are classified as the intermolecular forces. The interactions between molecules from these two energy terms is described pairwise, using Coulombic interaction (described here using a particle mesh Ewald method) and Lennard-Jones potential, respectively.

2.1.2 MD simulation finite difference method

The MD method is a time-dependent method. Time-dependent methods keep record of particles' previous movement, which is then used to predict the next step. MD simulations integrate Newton's second law of motion for atoms on an energy surface. The energy available for the molecules is distributed between potential and kinetic energy, and molecules are thus able to overcome barriers separating minima if the barrier height is less than the total energy minus the potential energy.[3] The dynamics is able to sample the whole surface when given a high enough energy closely related to the simulation temperature, but this will also require an impractically long simulation time. MD methods generate a series of time-correlated points in phase space in a series of finite time steps.[1] Newton's second Law of motion is given by equation below:

$$F = ma, \tag{2.5}$$

where F is the force applied on a particle, m is the mass of the particle and a is the acceleration of the particle in the direction of the applied force.

Since the system produces a multi-body problem, which is not easily simplified using analytical methods, the solution is determined numerically. Finite difference methods are then used to integrate Newton's second law of motion in order to break down the integration into pieces, each separated by a fixed time δt. Then, the total forces can be calculated on each particle with other particles as the vector sum of its interactions at time t. Assuming that the force in each time step is constant, the acceleration of the particles can be determined at time t, which is then combined with the velocity and the position of the particles. Then the new positions and velocities and acceleration at time $t + \delta t$ can be predicted. This continues until the full trajectories are produced that represents the entire motion of the particles of the system in the desired time.[1]

A variety of algorithms are available for integrating the equation of motion using finite difference methods. All these methods approximate the positions, velocities and accelerations using Taylor series expansions.[1] The expression for the Taylor series expansions for the position, velocity and acceleration are given by the following equations, respectively: [1]

$$\boldsymbol{r}(t+\delta t) = \boldsymbol{r}(t) + \delta t\boldsymbol{v}(t) + \frac{1}{2}\delta t^2\boldsymbol{a}(t) + \frac{1}{6}\delta t^3\boldsymbol{b}(t) + \frac{1}{24}\delta t^4\boldsymbol{c}(t) + \cdots \tag{2.6}$$

$$\boldsymbol{v}(t+\delta t) = \boldsymbol{v}(t) + \delta t\boldsymbol{a}(t) + \frac{1}{2}\delta t^2\boldsymbol{b}(t) + \frac{1}{6}\delta t^3\boldsymbol{c}(t) + \cdots \tag{2.7}$$

$$\boldsymbol{a}(t+\delta t) = \boldsymbol{a}(t) + \delta t\boldsymbol{b}(t) + \frac{1}{2}\delta t^2\boldsymbol{c}(t) + \cdots \tag{2.8}$$

$$\boldsymbol{b}(t+\delta t) = \boldsymbol{b}(t) + \delta t\boldsymbol{c}(t) + \cdots \tag{2.9}$$

$$\boldsymbol{c}(t+\delta t) = \boldsymbol{c}(t) + \cdots \tag{2.10}$$

where $\boldsymbol{r}$ is the position, $\boldsymbol{v}$ is the velocity (the first derivative of the position with respect to time), $\boldsymbol{a}$ is the acceleration (the second derivative of the positions with respect to time) and $\boldsymbol{b}$ and $\boldsymbol{c}$ represent higher order derivative of the positions with respect to time, and so on.[1]

Two algorithms for integrating Newton's equation of motion are briefly discussed. These algorithms are the leap-frog and the Verlet algorithm.

Leap-Frog algorithm

The leap-frog algorithm uses the following relationship for the position $\boldsymbol{r}(t+\delta t)$ and velocity $\boldsymbol{v}\left(t+\frac{1}{2}\delta t\right)$:

$$\boldsymbol{r}(t+\delta t) = \boldsymbol{r}(t) + \delta t \boldsymbol{v}\left(t+\frac{1}{2}\delta t\right) \tag{2.11}$$

$$\boldsymbol{v}\left(t+\frac{1}{2}\delta t\right) = \boldsymbol{v}\left(t-\tfrac{1}{2}\delta t\right) + \delta t \boldsymbol{a}(t) \tag{2.12}$$

In the leap-frog algorithm, the next velocities $\boldsymbol{v}\left(t+\frac{1}{2}\delta t\right)$ are calculated from the previous velocity $\boldsymbol{v}\left(t-\frac{1}{2}\delta t\right)$ at previous time $t-\frac{1}{2}\delta t$ and the acceleration $\boldsymbol{a}(t)$ at time t.[1] From the calculated velocities $\boldsymbol{v}\left(t+\frac{1}{2}\delta t\right)$ the positions $\boldsymbol{r}(t+\delta t)$can be deduced together with the positions at time $\boldsymbol{r}(t)$.[1] At time t the velocities can be calculated using the equation:

$$\boldsymbol{v}(t) = \frac{1}{2}\left[\boldsymbol{v}\left(t+\frac{1}{2}\delta t\right) + \boldsymbol{v}\left(t-\frac{1}{2}\delta t\right)\right] \tag{2.13}$$

This algorithm is simply summarised as velocities leaping over the positions to give the new values at time $t+\frac{1}{2}\delta t$ and the positions leaping over the velocity to give their new values at $t+\delta t$. This algorithm offers advantages such as explicit inclusions of the velocity calculation and does not require the calculation of the differences of large numbers. The other advantage of this method is that it does not require calculation of the kinetic energy contribution to the total energy at the same time as the positions are defined.[1]

Verlet Algorithm

The Verlet algorithm tracks the previous positions $\boldsymbol{r}(t-\delta t)$at time $t-\delta t$ and uses that with the positions $\boldsymbol{r}(t)$ at time t and the acceleration at time t to calculate the new positions. [1] The new velocities can be deduced by taking equation [2.14] and comparing it with the previous velocities. Note that the expression for the previous positions will take the same form as this equation except that the positive sign will be replaced with a negative sign after every odd numbered term. The relationship between the two equations can be written as follows: [1]

$$\boldsymbol{r}(t+\delta t) = \boldsymbol{r}(t) + \delta t\boldsymbol{v}(t) + \tfrac{1}{2}\delta t^2\boldsymbol{a}(t) + \ \ldots \tag{2.14}$$

$$\boldsymbol{r}(t-\delta t) = \boldsymbol{r}(t) - \delta t\boldsymbol{v}(t) + \tfrac{1}{2}\delta t^2\boldsymbol{a}(t) - \ \ldots \tag{2.15}$$

By adding equation [2.14] and [2.15], the following equation results:

$$\boldsymbol{r}(t+\delta t) + \boldsymbol{r}(t-\delta t) = 2\boldsymbol{r}(t) + \delta t^2\boldsymbol{a}(t) \tag{2.16}$$

Rearranging equation [2.16] and writing it in terms of the new position gives the following:

$$\boldsymbol{r}(t+\delta t) = 2\boldsymbol{r}(t) - \boldsymbol{r}(t-\delta t) + \delta t^2\boldsymbol{a}(t) \tag{2.17}$$

Although velocity does not appear explicitly in the Verlet algorithm, it can be calculated by dividing the difference between the previous position term $\boldsymbol{r}(t-\delta t)$ and the new position term $\boldsymbol{r}(t+\delta t)$ by $2\delta t$.[1] The equation for velocity be written as follows: [1]

$$\boldsymbol{v}(t) = \frac{[\boldsymbol{r}(t+\delta t) - \boldsymbol{r}(t-\delta t)]}{2\delta t} \tag{2.18}$$

2.1.3. Ensemble Methods

In liquid simulations, MD provides detailed structural motion of molecules, whilst statistical thermodynamics deals with the average behaviour of the particles in a system. As mentioned above, the dynamics simulation generates information at the microscopic level, such as atomic and molecular positions, velocities, accelerations, etc. This information is then required to be interpreted into macroscopic terms such as pressure, volume, temperature and internal energy. Statistical mechanics is used to provide such relationships.

From the representative collection of generated configurations, the sum of all states is approximated by an average over a finite set of configurations. Representative means the number of configurations with a given energy is proportional to that given by the Boltzmann distribution, and that all important parts of the phase space are sampled.[3] Statistical thermodynamics is based on the principle that thermodynamic quantities are averages of molecular properties.[2] In MD simulation, the ensemble methods are implemented in determining the average value of the behaviour of the molecular properties over all

replications generated by the simulation. The ensemble is defined as the collection of configurations.[3] Therefore, the average of those generated configurations is referred to as ensemble averages. There are several methods of ensemble averages in the theory of statistical thermodynamics. For now we are only concerned with micro canonical ensemble (NVE), canonical ensemble (NVT) and isothermal-isobaric ensemble (NPT). A detailed explanation of each of these thermodynamic ensemble methods is given below.

Micro Canonical Ensemble

The micro canonical ensemble, also called the NVE ensemble, is the collection of configurations with constant energy, constant number of particles and constant volume. The micro canonical ensemble calculates the number of available microstates Ω of the particles in the system. It then uses the Boltzmann entropy relation:

$$S = k_B ln\Omega \tag{2.19}$$

where S is the entropy and k_B is the Boltzmann constant. All other thermodynamics quantities are obtained from the calculated entropy.

There are two assumptions when using the micro canonical ensemble, namely the ergodic hypothesis and the statistical postulate. Firstly, the ergodic hypothesis is employed to convert the classical mechanics differential equations or the quantum mechanical eigenvalues into formulations for expressing the probability of finding the system in a specific microstate. The Ergodic hypothesis states that the time average is equal to ensemble averages: $\langle A \rangle_{time} = \langle A \rangle_{ensemble}$. Secondly, the statistical postulate states that given the isolated system is in equilibrium, it is found with equal probability in each its accessible microscopic states. This simply means that for a given Ω microscopic states corresponding to a particular energy level E_v, the probability P_v of finding the system in a macroscopic state v is given by:

$$\mathrm{P_v} = \frac{1}{\Omega(\mathrm{E,N,V})} \tag{2.20}$$

The micro canonical ensemble describes an isolated system where the momentum of the particles in the system is conserved; hence, the energy does not fluctuate.

Canonical Ensemble

The canonical ensemble, also called the NVT ensemble, is the collection of configurations of a system with constant number of particles, N, volume, V, and the temperature, T, whilst allowing energy to be transferred between the members of the ensemble.[2] However, the total energy of the ensemble is conserved. The thermodynamic potential of this ensemble is the Helmholtz free energy. The canonical ensemble can be looked at as a subsystem of the micro canonical ensemble. The kinetic energy is calculated as the sum of the contributions from the momenta:

$$\sum_{i=1}^{N} \frac{p_i^2}{2m_i} = \frac{3}{2} k_b T \tag{2.21}$$

In simulation, the initial velocities are chosen randomly from a Gaussian distribution, whereby the linear momenta are conserved. However, these velocities do not have to resemble the initial temperature, T_i. The temperature can be kept constant using several techniques, some of which are discussed here includes the Nose-Hoover method and the Berendsen loose coupling technique.

Isothermal-Isobaric Ensemble

The isothermal-isobaric ensemble, also called NPT ensemble, differs from the canonical ensemble in that the pressure, P, is kept constant with the number of particles, N and the temperature, T. Here the volume V is allowed to fluctuate between the members of the ensembles The thermodynamic potential of this ensemble is the Gibbs free energy. The external pressure can be applied to the system and kept constant through techniques such as the Berensen pressure coupling scheme. The other coupling technique used to control pressure and temperature is the Nose-Hoover method. These techniques are discussed below.

2.1.4 Temperature Control Method

Nose Hoover method

Temperature control in a simulation is needed for mimicking systems where the conditions correspond to those in a physical experiment. One such method is the Nose-Hoover method. In the Nose-Hoover temperature control method the system is supplied with a thermal reservoir, which is represented by an additional degree of freedom.

The potential of the reservoir has the form; $(f+1)k_BTlns$, where f is the number of degrees of freedom in the physical system, k_B is the Boltzmann constant, T is the desired temperature of the system and s is the additional degree of freedom. [1] The idea is to consider the heat bath as the integral part of the system by addition of artificial variable, s, associated with a mass, $Q > 0$, which effectively determines the strength of the thermostat, as well as velocity.[21] The kinetic energy of the reservoir has the form $\left(\frac{Q}{2}\right)\left(\frac{ds}{dt}\right)^2$. Its magnitude determines the coupling between the reservoir and the real system and thus influences the fluctuations in temperature. [1] According to Nose and Hoover, Q should be proportional to fk_BT. [1]

Berendsen Loose Coupling Technique

The Berendsen coupling technique is applied to control the temperature of the system as well as the pressure. Here the system is connected to the surrounding bath, which is at a constant temperature T_0, to slow down the scaling process. The scaling of each particle's velocity is accomplished by including a dissipative Langevin force in the equations of motions according to[17]

$$\boldsymbol{a}_i(t) = \frac{\boldsymbol{F}_i(t)}{m_i} + \frac{\boldsymbol{p}_i(t)}{m_i\tau}\left[\frac{T_0}{T(t)} - 1\right] \tag{2.22}$$

where $T(t)$ is the instantaneous temperature, and τ has units of time and is used to control the strength of the coupling.[7] The larger the value of τ the smaller the perturbing force and the more slowly the system is scaled to T_0. The pressure in the Berendsen coupling technique is computed using the following equation

$$P(t) = \frac{1}{V(t)}\left[Nk_BT(t) + \frac{1}{3}\sum_i^N \sum_{j>1}^N F_{ij} r_{ij}\right] \quad (2.23)$$

where V is the volume, N is the number of particles, F and r are the forces and distances between particles, respectively.[7]

2.1.5 The TIP3P Water Model

The TIP3P water model uses three sites of electrostatic and van der Waals interaction. In this water model there are two partial positive charges, δ+, on the two hydrogen atoms and a highly negatively charged site δ- located on the oxygen atom. The two positive charges on both hydrogen atoms are balanced by the negative charge of the oxygen atom. The van der Waals interactions between two water molecules is computed using the Lennard-Jones potential function with only a contribution from the oxygen atoms, without the computation of the hydrogen atoms. The CHARMM force field does modify the original methods and includes van der Waals parameters on the hydrogen atoms, but without modifying the charges. The hydrogen-oxygen distance, r(OH), is 0.9572 Å with a hydrogen-oxygen-hydrogen angle of 109.47 degree. Each hydrogen atoms has the partial positive charge value of 0.417δ+ and the oxygen atoms has the negative charge of -0.834.[1]

2.1.6 Heating

MD simulations are often initiated with minimised structures. Minimisation removes energies and overlapping from the structures. Therefore, a minimised structure is equivalent to a low energy structure, but it can be an unrealistic starting position for the simulation to follow. To overcome these unrealistic structures, the system is heated to bring it to the desired temperature T so that the information at the starting point is lost and allowing it to behave realistically. In starting an MD simulation, a set of initial velocities is required to generate the initial forces; these velocities are often randomly assigned in such a way that the Maxwell-Boltzmann distribution is reproduced[2]. The kinetic energy of these velocities is given by $3/2k_BT$, where the integer 3 represents the three dimensional system, and k_B and T is the Boltzmann constant and temperature, respectively.[2]

2.1.7 Periodic Boundary Condition (PBC)

To run a dynamics simulation with conserved number of particles, periodic boundary conditions (PBC) are applied. PBC ensures that the representative number of molecules is being simulated as if in infinitely diluted space. This, of course, also ensures that the system at the final stage contains the same number of molecules as in the initial stage. Moreover, since particles experience forces at the boundaries, PBC removes the problem of surface effects on the simulated box. PBC, when applied to the simulated cell during simulation, creates a periodic array of images surrounding the central box. Each and every atom in the central box is replicated throughout space to form an infinite array (in practice these arrays are also bound by a cutoff) of periodic images.[1,5]. Each particle in the periodic image moves in the same direction in the same position with the same momentum and energy as the corresponding particle in the original, or primary, box (the illustration is shown in figure 2.2 below). This prevents particles from escaping the box. When any particle in the central box moves outside the box, it is replaced by the corresponding particle in the periodic array of image. The central box is constantly refilled when an atom moves out of box.

There are different cells of different shapes that are used to simulate liquids with PBC. The most commonly used periodic cell are cubic, truncated octahedron, hexagonal prism, rhombic dodecahedron and elongated dodecahedron.[1] A particular periodic cell may be the right choice for a particular simulation but in principle, any cell that fills the space by translation operations of the central box in three dimensions, can be used. In all of these periodic cells, the cubic cell is the simplest periodic system to visualise and program. However, the truncated octahedron cell approximates a spherical simulation volume and is preferred to cubic cell when very large solutes are dealt with. [1]

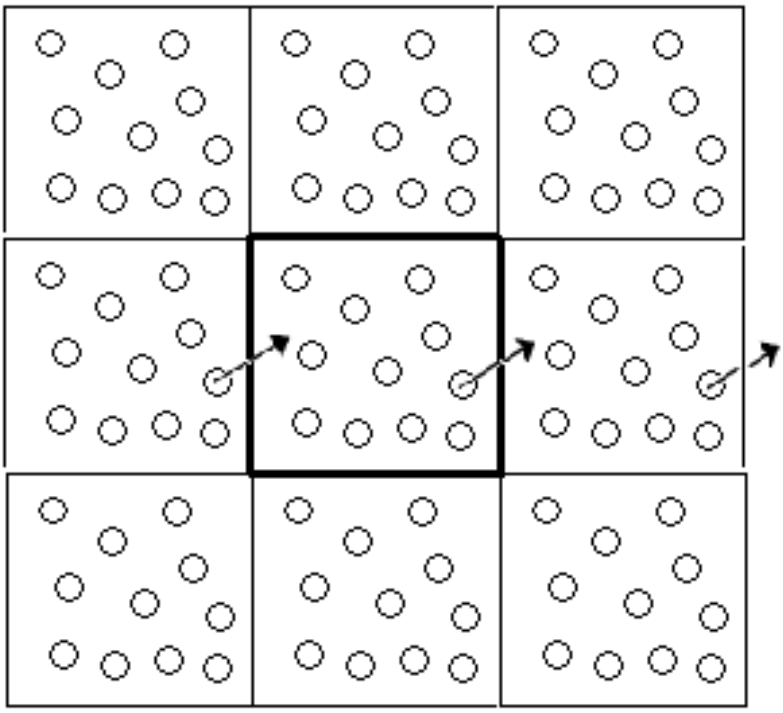

Figure 2.2 Schematic of periodic boundary conditions. The black shaded line central box represent the simulated box in 2-dimensions and the other surrounding boxes are its periodic images. The arrow shows the condition in which the atom in the central box moves out of the box is replaced by its periodic image which has the same position, velocity and direction.

2.1.8 Minimum Image Conversion

Nonbonded atomic pair-wise interactions at short range are crucial and are included into energy computation of the system. However, these interactions are computationally expensive to compute since in essence they should be calculated between all pairs of atoms in the system, even those in the image arrays.[1,4] The most common approach, if not the simplest to deal with the non-bonded interactions, is to apply the minimum image convention using a non-bounded cutoff.[1] During dynamics simulation in a periodic cell, each atom in the central box should see just one image of the atoms in the replicated infinite array of periodic images. Therefore, the energy is calculated between pair of atoms within the closest distance.[1]

2.1.9 Cutoffs

Cutoffs are used to compute the nonbonded interaction between atoms within the closest distance. In principle all pairs should be considered, but this becomes prohibitively expensive for a large number of particles. Since the nonbonded interaction is distance dependent and

dies off at very large distances (care should be taken for electrostatic interaction, which decreases much less rapidly than the van der Waals interaction), in practice the number of pairs used are restricted based on the separation between them. The cutoff values are always set to less than half the length of the simulated cell to avoid an atom seeing an image atom more than one, a consequence of the above-mentioned minimum image convention. Cutoffs have the tendency of introducing a discontinuity to both potential energy and force near the cutoff values, which means some fraction of potential energy is ignored. There are ways in which the discontinuity in energy can be counteracted; firstly, by using the shifted potential function. In the shifted potential function a constant term is subtracted from the potential at all values.[1] However, the problem with the shifted potential is that there can be a discontinuity in the force. When the shifted potential is applied, at the cutoff distance the force drops suddenly to zero just beyond the cutoff.[1] The dire consequence of this is that it brings instabilities in a simulation.[1] A shifted potential also results in deviation from the true potential. The preferred alternative to deal with the discontinuity in potential energy and forces at the cutoff value is to use the switching function, which assures a smooth approach of the energy change to the cutoff distance. The switching function is a polynomial function of the distance by which the potential energy is multiplied.[1] The form of the equation for the switching function is as follows:

$$\boldsymbol{v}'(r) = \boldsymbol{v}(r)\left[1 - 2(\frac{r}{r_c})^2 + (\frac{r}{r_c})^4\right] \tag{2.24}$$

where $\boldsymbol{v}'(r)$ is the switched potential, $\boldsymbol{v}(r)$ is the true potential r is the potential energy distance and r_c is the cutoff distance. The switching function has a value of 1 at $r = 0$ and a value of 0 at $r = r_c$. The advantages of using the switching function with group-based cutoffs is that energy is conserved and the potential is defined analytically at all points.[1]

2.1.10 Long Range and Short Range Forces

All nonbonded interaction can be divided into contributions from short range and long range forces. In an MD simulation of a system of many atoms, substantial treatment of these interaction forces, both at short and long distance, is very important. However, the treatment of the interactions involving the nonbonded charge-charge interaction, which is long range in nature, is of great concern in computer simulation and may result in disastrous events,

creating false energies if not treated properly. Several methods have been developed for the proper treatment of electrostatic interaction between non-covalently bonded pairs of atoms and provide greater accuracy, thus, minimising computational errors. The general short range and long ranges forces are explained in the subtitle following bellow and the treatment of electrostatics is expanded on.

Short Range Forces

All forces which decrease with a distant quicker than r^{-n}, where r denotes the distance and n is the dimensionality of the system, is classified as short range interaction. Short range interactions are treated by applying a nonbonded cutoff value to the potential V(r), as explained above. Examples include dispersion and higher order multipole interactions.

Long Range Forces

Long range forces are, in principle, infinitely ranged. A long range force is often defined as one in which the spatial interaction falls off no faster than r^{-n} where n is the dimensionality of the system. This force includes charge-charge interaction between ions and dipole-dipole interactions between molecules. These forces are problematic in computer simulations, since their range is greater than half the box length. In computer simulations long range forces are accounted for by the implementation of periodic boundary conditions into the simulation cell. One way of treating such forces more accurately would be to increase the size of the central box so that the screening neighbours would diminish the effective range of the potential.[4] The Ewald summation method of electrostatic interaction, Particle-Mesh Ewald (PME) is implemented for computation of the Coulombic interaction forces between atoms at long distances when periodic array of images are present.

2.1.11 Ewald Summation of electrostatic interaction

The Ewald summation method is the most effective technique for the computation of electrostatics. Ewald summation is a technique for efficiently summing the interaction between an ion and all its periodic images.[4] The Coulombic interactions that is the electrostatic interactions between a pair of interacting charges q_i, q_j varying with the

separating distance as $\frac{1}{r_{ij}}$, is calculated with the interacting array of periodic images surrounding the central box. The Ewald Summation method converges conditionally for electrostatic interaction energy evaluations.[6] Ewald summation can be used to treat electrostatic interactions during all phases of an MD simulation, for example, energy evaluation during minimisation, equilibration, and production. [6] The position of each box can be related to the central box by specifying a vector for each, of whose components are an integral multiple of the length of the box.[1, 4, 6] The charge-charge contribution to the potential energy due to all pairs of charges is described by the following equation [1,6]

$$V = \frac{1}{2}\sum_{i=1}^{N}\sum_{j=1}^{N}\frac{q_i q_j}{4\pi\varepsilon_0 r_{ij}} \tag{2.25}$$

where r_{ij} is the minimum distance between charges i and j and V is the potential energy and N denotes the number of ions in the system.[1, 6] There are $\frac{N(N-1)}{2}$ pairs of interacting ions in the system. [6] The total potential energy is summed over all pairs of ions. [6] This is the expression of the Ewald summation for the Coulomb interaction energy.[1] Consider a cell subjected to periodic boundary conditions surrounded by a number of periodic arrays of repeating images describes by repeating vectors $\boldsymbol{x}_1, \boldsymbol{x}_2, \boldsymbol{x}_3$ forming a supercell. [1, 4, 6] For every ion with a charge q_i at r_i there are also ions with a charge q_i at $r_i + n_1\boldsymbol{x}_1 + n_2\boldsymbol{x}_2 + n_3\boldsymbol{x}_3$ with n_1, n_2, and n_3 being arbitrary integers. [4, 6] The notation can then be simplified by rewriting the arbitrary repeat vectors, $n_1\boldsymbol{x}_1 + n_2\boldsymbol{x}_2 + n_3\boldsymbol{x}_3$ as $\boldsymbol{n}L$, where L represents the length of the supercell. The contribution of charge–charge interactions between the charges in the central box and all images of all particles in the surrounding boxes then is given by the following equation[1,6]

$$V = \frac{1}{2}\sum_{nbox=1}^{n}\sum_{i=1}^{N}\sum_{j=1}^{N}\frac{q_i q_j}{4\pi\varepsilon_0|r_{ij}+nL|} \tag{2.26}$$

2.1.12 Particle-Mesh Ewald (PME)

The Particle-Mesh Ewald (PME) procedure divides the potential energy into Ewald's standard direct and reciprocal sums and uses a conventional Gaussian charge distribution. The direct sum is evaluated explicitly by using a non-bonded cutoff and the reciprocal sum is approximated using a Fast Fourier Transformation (FFT) with convolutions on a grid, where

charges are interpolated between the grid points. However, PME does not interpolate but rather evaluates forces by analytically differentiating the energies.

References

1. Leach, A. R. Molecular Modelling: Principles and Applications; Longman, 2001.

2. Hinchliffe, A. Chemical Modeling from Atoms to Liquid; John Wiley & Sons, Ltd, 1999.

3. Jensen, F. Introduction to Computational Chemistry; J. Wiley and sons: England, 1999.

4. Allen, M. P. Tildesley, D. J. Computer Simulation of Liquids; Oxford Science Publication, 1987.

5. Alan Hinchliffe. Chemical Modeling From Atoms To Liquids; John Wiley & Sons, LTD. 1999

6. Hark Lee and Wei Cai, Ewald Summation for Coulomb Interactions in a Periodic Supercell, January 10, 2009.

7. Christopher J Cramer. Essentails of Computational Chemistry Theories and Models, second edition, John Wiley & Sons, Ltd, 2004.

Chapter 3

Computational Analysis - Analytical Methods

3.1 Introduction

The main goal of this thesis is to investigate the effect of an organic polymer on the diffusion of PGM complexes in aqueous solution. The relative rates of diffusion are importanting in bringing about the separation of individual PGM complexes from one another. The physical reasons that bring about varied distribution rates for the set of chemically very similar transition metal complexes has been difficult to understand from experimental methods. Here the strategy is to replicate the chromotographic elution trends using accurate MM force field developed at the Scientific Computing Research Unit Laboratories[18-20] This is done by calculating the diffusion rates from computer simulations. These are then compared with the experimental trends in elution times. In this chapter we detail the theory and methods used to calculate transport properties, such as diffusion, and techniques such as relative free energy calculations that reveal the chemical and physical rationale for the variation in diffusion of the PGM complexes.

The diffusion coefficient relates the particle flux to a concentration gradient. The amount of flow of a molecule through a given area per unit time is measured by its flux. Flux is proportional to the first derivative of its related property, see equation 3.7 below.[9] The general definition of diffusion is defined as the transport movement of the particles.[1,7,9] The rate of diffusion is given by its coefficient, D. The SI units of D is given by meter squared per second ($m^2.s^{-1}$).[7,9] There are two ways of calculating diffusion from MD simulations, (i) the mean square displacement (MSD), based on the Einstein relation between the diffusion coefficient and the MSD and the (ii) velocity autocorrelation function (VACF) based on Green-Kubo theory. Both methods give the same results and any of these can be used to compute the diffusion of a single molecule or a collection of molecules in a system.

3.1.1 Mean Square Displacement (MSD)

The diffusive motion of molecules is described by a random walk and lack of a simple linear path. As the molecules travel they collide and re-collide against one another, which prevents

them from following a straight path. One way of calculating D is by approximating a linear path from the molecular random walk. This is done by using the MSD of the molecular (or atomic) motion in a simulation which is governed by the Einstein relation in the theory of diffusion.

In computer simulations, the diffusion coefficient is calculated from equilibrium-simulation.[1,4,7] The Einstein relation of diffusion is based on Fick's law of diffusion and it is not applicable over short times.[1] The diffusion coefficient is calculated at infinite time using the relation[1,4]

$$D = \lim_{t\to\infty} \frac{1}{6t} < |r(t) - r(0)|^2 > \quad (3.1)$$

where $r(0)$ is the position of the molecule at time t = 0 and $r(t)$ is the position of the molecule at time t. The bracket, $\langle \dots \rangle$, represents the ensemble average. The quantity $< |r(t) - r(0)|^2 >$ is the MSD, which is averaged over the particles in a system of interest. The averaging contributes mainly towards reducing the statistical errors.[1] The diffusion coefficient is obtained by plotting the MSD against the time intervals from which it was calculated. The value of the slope, divided by an integer value of six, then expresses the diffusion coefficient, D.[1,7]

3.2. Computing Free Energy

3.2.1 Introduction

Selective ion binding is critical in ensuring efficient separation of hexachloro and tetrachloro PGM complexes. The distinct binding strength of these complexes to certain organic polymer functional groups in solution plays an important role in determining and achieving such selectivity in binding. The solvation free energy and binding free energy between the negatively charged metal complexes in water are determined in the presence of an organic polymer, with the aim of comparing their overall free energy differences.

3.2.2 Free Energy Methods

Free energy calculations are one of the most important aspects of computational chemistry. [11] The free energies of molecular systems describe their tendencies to associate and react. [12] The core of free energy simulation methodology is the fact that the free energy is the state function and therefore path independent; a non-physical pathway can be used to connect any two states. This idea is expressed in a hybrid Hamiltonian potential energy function $H(\boldsymbol{r},\ \lambda)$. This potential energy functions depends on the coupling parameter, λ[13]

$$H(\boldsymbol{r},\lambda) = H_E(\boldsymbol{r}) + (1-\lambda)H_R(\boldsymbol{r}) + \lambda H_P(\boldsymbol{r}) \qquad (3.2)$$

where $H_E(\boldsymbol{r})$ is the environmental part of the Hamiltonian that does not change, $H_R(\boldsymbol{r})$ is the reactant part of the Hamiltonian and $H_P(\boldsymbol{r})$ is the product part of the Hamiltonian.[13] Free energy calculations in this fashion are performed by defining the coupling parameter λ that describes the system such that the end points of the simulations corresponds to $\lambda = 1$ and 0, respectively, the nonphysical intermediates states are defined by intermediate values of λ. [14] Since the convergence of the free energy method depends on the change between two subsequent states, the move from the initial to final states should be done in a step wise fashion through the non-physical intermediates, with care taken to limit the change in free energy between two following states.[13] There are two distinct approaches of topological constructions when carrying out free energy calculations.[12] These approaches differ in how they describe the changing topology of the system.[14] The two methods are called single and dual topology.[12,14] In the single topology method, the change is formulated in terms of a system where the atom types and target internal coordinates (bonds, angles and torsions) of the system are modified to reflect the end points. The changes in the initial and final states are allowed to be defined using dummy atoms, given that the number of atoms is not always the same between these two states. [14] The single topology approach is widely implemented in programs GROMOS and AMBER. [12,14] In the dual topology method, the change is formulated in terms of a system where two complete versions of the changing group λcoexist at all times. One version represents the initial state and the other version represents the final state. All the atoms in the combined topology interacts with the system in an appropriately weighted mix based on the λ parameter, but the two topologies do not interact with one another. The atom type and the internal coordinates of the system never changes. The coupling constant, λ

effectively represents a scaling constant defining the mixture of the two topologies at any intermediate point. [14] The dual topology approach is widely implemented in programs such as CHARMM. [12,14]

During free energy simulations changes in bond length, as the move is made from the initial state to final state, could occur depending on the approaches followed. If a single topology method is used, its scheme does not allow changes in bond length with coupling constant, λ. Such contributions to the free energy are calculated using a potential of mean force (PMF) bond contribution.[14] Since both topologies are present in dual topology descriptions this is not a problem.

There are two different path based free energy methods that can be used to compute namely free energy perturbation (FEP) and thermodynamic integration (TI).[11,12,14] All of these methods are reported to be efficient in one way or another in calculating free energy differences. In the study by *Pearlman*[14] whereby these two methods where compared as implemented in the program AMBER, TI was reported to be more efficient than FEP when the dual topology approach is used, but both were comparable in efficiency with a single topology approach. It is also reported that FEP is more efficient with both single and dual topologies approaches for very long simulations.[14]

In addition to these two path-based free energy methods there is also the slow growth method [12]. However, for the purpose of this study we only make use of FEP and its implementation in the program CHARMM.

3.2.3 Free energy of Perturbation (FEP)

FEP methods have been found to be very accurate and it is highly preferred over other techniques to estimate free energy of association, characterised by non-covalent interaction between small molecules and solvent, and between small molecules and macromolecules.[15] FEP methods are based on the calculation of free energy difference between two sates. The free energy difference between two states, the initial, i, and final state, f, in FEP is calculated using the equation:

$$\Delta A = A_f - A_i = -k_B T \, ln\langle e^{-(H_f - H_i)/k_B T} \rangle_i \qquad (3.3)$$

where ΔA is the Helmholtz free energy difference between the initial state and final state; A_i denotes the Helmholtz free energy of the initial state and A_f denotes the Helmholtz free energy of the final state. H_i is the Hamiltonian appropriate to the initial state and H_f is the Hamiltonian appropriate to the final state and $\langle \quad \rangle_i$ refers to an ensemble average over a system represented by Hamiltonian H_i. k_B is the Boltzmann constant, and T is the temperature. For a small difference between the initial and final state, the minimum values of the Hamiltonian potential energy at the two states may not correspond to the resulting ensemble configurations.[14] Then, the problem can be generalised by describing the Hamiltonian $H(\lambda)$ as

$$H(\lambda) = \lambda H_f + (1 - \lambda) H_i \tag{3.4}$$

where the coupling constant λ has the values, $\lambda_0 = 0$, and $\lambda_n = 1$.[14] Equation [3.15] can now be generalised as follows:

$$\Delta A = A_f - A_i = \sum_{\lambda=0}^{1} -k_B T \, ln\langle e^{-\Delta H_\lambda / k_B T} \rangle_\lambda \tag{3.5}$$

where $\Delta H_\lambda = H_{\lambda+1} - H_\lambda$ is the Hamiltonian energy difference between the perturbed $(\lambda + 1)$ and unperturbed λ system, which involves windowing over λ intermediates states.[12,13]

3.2.4 Sampling Method

Consider equation [3.17] for the application of the free energy difference between two molecules A and B in different environments. In the liquid phase, their difference in free energy of solvation when moving from $A \rightarrow B$ is calculated by comparing their free energy change in the solvent and in vacuum, figure 3.1. A thermodynamic cycle representative of the free energy change between those two molecules, A and B in the two different environments, is given by:

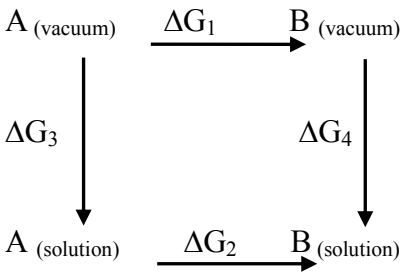

Figure 3.1 Schematic diagram representation of the free energy cycle for computing the free energy of solvation.

Determination of the free energy of binding, figure 3.2, follows the same rationale as the calculation in figure 3.1 but in this case their difference in free energy of binding when moving from $A \rightarrow B$ is calculated by comparing their free energy change in the organic solution and in aqueous solution.

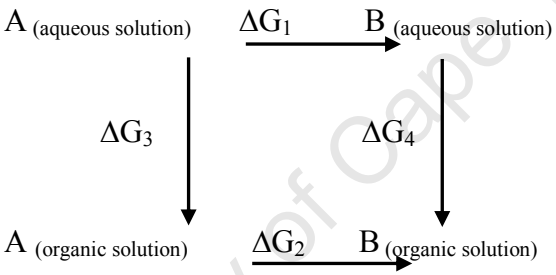

Figure 3.2 Schematic diagram representation of the free energy cycle for computing the free energy of binding.

where ΔG_1 and ΔG_2 are free energies differences between molecule A and B in vacuum phase (or aqueous solution) and in solution (or organic solution), respectively and ΔG_3 and ΔG_4 is the free energy to transfer molecule A and B from vacuum to solution (aqueous to organic solution for free energy of binding). Then, the difference in free energy of solvation of A and B is given by[12,16]

$$\Delta\Delta G = \Delta G_2 - \Delta G_1 = \Delta G_4 - \Delta G_3 \qquad (3.6)$$

Experimentally, the difference $\Delta G_3 - \Delta G_4$, where the same solute in different environments is of interest, can be determined. Standard experimental thermodynamic measurements can be used to calculate solvation and binding free energies, and the differences are readily available. However, through calculation it is the values of ΔG_1 and ΔG_2 that can be obtained using free

energy perturbation or integration. The free energy cycle shows that these values can be equated and the path independence of free energy makes the computational approach feasible.

3.3. Radial Distribution Functions (RDF)

Radial distribution functions (RDFs), also referred to as pair distribution functions (PDFs), are very useful for describing the structure of a solvent or solution. PDFs give the probability of finding the centre of a particle at a given distance from the centre of another particle, normalised to unity for the bulk probability. PDFs of liquids give intermediates between the solid and gas phases, with a small number of peaks at short distances, superimposed in a steady decay to a constant value at a longer distance corresponding to the bulk. Simulation calculations of the PDFs require sorting of the neighbouring atoms around each atom into distance bins; then the number of atoms in each bin is averaged over the entire simulation.[1] The equation defining the RDFs between a pair of two atoms in a spherical volume element is given as follows:[17]

$$\frac{1}{V} g_{AB}(r) = \frac{1}{N_A N_B} \langle \sum_{i=1}^{N_A} \sum_{j=1}^{N_B} \delta[r - r_{AiBj}] \rangle \qquad (3.7)$$

where V is the volume of the defined spherical shell, N is the total number of atoms within the volume of the shell, δ is the Dirac delta function and r is the radial distance.[17] The double summation within the ensemble average effectively counts the number of AB pairs separated by that distance, r.[17] Integrating equation [3.19] above over the full spherical volume yield[18]

$$\frac{1}{V} \int g_{AB}(r) = \frac{1}{N_A N_B} \langle \sum_{i=1}^{N_A} \sum_{j=1}^{N_B} \int \delta[r - r_{AiBj}] \rangle \qquad (3.8)$$

$$= 1$$

where the integral of the Dirac delta function is unity and the $\frac{1}{V}$ term is effectively a normalization constant for g. Equation [3.20] may thus be interpreted as a probability function.[18] Then, the probability of finding the two atoms A and B within some range Δr of distance r from one another can be expressed as follows:[17]

$$P\{A,B,r,\Delta r\} = \frac{4\pi r^2}{V} g_{AB}(r)\Delta r \quad (3.9)$$

where, in the limit of small Δr, the integral is approximated as $g_{AB}(r)$ times the volume of the thin spherical shell $4\pi r^2 \Delta r$.[17] All the g values greater than 1 indicate preferred locations for surroundings atoms, compared to bulk. In case of water molecules, it would be the preferred location of the solvation shell, while for the values below 1 it corresponds to under-populated regions. At larger r the function should be independent of distance. r, In homogeneous media, like fluids there should be an equal probability for any interatomic separation because the two atoms no longer influence one another's positions.[17]

3.4. Simulation Convergence

Convergence is formally defined as the acquisition of a sufficient number of phase points, through either Monte Carlo (MC) or MD methods, to thoroughly sample phase in a proper, Boltzmann-weighted fashion.[17] Calculating the root mean square deviation (RMSD) of the simulation structure is a good measure for a convergence test. The RMSD is computed using the following equation

$$RMSD = \sqrt{\frac{\sum_{i=1}^{N}(r_{i,sim} - r_{i,expt})^2}{N}} \quad (3.10)$$

Where N is the number of atoms in the macromolecule, and the positions r are determined in a coordinate system having the center of mass at the origin and aligning the principle moment of inertia along the Cartesian axes.[17] The purpose of monitoring RMSD is to provide a particular property whose convergence can be assessed and also offering a quantitative measure of how close the simulated structure is to the experimentally determined one.[17]

When there is no experimental data available for comparison, the RMSD is typically computed by using either the initial structure or the average simulated structure as a reference.[17]

3.5 Averages and Statistical Collection in MD Simulations

When performing MD the aim is to generate the necessary information about the atomic motion to calculate properties. Quantities such as positions, velocities, accelerations, and other necessary classical mechanics variables are calculated. This information is converted into macroscopic variables such as temperature, volume, pressure and internal energy. In order to execute this, MD uses statistical mechanics. Statistical mechanics averages the energy or structural properties over the time steps.[2,4] In statistical mechanics, the average values are defined as ensemble averages and is defined by the following equation:

$$\langle A \rangle_{ensemble} = \iint dp^n \, dr^n A(p^n, r^n) \rho(p^n, r^n) \tag{3.11}$$

where $\langle A \rangle_{ensemble}$ is the averaged statistical variable and $A(p^n, r^n)$ is the observable of interest and it is expressed as a function of the momenta, p, and position, r, of the system. The integration is over all possible values of p and r. $\rho(p^n, r^n)$ is the probability density and is given by the following equation:

$$\rho(\mathrm{p^n}, \mathrm{r^n}) = \frac{1}{\mathrm{Q}} \exp[-\mathrm{H}(\mathrm{p^n}, \mathrm{r^n}) / \mathrm{k_B T}] \tag{3.12}$$

where H is he Hamiltonian, T is the temperature, k_B is the Boltzmann constant and Q is the partition function, which is given by $Q = \iint dp^n \, dr^n exp[-H(p^n, r^n) / k_B T]$.

The kinetic energy is calculated as the sum of the kinetic energies of the individual atoms.[2] The temperature can be calculated by averaging the kinetic energy of the individual atoms from the derived statistical mechanics expression

$$\frac{1}{2}\langle \sum mv^2 \rangle = \frac{1}{2}(3N - N_c) N k_B T_{inst} \tag{3.13}$$

where $\frac{1}{2}\langle \sum mv^2 \rangle$ is the average of the sum of the kinetic energies of the individual atoms, $3N - N_c$ is the number of degrees of freedom, equal to three times the number of particles, N, minus the number of constraints, N_c, k_B is the Boltzmann constant and T_{inst} is the instantaneous temperature.[2]

References

1. Leach, A. R. Molecular Modelling: Principles and Applications; Longman, 2001.

2. Hinchliffe, A. Chemical Modeling from Atoms to Liquid; John Wiley & Sons, Ltd, 1999.

3. Jensen, F. Introduction to Computational Chemistry; J. Wiley and sons: England, 1999.

4. Allen, M. P. Tildesley, D. J. Computer Simulation of Liquids; Oxford Science Publication, 1987.

5. Alan Hinchliffe. Chemical Modeling From Atoms To Liquids; John Wiley & Sons, LTD. 1999

6. Hark Lee and Wei Cai, Ewald Summation for Coulomb Interactions in a Periodic Supercell, January 10, 2009.

7. Daan Frenkel & Berend Smit. Understanding Molecular Simulation From algoriths to Applications. Second edition, Computational Science Series Volume 1. Academic Press, 2002.

8. Li Wei-Zhong, Chen Cong, and Yang Jian. Heat Transfer-Asian Research, 37 (2), 2008

9. Peter, Atkins; Julio, De Paula. Atkins' Physical Chemistry; Eighth Edition; Oxford University Press, 2006.

10. K. J. Laidler, J. H. Meiser, Physical Chemistrys World student series edition, The Benjamin/Cummings Publishing Company, Inc, 1982.

11. Changjun Chen; Yi Xiao., J Comput Chem 31: 1368–1375, 2010.

12. Peter Kollman, *Chem. Rev.* 1993, *93,* 2395-2417.

13. B. R. Brooks, C. L. Brooks III, A. D. Mackerell, Jr., L. Nilsson, R. J. Petrella, B. Roux, Y. Won, G. Archontis, C. Bartels, S. Boresch, A. Caflisch, L. Caves, Q. Cui, A. R. Dinner, M. Feig,S. Fischer, J. Gao, M. Hodoscek, W. IM, K. Kuczera, T. Lazaridis, J. MA, V. Ovchinnikov,E. Paci, R. W. Pastor, C. B. Post, J. Z. PU, M. Schaefer, B. Tidor, R. M. Venable, H. L. Woodcock, X. Wu, W. Yang, D. M. York, M. Karpluss., J Comput Chem 30: 1545-1614, 2009.

14. David A. Pearlman, J. Phys. Chem. 1994, 98, 1487-1493.

15. M. Rami Reddy, U. C. Singh, Mark D. Erion., J Comput Chem 28: 491-494, 2007.

16. William L. Jorgesen and Laura L. Thomas., J. Chem. Theory Comput. 2008, 4.

17. Christopher J Cramer. Essentails of Computational Chemistry Theories and Models, second edition, John Wiley & Sons, Ltd, 2004.

18. Lienke, A.; Klatt, G.; Koch, K. R.; Robinson, D. J.; Naidoo, K. J. *Inorg. Chem.* 2001, *40*, 2352.

19. Naidoo, K. J.; Klatt, G.; Koch, K. R.; Robinson, D. J. *Inorg. Chem.* 2002, *41*, 1845.
20. Matthews, R. P.; Venter, G. A.; Naidoo, K. J. *J. Phys. Chem. B* 2011, *115*, 1045.].
21. Victor Ruhle, Berendsen and Nose-Hoover Thermostats, 8, 2007.

Chapter 4

Results

Introduction: Simulation Conditions, Systems and Methods

The geometry of the metal complexes being investigated are square planar and octahedral. The molecular structure of the polymer is given in chapter 1, section 1.5.3. CHARMM, version c33b2 was used to run all the MD simulation. A truncated octahedron periodic cell of dimensions 50.78008 Å x 50.78008 Å x 50.78008 Å was used to simulate the bulk solution properties at infinite dilute solution. The TIP3P water model by Jorgensen *et al.*[1] and Steinbach *et a.l*[2], was used in the solution simulations. The CSFF[3] was used for the polymer and the MSSF[4,5] for the complexes. The energies and forces due to the electrostatic interactions were calculated using the particle mesh Ewald (PME) method. Minimum image convention and application of a switching function were used.[6] The switching function modulates the interaction in a specified interval to smoothly reach zero at the cutoff. This was applied in the range 12.0Å-10 Å along with a neighbourhood list generated from pairs within a distance of 14.0Å from each other. The pair wise interactions were done on an atom-based selection algorithm.

The isobaric-isothermal ensemble (NPT) was used for the initial heating and equilibration of each system where the Nose-Hoover method, (Nose, S. (1984)[7], Hoover, W. G. (1985)[8] was used to control the temperature. For condensed phase diffusion analysis, simulations were performed using the NVT (canonical) ensemble.

The truncated octahedron periodic cell was generated from a cubic periodic cell with dimensional volume of 60 Å x 60 Å x 60 Å. A cubic cell was equilibrated for 1.0 ns, employing the NPT ensemble. Root mean square deviation (RMSD) analysis was used to determine the extent of the system's equilibration. A truncated octahedron cell was derived from the equilibrated cubic cell and then subjected to a further 1 ns of equilibration dynamics.

To rapidly equilibrate the polymer prior to incorporating it into the truncated octahedron periodic cell it was subjected to 1 ns equilibration in a TIP3P water sphere of 50 Å radius using stochastic boundary conditions. Upon inclusion into the truncated octahedron a further 9 ns of equilibration dynamics were run. The metals complexes and ammonium

cations were then randomly placed in the equilibrated systems, which was heated from 100K to 300K for 100ps followed by a final 1.0ns of equilibration.

The results of the diffusion trends of the different PGM chloro complex anions $RuCl_6^{2-}$, $RhCl_6^{3-}$, $PdCl_4^{2-}$, $OsCl_6^{2-}$, $IrCl_6^{2-}$ and $PtCl_6^{2-}$ in aqueous solution as well as in aqueous organic polymer solution are presented in this chapter. A comparison between the diffusion order in these two systems is done. It is also shown how distinct physical characteristics of the complexes control their diffusion order. The role of the water solvent in determining the diffusion order is highlighted. These factors are significant and lead to the diffusion order of the complexes in organic solution changing from that in aqueous solution.

For the diffusion, the calculations were performed in three different systems, all in the presence of ammonium cations to balance the charge of the system. The first system consists of water, ammonium cations and PGM chloro complexes. Both the second and third systems consist of water, ammonium cations, PGM complexes and organic polymers. Different polymers have been used in the latter system. The structures of these polymers, and a motivation for their specific composition, are given in (figure 1.2 and 1.5 ((a) and (b)), chapter 1, section 1.5, subsection 1.5.2).

In addition to this the free energy of solvation and free energy of binding results for the complexes $RuCl_6^{2-}$, $OsCl_6^{2-}$, $IrCl_6^{2-}$ and $PtCl_6^{2-}$ are also presented. Polymer one was used in the calculation. The trend between the diffusion coefficient of these complexes in aqueous solution and the free energy of hydration, as well as the relationship between diffusion and the free energy of binding to the polymer, is discussed.

4.1 Methods of Quantifying the Expected Trends in Diffusion

This section details the method used in quantifying the expected trends in diffusion rate of different PGMs chloro complex anions in water based on their size, charge density and solvation structure. Calculations of charge density and RDFs are given in the subsections below.

4.1.1 Analysis of Size and Charge Density

The selective separation and/or extraction of the PGMs involves the use of a polymer that should be able to selectively distinguish between the different metal anion complexes, based on physical property such as their different sizes, and chemical properties such as their

charges, interaction and solvation structure. The best way of differentiating these metals from each other during separation would be to understand how these properties influence one another. An important factor is the ability of the polymer to selectively bind to the chlorine ligand over the solvent. In this section an attempt is made to explain the pattern in diffusion rate is measured. This could be the cornerstone of a computational design method to develop better stationary phases.

The solvation of different PGM complexes has been studied with the calculation of their hydration shell in water,[9,10] but little has been said about what really contributes to their differing interaction with water and carbohydrates, which plays a major role in determining the retention order in an aqueous solution of an organic polymer. As part of our objectives, we have identified several factors that we believe should be essential in controlling the selective chlorine ligand interaction with the polymer. These factors, amongst others, include the size of the ion and the charge density, which depends both on the charge of an ion and the volume of the ion. The size of the complex in this case would be determined by calculating the distance from the metal center to the chlorine ligand. In the case of the hexachloro complexes, the metal complexes are spherical in shape and the distance from the metal center to the chlorine ligands gives the radius of the complex. For the square planar complex, the geometry is ellipsoidal and forms a disk-like shape; the radius could be determined by considering the four coordinated chlorine ligands. However, this makes it difficult to compare its size with that of the octahedral complexes due to the lack of axial chlorine ligands.

The trend in ionic radii is that ions with greater negative charge they tend to form large radius whereas ions which are less negatively charged their radius gets smaller. The highly negatively charged ions then they are likely to be more favourable to form greater water solvent association due to greater number of water molecules in the hydration shell. This what is going to be established later on this section. The $RhCl_6^{3-}$ complex is the largest, having a -3 charge, next is the class of hexachlorometallates, $RuCl_6^{2-}$, $OsCl_6^{2}$, $IrCl_6^{2-}$ and $PtCl_6^{2-}$ and finally the tetrachlorometallate complex, $PdCl_4^{2-}$, all of which have a charge of -2. It will be interesting to see how the octahedral complexes behave differently in solution to the square planar complex. Here is where we expect to see how the geometry of these complexes influences their behaviour in solution.

The volume, which is the determining measure of the size of the targeted metal complex species, is a function of the radius as show in equation 4.1 below. It is important to consider the charge of the anions as well, since this affects the interaction with its environment. More appropriately, we think of the charge smeared out on the surface of the

complex, and the charge density is therefore the defining factor. The volume of the octahedral complex can be estimated by the volume of a sphere:

$$V = \frac{4}{3}\pi r^3 \tag{4.1}$$

where V is the volume enclosed within the octahedral complex, and r is the radius of the octahedral metal complex. The charge density is given by the equation:

$$\rho = \frac{e^-}{V} \tag{4.2}$$

where e is the total charge of the octahedral anionic metal complex. Substituting equation [4.1] into [4.2] yields:

$$\rho = \frac{3 \times e^-}{4\pi \times r^3} \tag{4.3}$$

The charge density is directly proportional to the charge of the anion and indirectly proportional to its volume. In order to express the contribution of the volume, several calculations regarding their sizes and their hydration structures can be used.

The average bond distance and charge density for the different PGM hexachloro and tetrachloro coordinated complexes were calculated and the results are presented in table 4.1 below. Also given are the charge values for the chlorine ligands taken from the parameterised force fields for the different complexes, see table 4.2 below.

Table 4.1 The average M-Cl bond lengths (Å) of PGMs chloro complexes with their calculated charge density, ρ and bond length standard deviation, σ.

	$RhCl_6^{3-}$	$PdCl_4^{2-}$	$RuCl_6^{2-}$	$OsCl_6^{2-}$	$IrCl_6^{2-}$	$PtCl_6^{2-}$
r / Å	2.364	2.196	2.278	2.307	2.302	2.320
Σ	0.0399	N/A	0.0327	0.0382	0.0358	0.0301
ρ / x 10^{-3} eÅ^{-3}	54.2	45.1	40.4	38.9	39.9	38.2

e^- = elementary charge (1.602x 10^{-19} C)[20]

Table 4.2: This summarizes the parameterized force fields charges used for chlorine and PGMs. These charges were extracted from the force fields used in these simulations. The $\Delta(M^{+}\text{-}Cl^{-})$ is the calculated charge difference between the metal center and chlorine ligands.

	$RhCl_6^{3-}$	$PdCl_4^{2-}$	$RuCl_6^{2-}$	$OsCl_6^{2-}$	$IrCl_6^{2-}$	$PtCl_6^{2-}$
nCl^- (n= 4, 6)	-0.796	-0.582	-0.508	-0.522	-0.513	-0.528
$\Delta(M^{+}\text{-}Cl^{-})$	1.776	0.328	1.048	1.132	1.073	1.168

$RhCl_6^{3-}$ has the longest metal-chlorine bond and hence its calculated complex volume is the largest. Despite this, its charge density was calculated to be highest. This is due to its much greater charge of -3. The slightly larger bond length is thus insignificant in relation to the effect of the 50% higher charge, compared to the smaller -2 complexes. The overall trend in charge density obtained for these hexachloro complexes from highest to lowest is: $RhCl_6^{3-} > RuCl_6^{2-} > IrCl_6^{2-} > OsCl_6^{2-} > PtCl_6^{2-}$. It must also be noted that the difference in the charge density values calculated for these complexes is very small, see table 4.1 above, and this again shows why their chemical properties are similar and the difficulty to distinguish one from the other is a problem. The $RhCl_6^{3-}$ complex with its greater charge density is expected to form stronger solvent attraction, followed by $RuCl_6^{2-}$ and $IrCl_6^{2-}$, $OsCl_6^{2-}$ and finally $PtCl_6^{2-}$ being the least interacting. The order above is therefore the inverse of the expected trend in diffusion, based on charge density.

The charge density of the tetrachloro coordinated $PdCl_4^{2-}$ complex was not calculated, bearing in mind that its shape is an ellipsoid.

Another, albeit much simpler, indication of the magnitude of the complex-solvent interaction is the partial charges on the chlorine atoms. Comparison of these shows small differences within the series, and a different trend to that emerging from the charge density calculation. Intriguingly enough, the order of the chlorine charges of the metal complexes from the smallest to the highest match up with the order of the calculated charge density. The $RhCl_6^{3-}$ complex has the highest charge values on the chlorine ligands and subsequently the largest charge on the metal as well. Following that, the suggested diffusion order from slowest to quickest, assuming that this will follow the order of decreasing charge, is $PtCl_6^{2-} < OsCl_6^{2-} < IrCl_6^{2-} < RuCl_6^{2-}$. It is interesting to note that this trend is different from that emerging using charge density. The square planar complex was not included here since its charge density was not determined and direct comparison is not possible. The charge on the chlorine atoms are

however higher than on the octahedral dianions, so it is expected to diffuse slower within the approximation of using ligand atom charges for estimation.

4.1.2. Radial Distribution Function Calculations

As is well known from studying conductivity of simple monovalent aqueous ions, it is in fact the size of the solvated species that impacts mobility. In order to understand the hydration structure of the PGM chloro complex anions, the radial distribution functions (RDFs) were determined. The RDF provides an understanding of how many water molecules are likely to be found surrounding the PGM complex as well as a distribution of the distances at which these are likely to occur. The RDFs were calculated for the solute-solvent contacts, metal–O(water). This was done over 8.0 ns with PBC and the trajectory recentered around the complex prior to each frame being analysed. The TIP3P water model was used in a truncated octahedral periodic cell. Two thousands bins were chosen with the distance interval of 0.01 Å in order to provide a high resolution picture. The hydration shells were calculated only for those water molecules within a sphere of 20.0 Å around the complex. The graphs of g(r) against distance (Å) are given below in figure 4.1. The peaks correspond to the different solvent shells. The number of water molecules included in each hydration shell can be determined by integrating the area under the peak. Integration was performed from minimum to minimum bounding the peaks. Strong water attraction/association with the PGM complexes is indicated by high peaks in the g(r) plots. The hydration structure at longer distance becomes less as the interaction dies off.

A.

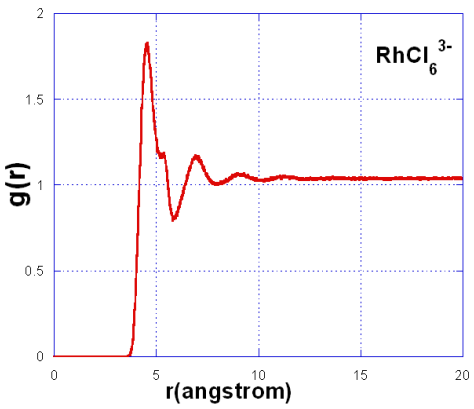

B.

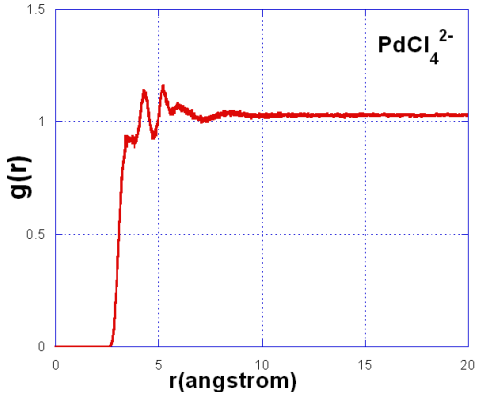

Continued on the next page

C.

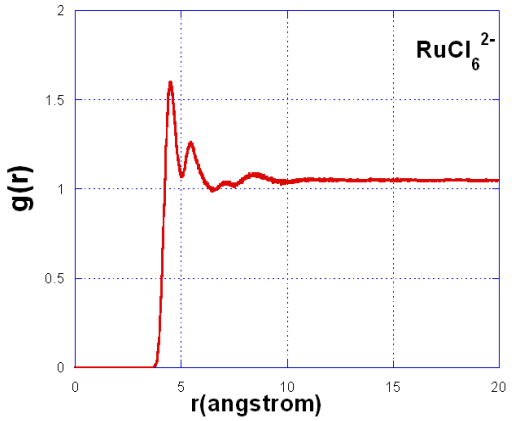

D.

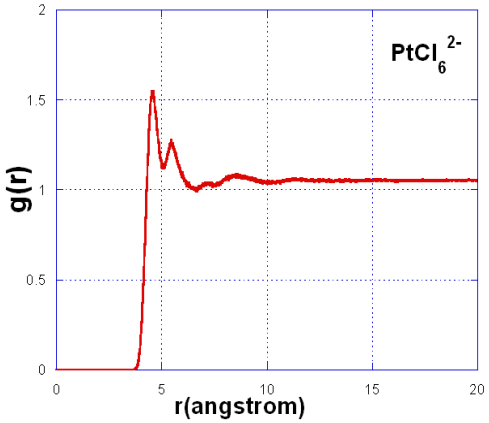

E.

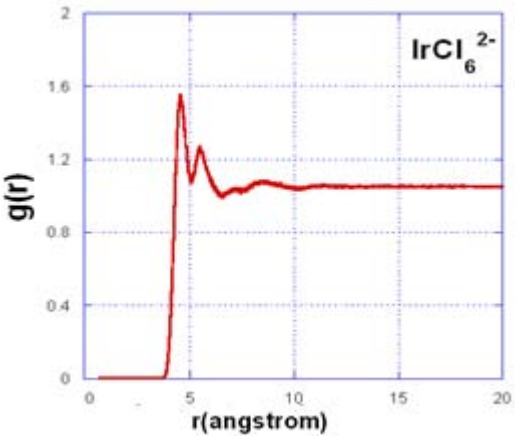

F.

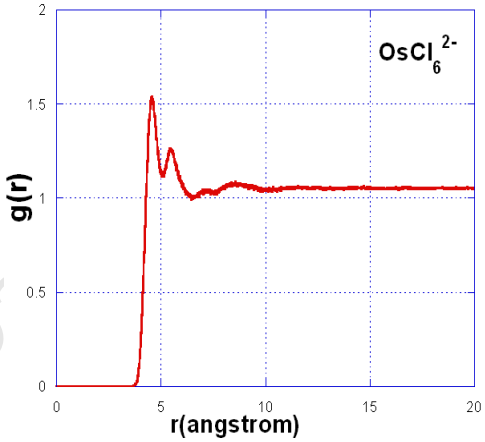

Figure 4.1: The figures A-F for complexes PdII, RhIII, RuIV, PtIV, IrIV, and OsIV, respectively, show the radial distribution functions for metal–O(water) configuration for the solvated PGM chloro-complexes.

Table 4.3: Summary of the M–O(water) features according to the RDFs. Continued on the next page.

	Rh(III)	Pd(II)	Os(IV)	Pt(IV)	Ir(IV)	Ru(IV)
r_0(Å)	3.51	2.58	3.57	3.60	3.61	3.58
1st g(r)	1.82	1.13	1.53	1.54	1.55	1.59
1str_{max}(Å)	4.58	4.30	4.58	4.56	4.55	4.48
1str_{min}(Å)	5.81	4.75	5.07	5.03	5.00	5.05
1stn_{M---O}	22.43	10.63	10.28	9.84	9.59	10.54
2nd g(r)	1.69	1.15	1.25	1.27	1.26	1.26
2ndr_{max}(Å)	6.93	5.18	5.49	5.47	5.49	5.47
2ndr_{min}(Å)	7.87	5.35	6.50	6.53	6.54	6.42

$2^{nd}n_{M---O}$	63.49	17.32	31.91	32.48	32.26	30.99

[a]r_0(Å) is the longest distance where the g(r) is zero. $1^{st}r_{max}$(Å) and $1^{st}r_{min}$(Å) is the maximum (turning point of the graph) and minimum (integration radii) distance of the first hydration shell and $2^{nd}r_{max}$(Å) and $2^{nd}r_{min}$(Å) are maximum and minimum (integration radii) distance of the second hydration shell. n_{M---O} is the metal---O(water) coordination number. Continued from previous page.

The RDF analysis shows that $RhCl_6^{3-}$ is clearly distinguishable from the other octahedral complex species and the square planar complex , see table 4.3 above. The four octahedral dianion complexes have very similar solvent structures and the g(r) values differ by less than 0.05. The first and second peak for the octahedral dianion species occur at ~4.5 Å and ~5.5Å. The coordination number,n_{M---O} for these octahedral complexes reveals approximately an equal number of water molecules interacting with the metal complex anions ranging between 9-10 in the first hydration shell and making them indistinguishable from one another, see table 4.3 above. This phenomenon has also been previously observed by Naidoo *et al.* and Matthews *et al.*[9,10] The square planar complex has the highest number of waters coordinated in the first hydration shell of all the dianionic species. The absence of the axial chlorine ligands might be the reason for this as water molecules above the plane get to move closer and get included in the hydration shell. However, the second hydration shells of the octahedral systems contain nearly double the number of waters than that of the square planar complex. This can be attributed to the fact that there are missing axial chlorine ligands in the square planar complex, therefore weaker or no interaction on top of the plane and a less structured manifold of water to be expressed at long distances, which results in less water molecules in the second hydration shell. Its solvated structure becomes extremely dispersed. The octahedral $RhCl_6^{3-}$ complex on the other hand, contains double the number of waters coordinated in its first and second hydration shells compared to the octahedral dianionic species. The observations from the trianion RDF mirrors the size and charge density calculated above. Again, the very small differences that separate the dianionic octahedral complexes in their RDFs highlight the difficulty in developing recognition mechanisms in aqueous solution. Nonetheless, using effective radii for the hydrated complexes based on the position of the first peak in the RDF results in the following expected trend for diffusion in the octahedral species: $RhCl_6^{3-} \sim OsCl_6^{2-} < PtCl_6^{2-} < IrCl_6^{2-} < RuCl_6^{2-}$. Other possible measures could be the 1^{st} minimum and the integration number under the first peak. These are presented and further

discussed when the diffusion results are rationalised as it becomes a useful measure of estimating the effective size of the complex in solution.

4.2. Interactions between the PGM Complex and Polymer in Aqueous Solution

4.2.1. Introduction

In solution, the main attractive interaction between the metal complex and polymer is expected to take place both between the partially positive hydrogen of the dextran hydroxyl groups and the methyl groups on the polymer with the triangular faces of the hexachloro octahedron, and via the edges of the tetrachloro complex.[11] The extent to which the polymer and the metal complex anions interact is of course also dependent on the orientation of the polymer with respect to the complex; this can shift between the aforementioned attractive H··· Cl interaction and a potentially repulsive O··· Cl interaction. In addition, the solvation structure of the metal complexes and the glucose-like monomers and ether linkages need to be disrupted to affect these interactions.

Figure 4.2 below shows snapshots from the MD trajectories at the points during which the interaction was highly stabilising. Figure 4.3 shows the histograms from equilibrium MD of the PGM complex-polymer (polymer one, the single strand) distances.

The interaction energy time series plots were constructed from 8.0 ns of simulation. The interaction energy was calculated between the different PGM complexes and all the polymer atoms, excluding the water solvent. The plots for the interaction energy time series for polymer one (consisting of one interconnected fragment) and polymer two (having two separate fragments), respectively are given in Appendix C, figure 4.4 and 4.5. Across the time series the distance between the polymer and PGM complex was also determined. This distance was taken as the shortest distance, taken across all possible atoms of the polymer and the metal atom of the complex. The variation of the interaction energy with the distance is shown in the same axis on figure 4.4 and 4.5 below.

4.2.2 Interaction Time Series from Molecular Dynamics

The interaction energies was calculated by computing the total energy which includes which include hydrogen bond, van der Waals and electrostatic energy. The interaction time series plots, (see appendix C, figure 4.4 and 4.5 below), and interaction-distance plots on the same axis, figure 4.4 and 4.5 are marked by infrequent intervals of strong interaction represented by peaks occurring on the negative axis. Table 4.4 and 4.5 below gives similar data for the distances. Averages, minimum and maximum values, as well as standard deviations were calculated.

Table 4.4: Summary of the calculated average interaction energy, $E_{int}^{ave}(kcal/mol)$, standard deviation, E_{int}^{σ}, maximum interaction energy, $E_{int}^{max}(kcal/mol)$, and minimum interaction energy, $E_{int}^{min}(kcal/mol)$ for $RhCl_6^{3-}$, $PdCl_4^{2-}$, $PtCl_6^{2-}$, $OsCl_6^{2-}$, $IrCl_6^{2-}$ and $RuCl_6^{2-}$ complexes against polymer one.

Complex	$PdCl_4^{2-}$	$PtCl_6^{2-}$	$IrCl_6^{2-}$	$OsCl_6^{2-}$	$RuCl_6^{2-}$	$RhCl_6^{3-}$
E_{int}^{ave}	-0.37	-1.55	-1.22	-1.15	-1.75	-0.27
E_{int}^{σ}	1.28	2.80	2.51	2.78	3.26	0.77
E_{int}^{min}	2.98	0.89	1.58	1.73	0.81	2.56
E_{int}^{max}	-15.03	-20.50	-21.00	-21.53	-20.96	-10.96

Table 4.5: Summary of the calculated average distance, $r^{ave}(Å)$, standard deviation, r^{σ} maximum distance, r^{max}, and minimum distance, r^{min} for $RhCl_6^{3-}$, $PdCl_4^{2-}$, $PtCl_6^{2-}$, $OsCl_6^{2-}$, $IrCl_6^{2-}$ and $RuCl_6^{2-}$ complexes against polymer one.

Complex	$PdCl_4^{2-}$	$PtCl_6^{2-}$	$IrCl_6^{2-}$	$OsCl_6^{2-}$	$RuCl_6^{2-}$	$RhCl_6^{3-}$
r^{ave}	13.75	12.25	12.69	11.37	12.69	13.44
r^{σ}	5.93	6.34	6.61	5.01	5.94	6.07
r^{max}	34.74	34.56	35.90	29.57	29.94	31.67
r^{min}	2.50	3.22	2.98	3.05	2.99	3.00

The average interaction energy is quite low, compared to the maximum values, and this is also evident from the average separation distance, which is large and mostly beyond the non-bonded cutoff of 14 Å, see table 4.4 and 4.5. Although the complexes interact strongly at certain periods along the simulation, the equilibrium does seem to lie more towards a hydrated ion than one interacting strongly with the polymer. Standard deviations for both are also very large, indicating that the systems undergo a range of interactions across all

distances. The trend in maximum interaction energies largely mirror that of the average interaction; the tetravalent octahedral complexes fall in a narrow band of ~20 kcal/mol, the divalent Pd(II) complex is lower by ~15 kcal/mol, and the trivalent Rh(III) complex is, surprisingly, the lowest, at ~10 kcal/mol. From the charge density and partial charges of the chlorine atoms the strongest electrostatic interaction is expected for the Rh(III) complex. However, the solvent shell is also largest, consequently having a large effective radius, and water molecules located in the solvent shell should feel the strongest electrostatic attraction, requiring more energy to remove. The lesser interaction is thus not so much due to intrinsic properties of the complex, but due to the larger structured solvent shell that requires more energy to disrupt and a large separation consequently being maintained throughout the simulation. This latter observation is returned to in more detail below when statistics of the separation distances are looked at. Out of all the complexes studied, the maximum repulsive interaction occurs for the planar $PdCl_4^{2-}$ complex; possibly a consequence of its unsymmetrical ellipsoid shape and smaller size. Note that this species does have the shortest M-Cl bonds, table 4.1, smallest metal-chlorine charge difference, table 4.2, and from the RDFs the first solvation shell maximum occurs at the closest distance of all the complexes studied. The strong repulsive interaction energy for $RhCl_6^{3-}$, which is only slightly less repulsive than the $PdCl_4^{2-}$ complex, is again very likely due to its higher overall charge. This leads to strong electrostatic interaction, and in principle should therefore result in stronger repulsion as well. Whereas the trend in average and maximum/minimum separation distances does not exactly reflect that of the interactions, the two weakest interacting systems are however, on average the furthest from the polymer. The square planar complex has the closest approaching distance; due to the absence of axial ligands, the Pd(II) complex is able to move close if interacting groups are in line with these vacant axial regions. The octahedral complexes (even the trianion) all approach the polymer ~3 Å at their closest. It is significant that at this distance there can be no hydration shell waters between the complex and the polymer. There is thus evidence of a favourable equilibrium allowing hydration waters to be exchanged for chemically similar hydroxyl groups or other interacting functional groups sharing less similarity to the solvent.

A.

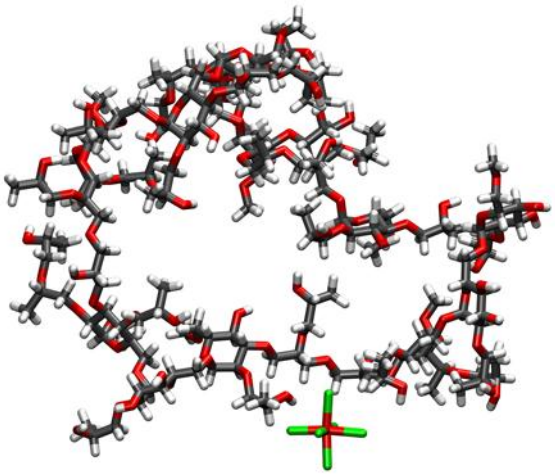

B.

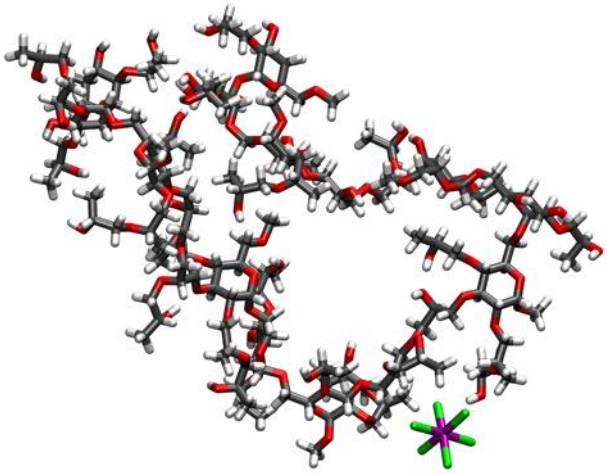

C.

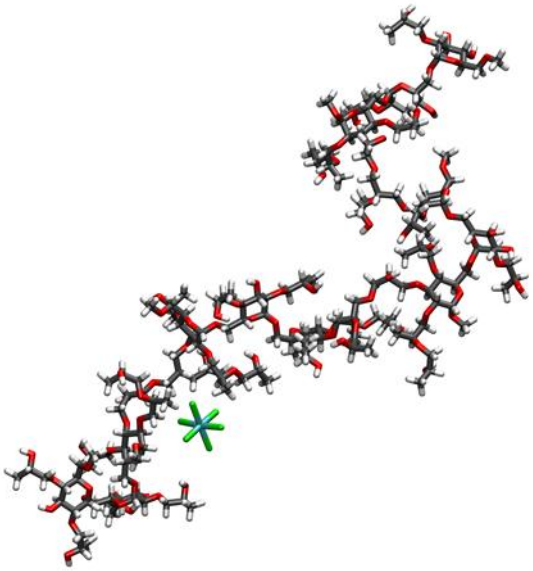

D.

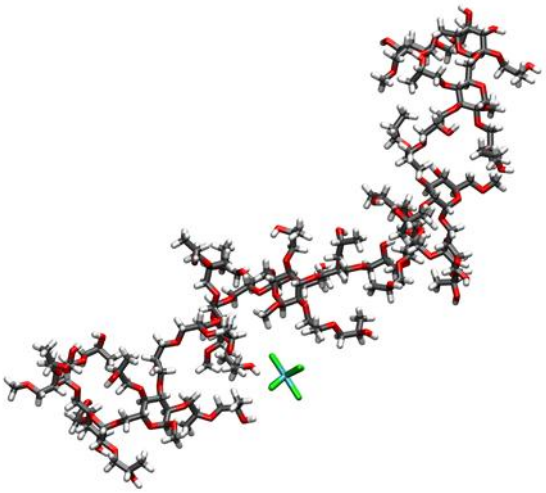

Continued on the next page

E. F.

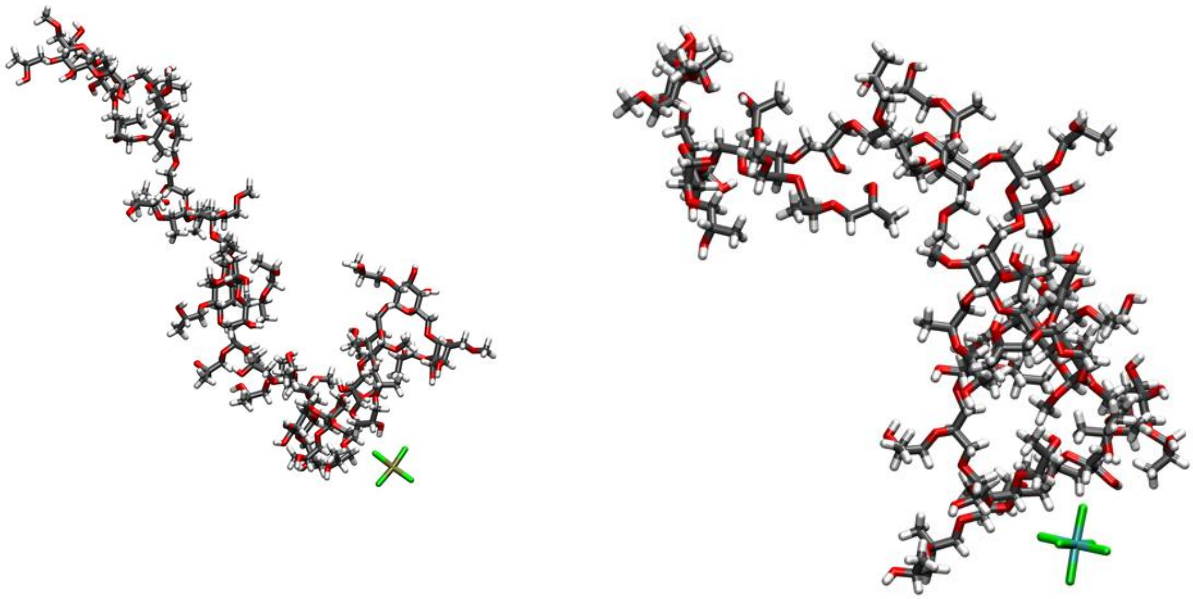

Figure 4.2: Selected trajectory snapshots, excluding water for clarity, of high attractive interaction occurring between the PGM complexes and the single polymer unit; (A) $OsCl_6^{2-}$ (at 6637.75 ps), (B) $PtCl_6^{2-}$ (at 4670.00 ps), (C) $IrCl_6^{2-}$ (at 3545.05 ps), (D) $RuCl_6^{2-}$ (at 8575.5 ps), (E) $PdCl_4^{2-}$ (at 4667.10 ps) and (F) $RhCl_6^{3-}$ (at 2185.25 ps). Continued from previous page.

Several features, useful in constructing an average picture of the dynamics of the complex-polymer interaction, should be noted, figure 4.2. The complex never seems to become enveloped by the polymer, and interaction occurs at the surface of the polymer with a select few residues. These residues almost always exclude the sugar ring and only occasionally include the glycosidic linkage, but almost always include hydroxyls on the propyl and ether chains. Where strong interaction occurs the partially positive hydroxyl protons face the partially negative PGM complex chlorine atoms. Surprisingly, the non-polar hydrogens on these chains also seem to play a non-negligible role in stabilising the interaction. This latter observation is clearly seen in the $IrCl_6^{2-}$ and $RhCl_6^{3-}$ snapshots. Here the metal complex is in a pocket surrounded by methylene hydrogens. These snapshots, although excluding water molecules for clarity, also illustrate that the metal complexes are able to exchange water molecules from their solvation shell in favour of interaction with the polymer atoms.

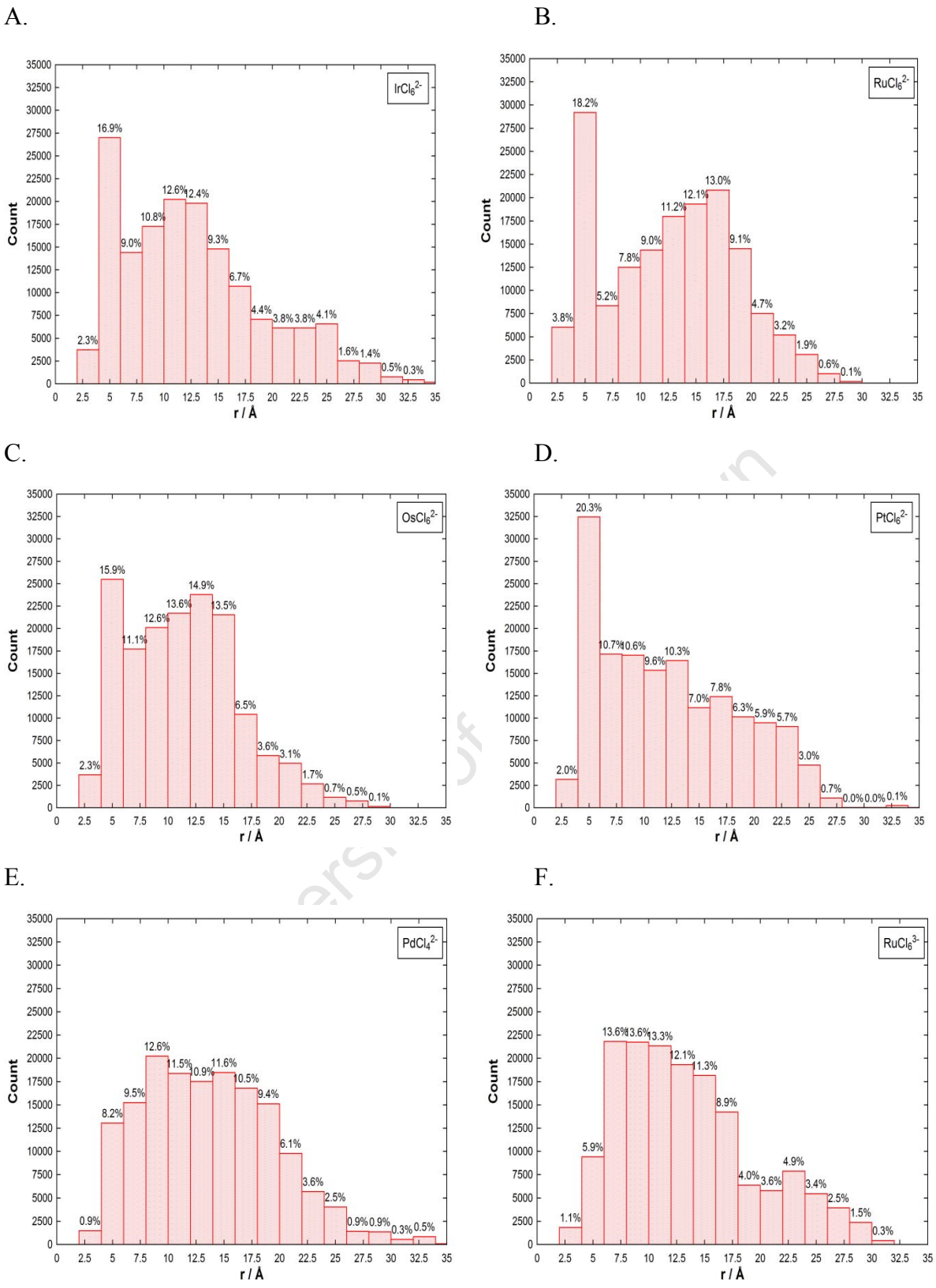

Figure 4.3: Histograms A-F for complexes $IrCl_6^{2-}$, $RuCl_6^{2-}$, $OsCl_6^{2-}$, $PtCl_6^{2-}$, $PdCl_4^{2-}$ and $RhCl_6^{3-}$, respectively, is showing the PGMs complex-polymer distance distribution. The percentage each bar contributes to the total count is also shown.

To better characterise the behaviour in solution, statistics of the separation distance during the trajectories can also be looked at. The histograms from equilibrium MD of the PGM complex-polymer (polymer one, the single strand) distances have also been calculated. The four hexachloro coordinated complex dianions; $PtCl_6^{2-}$, $OsCl_6^{2-}$, $IrCl_6^{2-}$ and $RuCl_6^{2-}$ show similar patterns of distribution. The octahedral dianion complexes stay within 5 Å of the polymer between 2 and 4% of the simulation time. This corresponds to direct contact between the complex and the polymer. The next band occurs just beyond 5 Å, and at this distance the complexes stay between 15% and 20% of the simulated time. It is also the dominant coordination distance occurring for these complexes. Beyond these regions, ~60% of the simulation time is spent within the non-bonded cutoff. At this region, all the complexes have roughly the same distribution band with Rh(III) the highest percentage distribution.

The square planar Pd(II) complex shows a distribution lacking a preferred close separation distance. Therefore it exhibit unfavourable exchange of hydration waters in favour of polymer coordination.

Similarly, the Rh(III) octahedral trianion largely maintains its completely solvated form, its diffusive motion concentrated between 7 and 20 Å of the polymer. This is consistent with the tightly bound solvation shell of the $RhCl_6^{3-}$ complex, as is also seen from the radial distribution functions above, see figure 4.1, table 4.3. By monitoring the trajectory it was confirmed that highly attractive interaction peaks correspond to the polymer and the metal complex moving within close proximity. In contrast, the smallest peaks at the negative region and the zero or positive interaction do not necessarily correspond to intervals in which the polymer and the metal complex are far apart. Other than rotation of the complexes in solution the hydroxyl groups on the polymer also rotate, leading to regions where the interaction is less stabilising due to the dominance of charge repulsion. The spatial orientation of the partially negative hydroxyl and glycosidic oxygen are not always ideally arranged to limit repulsion with the negatively charged metal complex.

Looking at the distance-interaction time series plots figure 4.4 and 4.5 below (also refer to appendix C), it was observed that the hexachlorometallates of charge -2 produce broader peaks, especially for polymer one, however, at the same time it has been observed that the hexachlorometallates with a charge of -3 produces sharp peaks. We also found that the tetrachlorometallate, $PdCl_4^{2-}$ and the hexachlorometallate, $RhCl_6^{3-}$ produces a similar pattern of behaviour. This will become important again within the context of discussing the

diffusion results, where these two systems showed similar behaviour in their mass transport ability.

Comparison of the interaction between the metal complexes and the polymer in the systems having either polymer one or polymer two shows that the general interaction profiles are similar. With polymer two the interaction energy time series plots show slightly broader peaks compared to those produced by polymer one. Overall though, no significant differences were found that would lead to different conclusions being reached.

A. OsIV

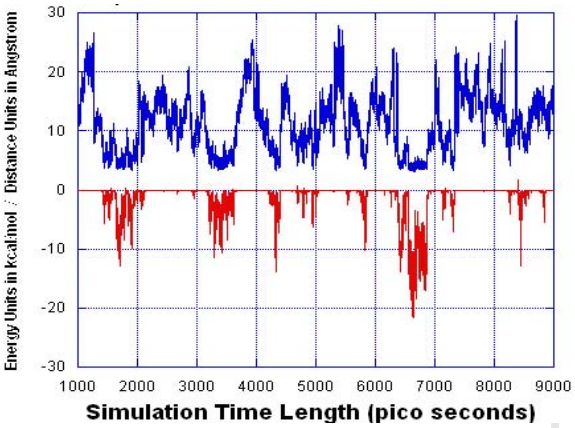

B. PtIV

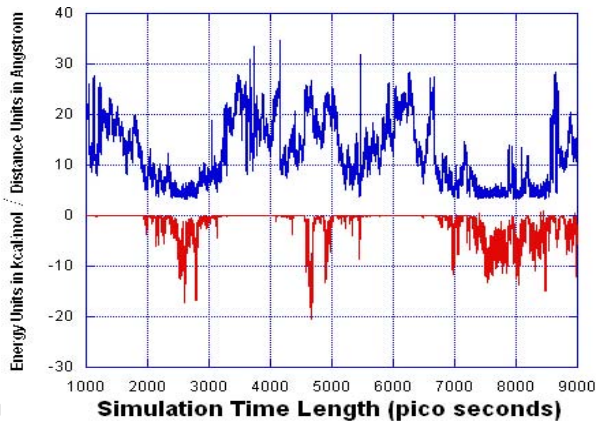

C. IrIV

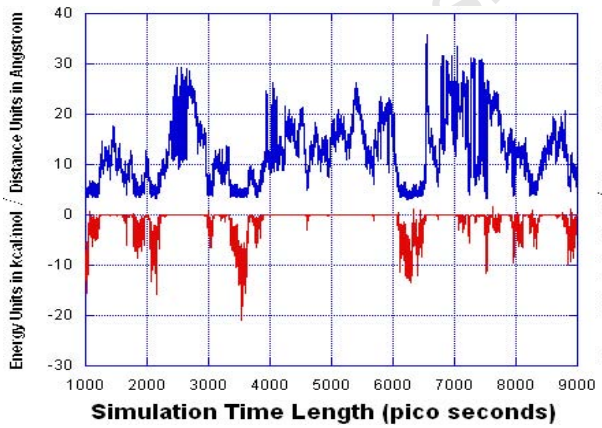

D. RuIV

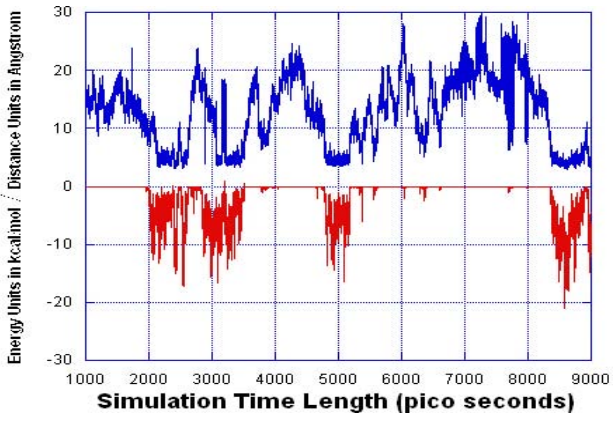

Figure 4.4. The interaction energy and distance time series plots between the PGM with the polymer one shown on figure A-F for complexes OsIV, PtIV, IrIV, RuIV, PdII and RhIII, respectively. The plots on top give the time series of the distance between different metal complex anions to the polymer one. The distance was calculated between the metal center of the metal complex anion to the nearest atom of the polymer one. The plots below are the interaction energy of the metal complex anions with the polymer. Continued on the next page.

E. PdII F. RhIII

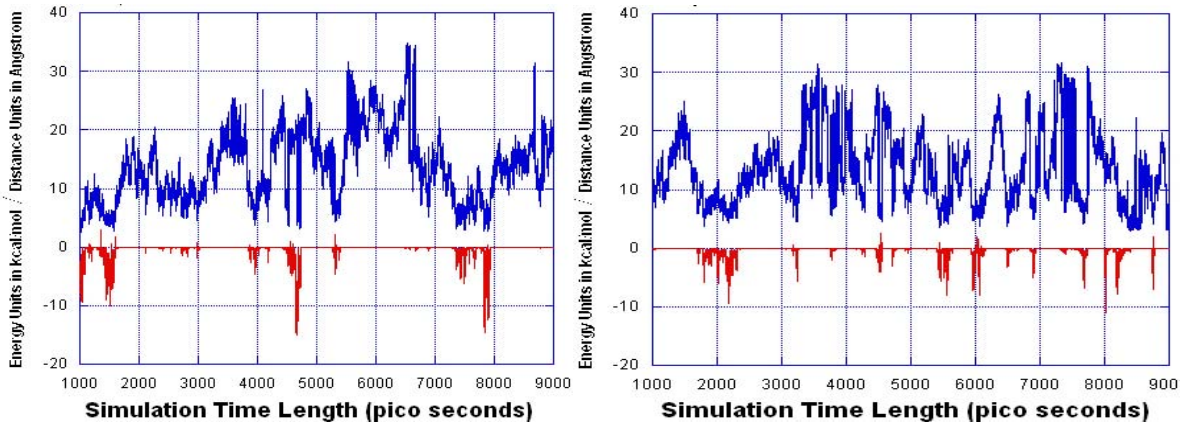

Figure 4.4. The interaction energy and distance time series plots between the PGM chloro complex anions and the polymer one are shown on figure A-F for OsIV, PtIV, IrIV, RuIV, PdII and RhIII containing complexes, respectively. The plots on top give the time series of the distance between different metal complex anions to the polymer one. The distance was calculated between the metal center of the metal complex anion to the nearest atom of the polymer one. The plots below are the interaction energy of the metal complex anions with the polymer.

A. OsIV B. IrIV

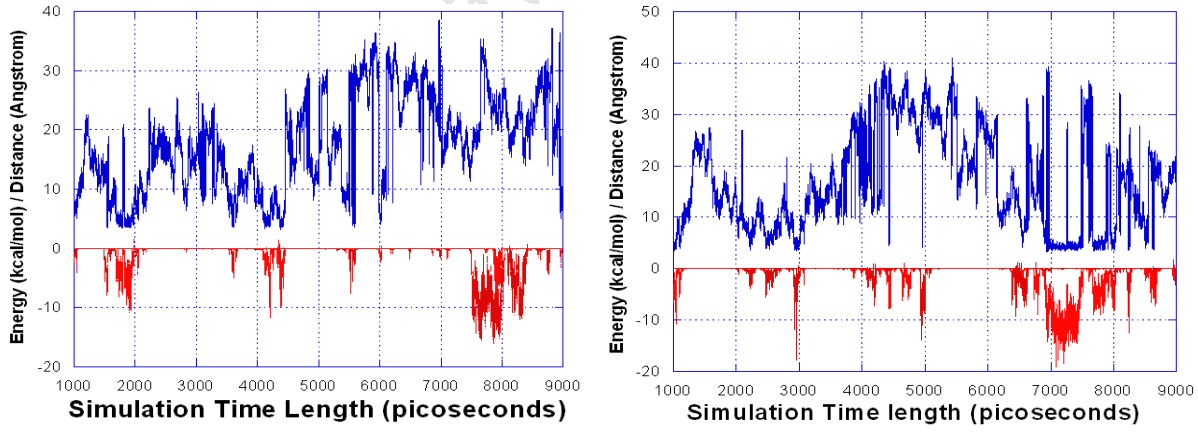

Figure 4.5. The interaction energy and distance time series plots between the PGM chloro complex anions and the polymer two are shown on figure A-F for OsIV, IrIV, PtIV, RuIV, PdII and RhIII containing complexes, respectively. The plots on top give the time series of the distance between different metal complex anions to the polymer two. The distance was calculated between the metal center of the metal complex anion to the nearest atom of the polymer one. The plots below are the interaction energy of the metal complex anions with the polymer. Continued on the next page.

C. PtIV

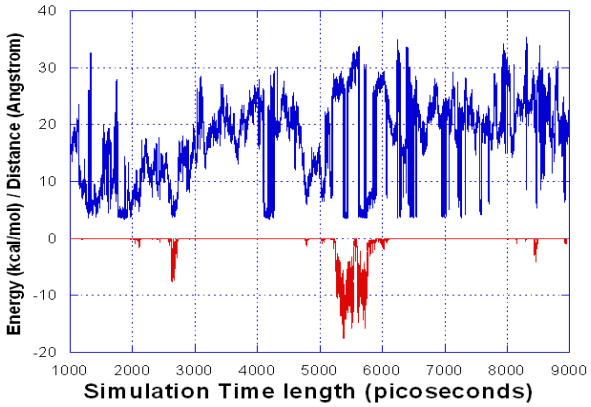

D. RuIV

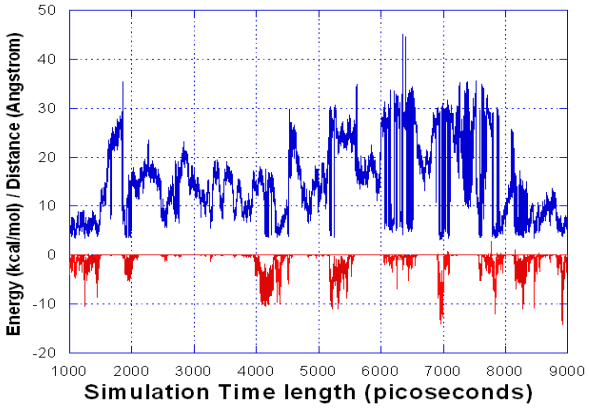

E. PdII

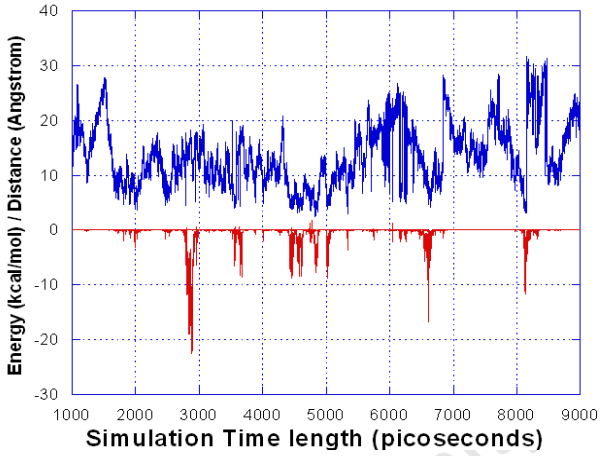

F. RhIII

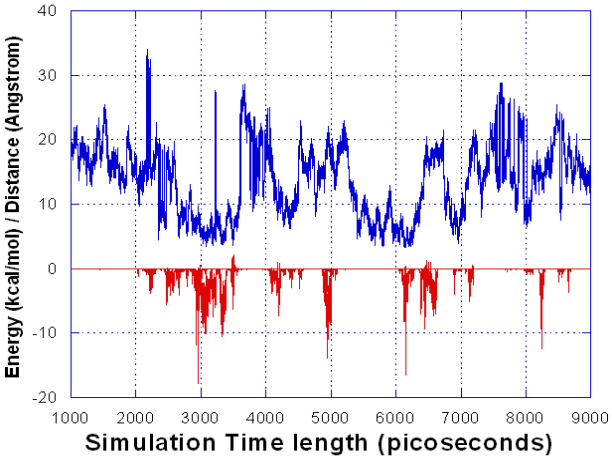

Figure 4.5. The interaction energy and distance time series plots between the PGM chloro complex anions and the polymer two are shown on figure A-F for OsIV, IrIV, PtIV, RuIV, PdII and RhIII containing complexes, respectively. The plots on top give the time series of the distance between different metal complex anions to the polymer two. The distance was calculated between the metal center of the metal complex anion to the nearest atom of the polymer one. The plots below are the interaction energy of the metal complex anions with the polymer. Continued from previous page.

4.3. Calculation of Diffusion Coefficients

The motion of the PGM chloro complex anions in aqueous solution is controlled by both the solvent interaction and the interaction with the polymer. It was shown in section 4.2 above how the different PGM complexes interact with the polymer. In section 4.1 above, the solvation structures for these complexes were shown to differ based on their geometry and overall charge. Complexes with a similar geometry and similar charge however, have very

similar solvation structures and effective sizes in solution. In this section the diffusion rate of the complexes in aqueous solution and in the presence of the organic polymer(s) are determined. Furthermore, a comparison is made between the MD computed diffusion coefficients and experimentally measured retention order. Reproduction of the computed values with the experimental measurements further consolidates the reliability of this method to study the behaviour of these systems in solution. The diffusion coefficient values of PGMs in water are given in table 4.6 below and the trend is shown in figure 4.6. Table 4.7 and 4.8 below shows the diffusion of PGMs in water in the presence of different polymers and their trend is shows in figure 4.7 and 4.8, respectively. Finally, the comparison of the MD computed diffusion rate trend with the experimental measurements is given in table 4.10. Plots of the mean-square-displacement versus time, central to the calculation from simulation, are given in appendix A, figure 4.1-4.3. The trajectories were extracted from 8.0 ns of simulation and were unfolded when calculating the diffusion coefficient to make the trajectory continuous by removing PBC imaging.

The typical MSD plots should be linear with an increasing slope. The plots obtained here are all linear over a short time interval. (see appendix A, figure 4.1-4.3). A total of 8.0 ns of simulation data was used to correlate and the linear fitting to estimate the diffusion coefficient was done in an interval of 1.0 ns. It is well-established that the data beyond a 1 ns time frame are not usable due to a statistical uncertainty from a lack of time frames correlating to these points. Secondly, the diffusion is an average property and is computed by averaging over the motion of all the molecules in a system over a desired time length. In this case, diffusion is computed from the distance travelled by a single ion, which severely hampers the quality of data from short simulation times. The second problem can only be remedied by using large simulation times, the approach used here, or increasing the concentration of species whose diffusion is of interest. A popular method of calculating errors in diffusion calculations is to divide the data into several blocks (or run several simulations concurrently) and then to calculate the diffusion coefficients over each of these blocks. Averaging of the calculated values is then done, and errors worked out in the usual way using deviations from the average. However, this approach could not be used due to the length of simulation required for each block in order to gain statistically meaningful, linear diffusive motion.

4.3.1. Diffusion Coefficients of PGM complexes $RuCl_6^{2-}$, $RhCl_6^{3-}$, $PdCl_4^{2-}$, $OsCl_6^{2-}$, $IrCl_6^{2-}$ and $PtCl_6^{2-}$ in water

Table 4.6. Diffusion coefficient values for $RuCl_6^{2-}$, $RhCl_6^{3-}$, $PdCl_4^{2-}$, $OsCl_6^{2-}$, $IrCl_6^{2-}$ and $PtCl_6^{2-}$complexes in water. The values were calculated from linear fits to 1.0 ns of data calculated over a total simulation time of 8 ns.

PGMs	MSD against Δt: Diffusion Coefficient, D , x 10^{-5} cm^2 s^{-1}
$IrCl_6^{2-}$	2.039
$PtCl_6^{2-}$	1.743
$RuCl_6^{2-}$	1.489
$PdCl_4^{2-}$	1.480
$OsCl_6^{2-}$	1.038
$RhCl_6^{3-}$	0.637

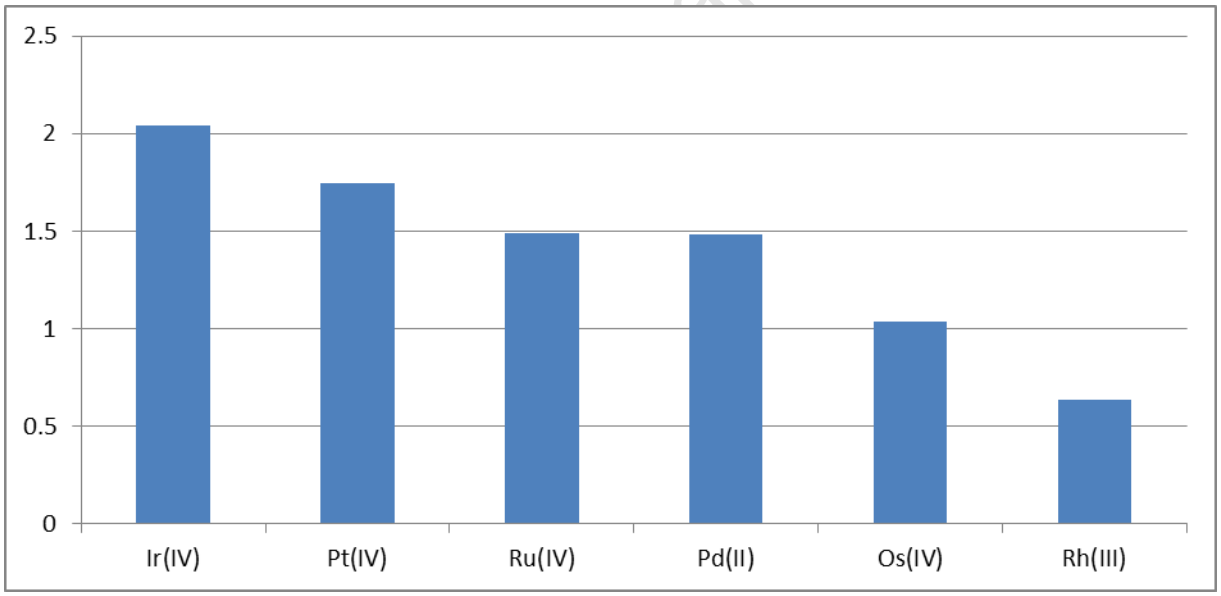

Figure 4.6. The Diffusion coefficients for $RuCl_6^{2-}$, $RhCl_6^{3-}$, $PdCl_4^{2-}$, $OsCl_6^{2-}$, $IrCl_6^{2-}$ and $PtCl_6^{2-}$ complexes in water, in 10^{-5} cm^2 s^{-1}

$RhCl_6^{3-}$ is found to have the slowest diffusion rate of all the complexes in water, figure 4.6 above. The slow diffusion rate of this metal ion complex in aqueous solution is not surprising given its stronger interaction with water solvent due to its higher negative charge of -3 and subsequent larger effective size. This also corresponds to its calculated largest hydration shell, see table 4.3 above. This is the same result as shown by *Naidoo et al.* And Matthews *et al.* on

the hydration shell of PGMs.[9,10] All the method followed from charge density, consideration of charge of chlorine ligands, RDFs and interaction energies predict $RhCl_6^{3-}$ to be the slowest diffusing. With all due course this has been found to be the case. However, charge densities predict $RuCl_6^{2-}$ to be the next slowest, and $PtCl_6^{2-}$ the fastest and this trend is not reproduced here. Actual, other than the on point predictions of $RhCl_6^{3-}$ by charge density and metal-chlorine charge difference with the diffusion rate, the other PGMs chloro complex anions diffusion order do not match with the expected order of the above mentioned properties.

Switching to an effective size argument, there are several different measures of size, all determined from the RDF data. Using the first maximum in the RDFs makes $PdCl_4^{2-}$ the smallest, a result again not fitting these diffusion coefficients. Furthermore, $RuCl_6^{2-}$ is predicted to be next smallest; again this does not fit the diffusion data. More encouraging is using the first minimum. Although $PdCl_6^{2-}$ is predicted to be smallest and hence should diffuse quickest, the predicted hydrated ion size of the remaining ions fit the trend very well. Excluding Pd(II) the size in decreasing order is $RhCl_6^{3-} > OsCl_6^{2-} > RuCl_6^{2-} > PtCl_6^{2-} > IrCl_6^{2-}$. It should be noted that the variation in size of the tetravalent octahedral complexes is extremely narrow, and does not quite suggest the order of differences in diffusion as seen here. Turning to integration numbers provides even more satisfying insight, and sheds light on the apparent anomaly of $PdCl_4^{2-}$. Integration over the first peak (from zero the first minimum), gives a total number of waters (10.63) that is more than any of the dianionic octahedral complexes, and in fact very close to that of $RuCl_6^{2-}$ (10.54). Of course, the diffusion coefficient of this species is also closer to $RuCl_6^{2-}$. Bearing in mind that this species is in fact not spherically symmetrical, it is perhaps not surprising that the integration number is more meaningful than the location of the anisotropically determined peak. Thus using the number of water molecules in the solvent shell, rather than the size of the shell, suggests the complex should diffuse slower than expected, fitting the trends seen here.

4.3.2. Diffusion Coefficients of PGM Complexes $RuCl_6^{2-}$, $RhCl_6^{3-}$, $PdCl_4^{2-}$, $OsCl_6^{2-}$, $IrCl_6^{2-}$ and $PtCl_6^{2-}$ in Aqueous Polymer Solution

In this section diffusion results of the complexes in the presence of the polymer(s) are compared with that in water. Before discussing the results in detail, the two types of polymers used are compared to estimate the effect of polymer size on the results. For convenience a table is also provided that summaries the change from pure water to polymer solution in terms

of percentages. It is very encouraging that these results mostly exhibit the same ordering in the trend, except for the position of the $RuCl_6^{2-}$ complex. Within the same polymer system the diffusion coefficients are however, very close in value and that alone accentuates the difficult in predicting and understanding the behaviour of these related complexes. As was the case with the discussion of the interaction energy and in the interest of consistency, only the results with polymer one will be discussed in detail.

Table 4.7: Diffusion coefficients for the PGM complexes in presence of the single polymer strand (polymer one). The Diffusion coefficient values were fit to a 1 ns region from a total simulation time of 8 ns simulation.

PGMs	MSD against Δt: Diffusion Coefficient, D , x 10^{-5} cm^2 s^{-1}
$RhCl_6^{3-}$	1.445
$PdCl_4^{2-}$	1.389
$RuCl_6^{2-}$	1.325
$IrCl_6^{2-}$	1.289
$PtCl_6^{2-}$	0.974
$OsCl_6^{2-}$	0.759

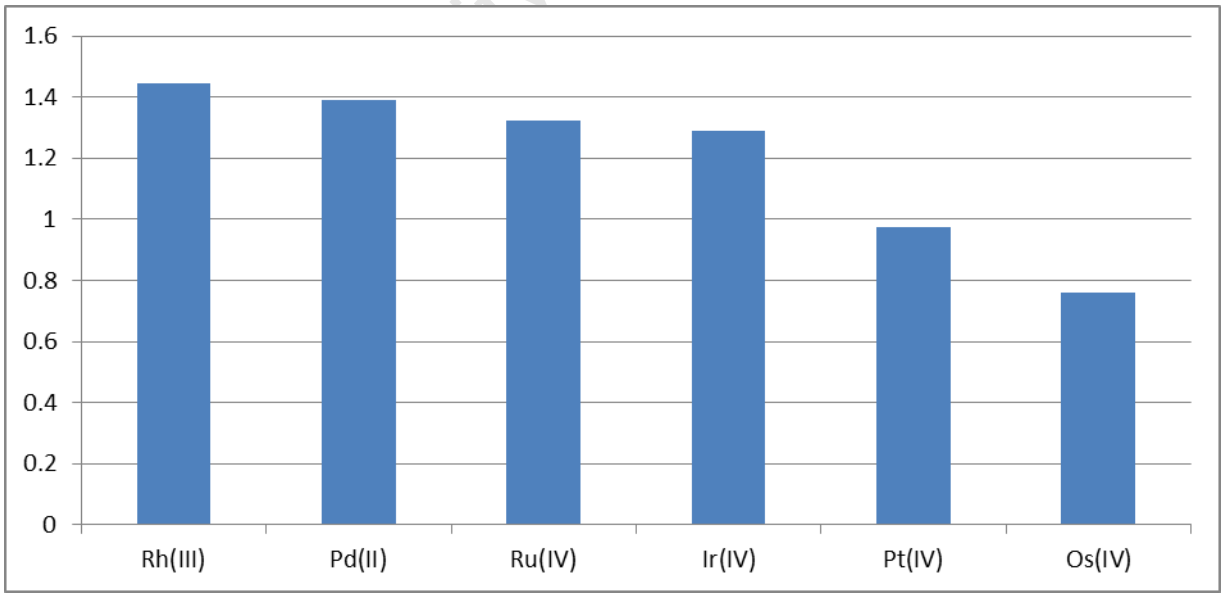

Figure 4.7: Diffusion plots for complexes $RhCl_6^{3-}$, $PdCl_4^{2-}$, $RuCl_6^{2-}$, $IrCl_6^{2-}$, $PtCl_6^{2-}$and $OsCl_6^{2-}$ in a system with polymer one in water.

Table 4.8: Diffusion coefficients for the PGM complexes in presence of the two polymer strands (polymer two). The Diffusion coefficient values were fit to a 1 ns region from a total simulation time of 8 ns simulation.

PGMs	MSD against Δt: Diffusion Coefficient, D, $x10^{-5}$ $cm^2.s^{-1}$
$RhCl_6^{3-}$	1.355
$PdCl_4^{2-}$	1.129
$IrCl_6^{2-}$	1.070
$PtCl_6^{2-}$	1.062
$RuCl_6^{2-}$	1.027
$OsCl_6^{2-}$	0.856

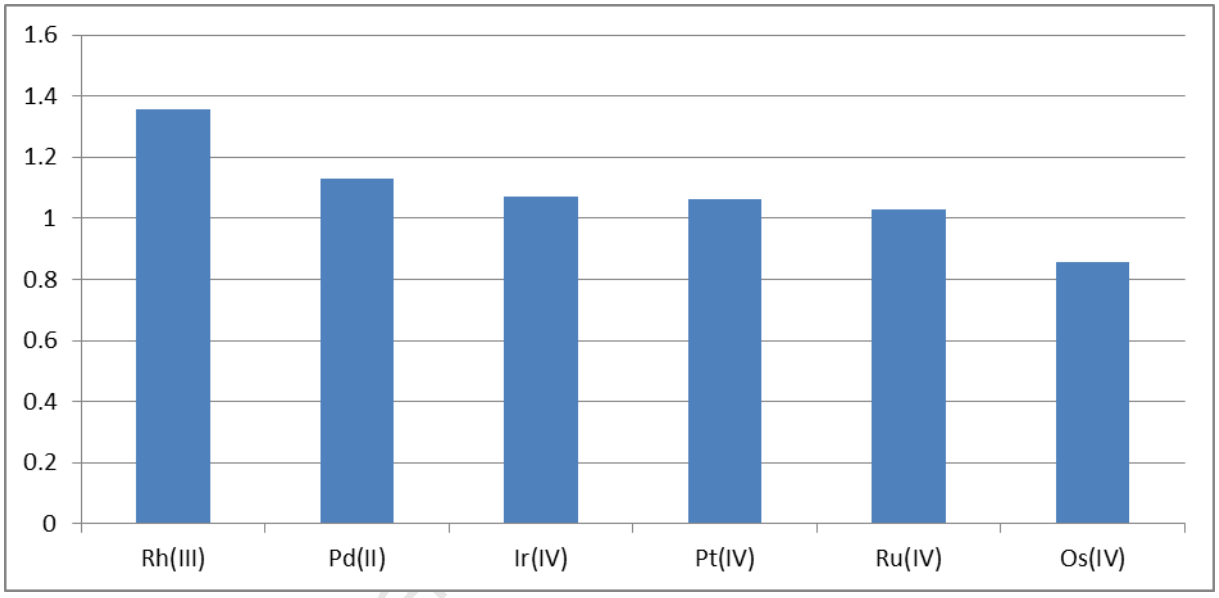

Figure 4.8: Diffusion plots for complexes $RhCl_6^{3-}$, $PdCl_4^{2-}$, $IrCl_6^{2-}$, $PtCl_6^{2-}$, $RuCl_6^{2-}$ and $OsCl_6^{2-}$ in a system with polymer two in water.

Table 4.9.Summary of the percentage drop and rise in diffusion rate of$RuCl_6^{2-}$, $RhCl_6^{3-}$, $PdCl_4^{2-}$, $OsCl_6^{2}$, $IrCl_6^{2-}$ and $PtCl_6^{2-}$ complexes moving from a system with water only to an aqueous solution with polymers. The downward arrow ↓represent drop in diffusion values in the presence of polymers and the upward arrow ↑represent rise in diffusion values in the presence of polymers. Continued on the next page.

	Polymer One	Polymer Two	Diffusion Coefficient, D, in water	Diffusion Coefficient, D, polymer one	Diffusion Coefficient, D, polymer two
$IrCl_6^{2-}$	↓36.77%	↓47.52%	2.039	1.289	1.070
$PtCl_6^{2-}$	↓44.08%	↓39.07%	1.743	0.975	1.062
$RuCl_6^{2-}$	↓11.00%	↓31.01%	1.489	1.325	1.027
$PdCl_4^{2-}$	↓6.14%	↓23.73%	1.480	1.389	1.129
$OsCl_6^{2-}$	↓26.90%	↓17.55%	1.038	0.759	0.856
$RhCl_6^{3-}$	↑55.96%	↑53.03%	0.637	1.445	1.355

Except for the $RhCl_6^{3-}$ complex, all species show a drop in diffusion rate in the presence of the polymer, the order being $PtCl_6^{2-}$ > $IrCl_6^{2-}$ > $OsCl_6^{2-}$ > $RuCl_6^{2-}$ > $PdCl_4^{2-}$. On the other hand, the absolute trend from fastest to slowest is $RhCl_6^{3-}$ > $PdCl_4^{2-}$ > $RuCl_6^{2-}$ > $IrCl_6^{2-}$ > $PtCl_6^{2-}$ > $OsCl_6^{2-}$. In interpreting these values average interaction energy and distances are used as reported in tables 4.4 and 4.5. If the assumption is made that the factor influencing this drop the most is the interaction, the prediction should be, from largest change to least, $RuCl_6^{2-}$ > $PtCl_6^{2-}$ > $IrCl_6^{2-}$ > $OsCl_6^{2-}$ > $PdCl_4^{2-}$ > $RhCl_6^{3-}$. Indeed the $PtCl_6^{2-}$ and $IrCl_6^{2-}$ complexes show large drops, followed by $OsCl_6^{2-}$ and $PdCl_4^{2-}$. However, the $RuCl_6^{2-}$ complex does not fit this trend, having shown the highest interaction and but one of the least changes in diffusion coefficient. Looking solely at the minimum interaction as metric, the trend expected should be $OsCl_6^{2-}$ > $IrCl_6^{2-}$ > $RuCl_6^{2-}$ > $PtCl_6^{2-}$ > $PdCl_4^{2-}$ > $RhCl_6^{3-}$. This shows virtually no correlation and is clearly not an appropriate metric.

Distances from polymer to complex can also be looked at, assuming that the complex is slowed down when nearing the polymer – an argument of course based on interaction energy as well, with a similar trend expected. Nonetheless, using averages the expected trend is slightly different from that gained by looking at interaction, $OsCl_6^{2-}$ > $PtCl_6^{2-}$ > $IrCl_6^{2-}$ ~ $RuCl_6^{2-}$ > $RhCl_6^{3-}$ > $PdCl_4^{2-}$. This shows some similarity but remains largely unsatisfactory in giving a consistent interpretation.

Trends aside, the next most interesting result is the diffusion behaviour of the Rh(III) complex. The reason for this is obviously being the fact that it has greater number of water molecules on its hydration shell which resulted into slower diffusion rate in water. However,

the sudden increase on its diffusion in the presence of polymer is due to the results that for polymer to bind to the complex it has to disrupt its solvation structure. As that happens, the polymer subsequently bind weakly to the metal complex due to the larger solvation structure and the disturbed solvation structure result into free movement of the complex, hence increase on its diffusion. It has an unexpected increase in mobility in the presence of the polymer, by more than 55%, irrespective of the choice of polymer. Although it has the weakest interaction of all investigated complexes, and consequently a high separation distance, the interaction is still attractive. Of course, it has a solvation shell that is more than double the size (see integration numbers of Rh(III) in table 4.3) of the other octahedral complexes and would consequently be most sensitive to a disrupting presence on its effective size, at similar distances. This finding strongly supports our argument of using an effective size in solution to describe the diffusion coefficients, rather than the absolute value of the interaction.

4.3.3 Comparison of the Experimental Elution order and the Computationally Calculated Diffusion Coefficients

The objective here is to compare the calculated trend in diffusion coefficients with the experimentally determined retention order, as a means to validate the quality of the model. Confirming this will answer whether computer aided molecular design and MD simulation can be used, with high reliability, to assist rational design of stationery phases for the selective separation and extraction of PGM complexes in aqueous solution. The retention order for the different complexes in solution demonstrates distinct chemical properties associated with each of these.

The experimental retention time order for different PGM chloro complex anions is given in figure 4.9. Comparison of the diffusion results for the complexes in aqueous solution with polymer one and polymer two with the experimental retention time order is given in table 4.10 below. The experimental results include four different retention time measurements; in each separation a different polymer was used with different solvents, figure 4.9.

Table 4.10 Summary of the comparison of the experimental retention order of the complexes in an inorganic solvent using Sephadex® gel, Toyopearl® gels and other different stationery phase with the computational calculated diffusion rate in water using a polymer based on the Sephadex LH-20 structure. The diffusion order from fastest to slowest read horizontally from the top to bottom.

Experimental elution order from the fastest to the slowest.				**Calculated diffusion order from the fastest to the slowest**	
RuIV	RhIII	RhIII	RhIII	Polymer One	Polymer Two
RhIII	PdII	PdII	RuIV	RhIII	RhIII
PdII	PtIV	PtIV	IrIV	PdII	PdII
PtIV	OsIV	OsIV	PtIV	RuIV	IrIV
IrIV				IrIV	PtIV
OsIV				PtIV	RuIV
				OsIV	OsIV
ref. 12	ref. 16	ref. 17	ref. 18		

A.

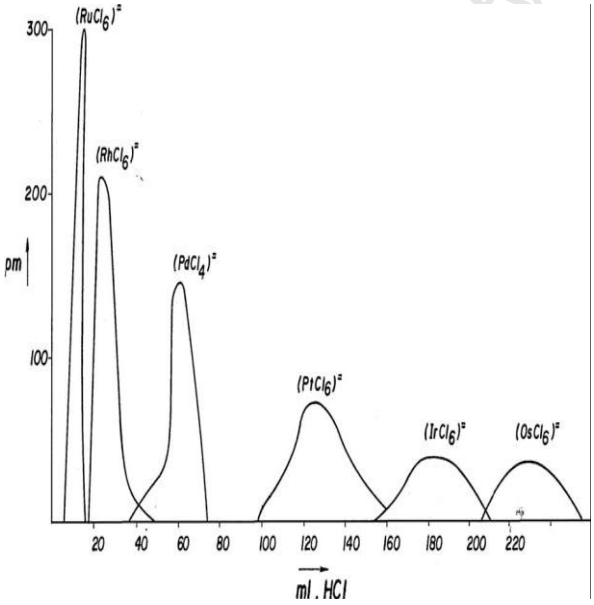

B.

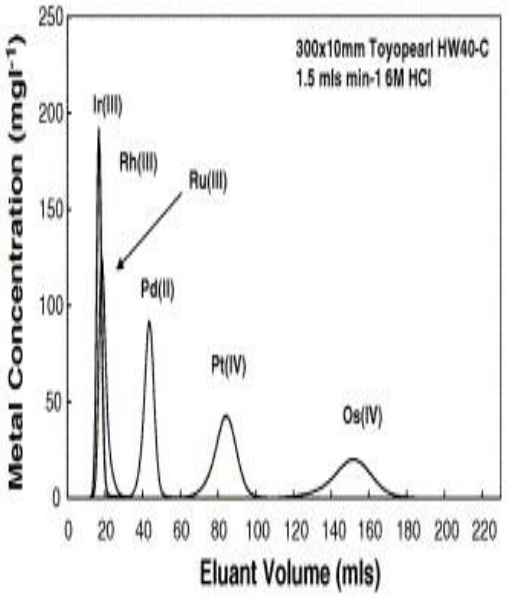

Continued on the next page

C. D.

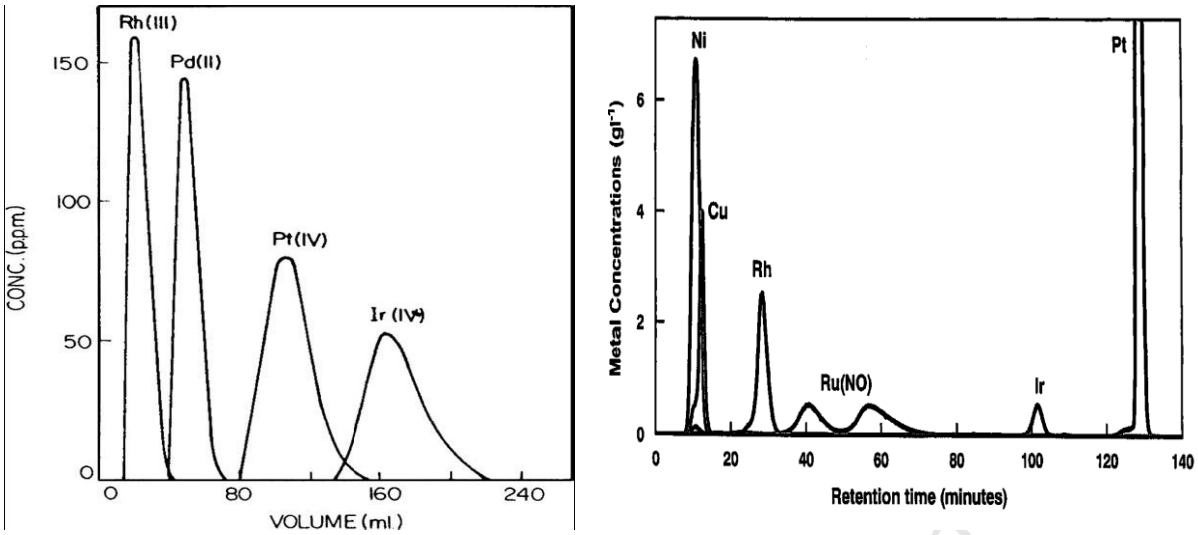

Figure 4.9. The chromatogram illustrations of retention time order for some PGMs in chromatographic media. The figures according to their sequential labeling were adapted from (A). The chromatographic separation of PGMs using Sephadex® in 1 M HCl [12], (B), A chromatographic elution of PGMs using Sephadex G-10 in 1 M NaCl[16], (C), A chromatographic separation of PGMs using Toyopearl® in 6M HCl[17], and (D), The chromatographic separation of the PGMs comprises a support functionalised with substituted amine groups [18] Continued from previous page.

The calculated diffusion order in polymer one is $RhCl_6^{3-}$> $PdCl_4^{2-}$> $RuCl_6^{2-}$> $IrCl_6^{2-}$> $PtCl_6^{2-}$> $OsCl_6^{2-}$. In polymer two this order is $RhCl_6^{3-}$> $PdCl_4^{2-}$> $IrCl_6^{2-}$> $PtCl_6^{2-}$> $RuCl_6^{2-}$ > $OsCl_6^{2-}$. This order and the difference between their diffusion coefficient values in comparison to that in water were discussed above in section 4.3.2.

The experimentally measured retention time order, from the first eluted to the last (i.e. in order of decreasing mobility for easy comparison with the results given above), for some of the PGM complexes are:

1. The chromatographic separation of PGMs using Sephadex® in 1 M HCl by G. Schmuckler[12]: $RuCl_6^{2-}$ > $RhCl_6^{3-}$> $PdCl_4^{2-}$> $PtCl_6^{2-}$> $IrCl_6^{2-}$> $OsCl_6^{2-}$.
2. A chromatographic elution of PGMs using Sephadex G-10 in 1 M NaCl by G. Schmuckler et al.[16]: $RhCl_6^{3-}$> $PdCl_4^{2-}$> $PtCl_6^{2-}$> $IrCl_6^{2-}$.
3. A chromatographic separation of PGMs using Toyopearl® in 6M HCl by R. A. Grant et al[17]: $IrCl_6^{3-}$> $RhCl_6^{3-}$> $RuCl_6^{3-}$> $PdCl_4^{2-}$> $PtCl_6^{2-}$> $OsCl_6^{2-}$.
4. This chromatographic separation of the PGMs comprises a support functionalised with substituted amine groups by Moine et al.[18]: Rh(III) >Ru(NO)> Ir(IV) > Pt(IV).

These results are exactly as they appear in their respective patents. Note that the Ru complex was given in the form Ru(NO)[18]. This complex is reported to be separated by converting it into the nitrosyl complex retaining the nitrosyl complex temporarily on the chromatography column and subsequently eluted by oxidizing or reducing eluent. Its presence in the solution is in the form $[Ru(NO)Cl_5]^{2-}$ or either $[Ru(NO)Cl_4(H_2O)]^-$.[19] Another important thing to note is that the elution order reported in the patent by Schmuckler[12] is: $RuCl_6^{2-}$ > $RhCl_6^{2-}$> $PdCl_4^{2-}$> $PtCl_6^{2-}$> $IrCl_6^{2-}$> $OsCl_6^{2-}$. However, it was claimed that the $RhCl_6^{2-}$ species is rather the $RhCl_6^{3-}$ species. This also leaves uncertainty if the $RuCl_6^{2-}$ species being separated is rather the $RuCl_6^{3-}$ species. This comes as no surprise since the trivalent species of these complexes are always eluted first in the column.[12,16-18]

From the first three it appears that the use of different dextran-based chromatographic media and different solvent composition does not affect the order of elution, with the same order apparent in all. The result given by Moine *et al.*[18] shows a slightly different trend from the other three, with the position of Ir(IV) and Pt(IV) switched around. Our calculated values show a very high degree of similarity to these reported values. In general, the $OsCl_6^{2-}$ complex is the slowest, followed by $IrCl_6^{2-}$ and $PtCl_6^{2-}$, with the $RhCl_6^{3-}$ and $PdCl_4^{2-}$ complexes the quickest, the higher charged system dominating. Comparison of tetravalent Ru(IV) with the results by Moine *et al.*[18] match the trend but caution is necessary since this complex may be separated in two different species, $[Ru(NO)Cl_5]^{2-}$ or either $[Ru(NO)Cl_4(H_2O)]^-$. Comparison of the diffusion trend of the PGM complexes in a system with polymer two (a Sephadex-type polymer) with results of reference 10, figure 4.9, D, shows only a discrepancy in the order of the $RuCl_6^{2-}$ complex, nevertheless, the diffusion coefficient order for $RhCl_6^{3-}$ > $IrCl_6^{2-}$ > $PtCl_6^{2-}$ matches very well.

It is obvious that different polymers and different solvents are used to improve the selectivity towards different PGM chloro complex anions during separation.

Importantly, the surprising behaviour of the Rh(III) complex in that it speeds up is also seen in experiment – more so, all trianions complexes diffuse quicker in the presence of the separating medium.[17]

From the MD simulation results reported here and comparison with various experimental trends, it is clear that computer aided design can assist in the development of better separation phases.

4.4. Free Energy of Association Between the PGM Complex and the Polymer

Free energy differences result from the varying free energy of association characterised by non-covalent interaction between small solute molecules, solvent molecules and macromolecules.[20] Free energy differences are widely used to measure relative solvation of molecules and ions and binding free energies.[20] In this section, the investigation of the solvation and binding free energy of the PGMs complexes in water and in a solution with organic polymer is conducted using the technique of free energy perturbation (FEP). These free energy calculations are performed to extract information about the comparative binding pattern for the different metal complexes with respect to their size, shape and charge. The free energy simulations were performed in water with polymer one. Differences were computed between the PGMs complexes in pure water and in aqueous solution with organic polymer. The schematic diagram showing the free energy circle is given in Chapter 3, section 3.2.4, figure 3.1 and 3.2.

4.4.1 Procedure for Performing FEP calculations

The dual topology scheme was used to define the stepwise transition between the various complexes. The anion topologies were constructed with the non-bounded exclusion list to avoid mixing of atoms interacting across the segment, hence, enabling smooth sampling when transferring from one independent segment to another. All the calculations were performed using the CHARMM program. The free energy simulations were carried out in a stepwise manner through non-physical intermediate states, coupled to a parameter, λ.[15] These intermediate states (or windows) are set up to slowly produce the structural transformation from one complex to the next. A value of $\lambda = 0$ describes the initial point where the atoms present are purely those from the initial structure; $\lambda = 1$ describes the end point, where only atoms of the ending structure are present. The non-physical intermediate states are defined by intermediate values of the coupling parameter, e.g. 0.1, 0.2, etc.[21] A series of free energy calculations was therefore performed, each broken down into 37 windows, run at different λ values with gaps $\Delta\lambda = 0.025$ between steps. To allow for smooth convergence of the method at the end points, the initial value was calculated at $\lambda = 0.05$ and final value at $\lambda = 0.095$. For integration between the intervals double-wide sampling was used. This method requires that

integration at each λ value is performed in two steps; from each point to the midpoint between adjacent steps, both forwards and backwards.

The simulation length of each window was 430 picoseconds with the first 30 picoseconds used for equilibration and 400picoseconds of dynamics production. To avoid the hybrid structure of the two residues of PGM chloro complex anions, in which the free energy difference is determined, to move away from each other during energy calculation a harmonic constrain was applied throughout the production dynamics simulation. This allowed free rotation of the segments but a minimal linear translation. The segment is defined by double residues combined together in which each residue describes the topology of a PGM chloro-complex anions bond connectivity, angles, dihedral and improper dihedrals and charges. A force constant of 50 kcal mol^{-1} $Å^{-1}$ was used. The complexes were randomly placed into the system in any position which is 8.0 angstrom away from the polymer. The starting position for all the system was exactly the same. The calculation was done without Ewald summation to approximate the electrostatics; instead a standard switching function was applied. The cuton and the cutoff values was 10 and 12, respectively. The Nose-Hoover method was used to control the temperature, and a Verlet integration method. The simulation was run using a truncated octahedron cell and periodic boundary conditions.

The free energy results are given in the table 4.10 below. Other than the calculations to determine free energy of association, free energy of hydration was also determined. Three sets of simulations were thus performed under different conditions, one in vacuum, one in water and the other one in water in the presence of the polymer. The vacuum/water simulations were used to calculate free energy of hydration and the water/polymer simulations for free energy of association. It is customary to check the convergence and calculate an estimation of the error by doing the perturbation in both a backwards and forwards direction. Other than the difference in sign these should ideally produce very similar values. In reporting the results the direction of the arrows indicates the direction of the integration from the initial state to the final state. Free energy differences were only calculated between pairs of octahedral complexes with same the same overall charge and coordination; thus only the four dianion octahedral complexes $RuCl_6^{2-}$, $IrCl_6^{2-}$, $PtCl_6^{2-}$ and $OsCl_6^{2-}$ were used. The slowest diffusing $OsCl_6^{2-}$ complex was used as reference point and the remaining three complexes calculated relative to it.

A negative free energy of hydration resulting from the perturbation of complex A to complex B can be interpreted as complex B having a larger (negative) free energy of

hydration, and thus a more favourable solvation. Likewise, a positive difference implies A has a more favourable hydration. A similar conclusion holds for the association with the polymer. Finally, these values were calculated under conditions of constant volume and constant temperature, the canonical ensemble, and thus corresponds closest to Helmholtz free energies. Symbols $\Delta A/\Delta\Delta A$ rather than $\Delta G/\Delta\Delta G$ were thus used.

4.4.2. FEP results for $RuCl_6^{2-}$, $IrCl_6^{2-}$, $PtCl_6^{2-}$ and $OsCl_6^{2-}$ in Water and Aqueous Polymer Solution.

Before elaborating on the trends in solvation and binding, the accuracy of the results is discussed first. Table 4.11 shows that for all simulations the forward and backward perturbations differ by less than 2.0 kcal mol^{-1}. Perturbations using less windows (19) were done initially, but the errors associated with these calculations were considered unacceptable (see Appendix B, table 4.1). Subsequently, the perturbations over 37 windows showed smaller errors lying within an acceptable criterion of 2.0 kcal mol^{-1}, and these results are used for further discussion in this section.

Table 4.11. Free energy changes for the different PGM complexes are presented below for both forward and backward simulation. The calculated free energy of solvation and binding are given by $\Delta\Delta A_{(binding)}$ and $\Delta\Delta A_{(solvation)}$. 37 λ steps were used. The simulation length of 430 ps was used.

	ΔA kcal/mol	**ΔA kcal/mol**	**ΔAkcal/mol**	**$\Delta\Delta A_{(binding)}$ kcal/mol**	**$\Delta\Delta A_{(solvation)}$ kcal/mol**
37 λ steps	*Water*	*Organic solution*	*Vacuum*	*Organic solution*	*Aqueous solution*
$PtCl_6^{2-} \rightarrow OsCl_6^{2-}$ $PtCl_6^{2-} \leftarrow OsCl_6^{2-}$	25.993 -25.184	23.454 -23.424	23.593 -24.834	-2.539 1.760	2.400 -1.760

$IrCl_6^{2-} \rightarrow OsCl_6^{2-}$ $IrCl_6^{2-} \leftarrow OsCl_6^{2-}$	16.412 -15.158	15.272 -13.433	7.613 -8.852	-1.139 1.724	8.798 -6.305
$RuCl_6^{2-} \rightarrow OsCl_6^{2-}$ $RuCl_6^{2-} \leftarrow OsCl_6^{2-}$	-33.580 28.933	-35.766 32.289	-31.145 29.594	-2.186 3.356	-2.434 -0.661

As arbitrary reference point the slowest diffusion complex was chosen and all perturbations were done relative to the $OsCl_6^{2-}$ complex. Results show that all systems have an hydration free energy that is more favourable to Os(IV), in the order $OsCl_6^{2-}$ < $RuCl_6^{2-}$ (-0.6 kcal mol^{-1}) < $PtCl_6^{2-}$ (-1.8 kcal mol^{-1}) < $IrCl_6^{2-}$ (-6.3 kcal mol^{-1}). For easy discussion the trend in diffusion for these complexes are repeated here, that is from slowest to fastest (in pure water) $OsCl_6^{2-}$ < $RuCl_6^{2-}$< $PtCl_6^{2-}$ < $IrCl_6^{2-}$. This shows that the complex with higher hydration free energy diffuses faster, with the exact order replicated. To interpret the results and elaborate on their relationship to diffusion, the well-known relation for free energy is used:

$$\Delta G = \Delta H - T\Delta S$$

This includes a contribution from enthalpy, which is estimated to be approximately equal to the internal energy, ΔU, and a contribution from the entropy. As discussed in section 4.1 these systems are all expected to have very similar interaction energy with the aqueous solvent, and the important differential between them must lie in the entropy term. For the near-rigid, similar PGMs complexes a large contribution comes from the rotational motion of the complex as it moves through solution. As the rotational motion becomes more pronounced the $-T\Delta S$ term becomes more negative, and the free energy increases. These results therefore suggest that the rotation of the complexes increases in the order $OsCl_6^{2-}$ < $RuCl_6^{2-}$< $PtCl_6^{2-}$ < $IrCl_6^{2-}$. If it is now assumed that a quicker rotation is a result of lesser drag by the surrounding water molecules, this implies the quicker rotating anion has a larger translational diffusion. This is precisely the result emerging here.

Regarding the free energy studies in the presence of the polymer the order, from strongest to weakest binding, is $OsCl_6^{2-}$ > $IrCl_6^{2-}$ ~ $PtCl_6^{2-}$ > $RuCl_6^{2-}$. This ordering is less clear to explain. It must be noted however, that although this does not agree with the enthalpy ordering (as illustrated by the interpretation of free energies in aqueous solution and the contribution from entropy), it does show partial agreement to the average distances reported

in section 4.2.2. The Os(IV) complex remained closest on average, showing the highest binding affinity, followed by the other systems. Already an agreement between the average distances and diffusion coefficients was shown, and here it is reasonable to assume that the complex with the higher binding affinity should show a closer proximity to the polymer during the simulation. Rather than the average separation, calculated over 8.0 ns of simulation with a large standard deviation, the histogram of separation distances between the polymer and complex is referred to. This allows for a calculation of the proportion of time spent during the simulation within a specified cut off distance to the polymer, i.e. interacting strongly. Summing over the first peaks from ~2.5 to ~12.5 Å, the proximity of the complexes to the polymer can be arranged in the order $RuCl_6^{2-}$ (55.2%) < $PtCl_6^{2-}$ (63.5%) ~ $IrCl_6^{2-}$ (64%) < $OsCl_6^{2-}$ (70.4%). This order follows the free energy of binding, with the weakest binding complex first and the strongest last.

References

1. W .L. Jorgensen, & C. Jenson, *J. Comput. Chem. 19*, 1179-1186, (1998).

2. P. J. Steinbach, & B. R. Brooks, *Proc. Natl. Acad. Sci. (USA). 90*, 9135-9139, (1993).

3. M. Kuttel, J. W. Brandy and K. J. Naidoo, J. Comput. Chem., 2002, 23: 1236-1243.

4. A. Lienke, G. Klatt, D. J. Robinson, K. Koch, and K. J. Naidoo Inorg. Chem., 2001, 40(10), pp 2352-2357.

5. G. Klatt, D. J. Robinson, K. Koch, and K. J. Naidoo Inorg. Chem., 2002, 41(7), pp 1845-1849.

6. T. Darden, D. York, & L.G. Pedersen, *J. Chem. Phys. 98*, 10089 – 10092, (1993).

7. S. Nose, (1984), *Mol. Phys. 52*, 255 – 268, (1984).

8. W. G. Hoover, W. G., *Physical Review A. 31*, 1695-1697, (1985).

9. Kevin J. Naidoo, Gunter Klatt, Klaus R. Koch, and David J. Robinson, Inorg. Chem. 2002, 41, 1845-1849.

10. Richard P. Matthews, Gehard A. Venter and Kevin J. Naidoo, J. Phys. Chem. B 2011, 115, 1045–1055.

11. Katherine J. Bell, Arjan N. Westra, Rebecca J. Warr, Jy Chartres, Ross Ellis, Christine C. Tong, Alexander J. Blake, Peter A. Tasker,* and Martin Schroder*, Angew. Chem. Int. Ed. 2008, 47, 1745-1748.

12. Gabriella Schmuckler, U.S. Patent, 4885143, 1989.

13. Richard A. Grant and Yvonne Taylor, U.S. Patent, 5879644, 1999.

14. Peter A. Tasker, Christine C. Tong, Arjan N. Westra, Coordination Chemistry Reviews, 251 (2007), 1868-1877.

15.Ross J. Ellis,Jy Chartres, Kathyyn C. Sole Timothy G. Simmance, Christine C. Tong, Fraser J. White Martin Schroder and Peter A. Tasker, ChemComm, 2008, DOI: 10.1039/b815895a.

16. R. A. Grant, Y. Taylor, U.S. Patent 5,879,644, 1999.

17. G. Levitin, G. Schmuckler / Reactive & Functional Polymers 54 (2003) 149–154.

18. L. Moine, D. C. Sherrington, R. A. Grant, U.S Patent 7,354,517, 2008.

19.http://osdir.com/patents/Metallurgical-processes/Chromatographic-method-separating-ruthenium-platinum-group-metals-07163570.html.

20. M. Rami Reddy, U. C. Singh, Mark D. Erion., J ComputChem 28: 491-494, 2007.

21. David A. Pearlman, J. Phys. Chem. 1994, 98, 1487-1493.

Chapter 5

Conclusion

In this dissertation, features of the chromatographic column separation of PGMs in aqueous solution are modelled using MD and free energy computer simulations. Theoretical diffusion times were calculated and compared to experimental retention times. These results were found to show good agreement with the measured experimental retention order[1-3] for $RhCl_6^{3-}$, $PdCl_4^{2-}$ and $OsCl_6^{2-}$ complexes with polymer one and two. The other three complexes, $PtCl_6^{2-}$, $IrCl_6^{2-}$ and $RuCl_6^{2-}$ show deviation from the expected order.[1-3]. However, for all the PGM complexes the diffusion order is consistent with the experimental order in the general trend of $MCl_6^{3-} > MCl_4^{2-} > MCl_6^{2-}$. The computer predicted diffusion order of the $PtCl_6^{2-}$ and $IrCl_6^{2-}$ complexes was $IrCl_6^{2-} > PtCl_6^{2-}$. This was found to be opposite to the retention time order of Schmuckler *et al* and Grant *et al* [1-2] but consistent with the retention time order of Moine, Sherrington and Grant.[4] In addition, the retention time order of Moine *et al.* agreed exactly with the diffusion order of PGMs when polymer two (consisting of two separate dextrans) was used. These results show that the use of MD simulations to model the separation of PGM complexes are warranted and able to reproduce experimental measurements. This model however, can be further developed to predict and formulate processes that can be implemented for the separation of precious metals. The outcomes of separation are still mostly dependent on the extraction steps followed and the choices of solvent and polymer used. This alone continues to offer immense challenges for the industrial extraction of PGMs, where the need for identifying and understanding the separation mechanism taking place during solution is urgently needed. This study provides a platform that can lead to the development of more sophisticated methods, which can serve as the corner stone to address those challenges in future.

The interaction energy of the complexes was not clearly categorised and correlated with the diffusion. However, thee trend in which these complexes interact with the polymer in solution also obey the rule based on the order: $MCl_6^{3-} > MCl_4^{2-} > MCl_6^{2-}$. Their sophisticated interacting behaviour in the solution shows why their separation is difficult to understand.

Nevertheless, their solvation structure is well studied and their trend in solvation is understood based on their charges and effective radii. The order: $MCl_6^{3-} > MCl_4^{2-} > MCl_6^{2-}$ is

consistently retained as it is given from the most solvated to the least solvated. It has been found that their solvation is crucial when looking at the interaction with the polymer. The $RhCl_6^{3-}$ complex, which has the largest solvation shell due to its higher charge of -3, speeds up in the presence of the polymer due to disruption of the solvent shell. The challenge lies in developing polymers that will effectively disrupt the solvation of these complexes and offer strong interaction with them

The free energy of binding ranking did not match with the diffusion rate order. Two aspects have been identified as the main cause of this namely the number of λ steps chosen, which may have contributed to poor convergence, and the treatment of constraints to limit the drift during the perturbation. However, the free energy of solvation was found to match exactly with the diffusion in water in this order from the slowest to the fastest: $OsCl_6^{2-}$ < $RuCl_6^{2-}$< $PtCl_6^{2-}$ < $IrCl_6^{2-}$.

For future work, improved convergence in free energy of binding can be achieved by choosing the number of λ steps wisely and by developing more sophisticated protocols to constrain the polymer in structural perturbation. All results consistently agree within the classes of charge and complex size, but differentiating between complexes of similar properties remains difficult. The development of polymers that will disrupt the solvation of these complexes in water could prove beneficial to investigating the binding behaviour more accurately.

Reference

1. G. Schmuckler, U.S. Patent 4,885,143, 1989

2. G. Levitin, G. Schmuckler / Reactive & Functional Polymers 54 (2003) 149–154

3. R. A. Grant, Y. Taylor, U.S. Patent 5,879,644, 1999

4. L. Moine, D. C. Sherrington, R. A. Grant, U.S Patent 7,354,517, 2008

Appendix

A. MSD vs Change in time Plots

Diffusion plots for $IrCl_6^{2-}$, $PtCl_6^{2}$, $RuCl_6^{2-}$, $PdCl_4^{2-}$, $OsCl_6^{2-}$ and $RhCl_6^{3-}$ in water solvent

A

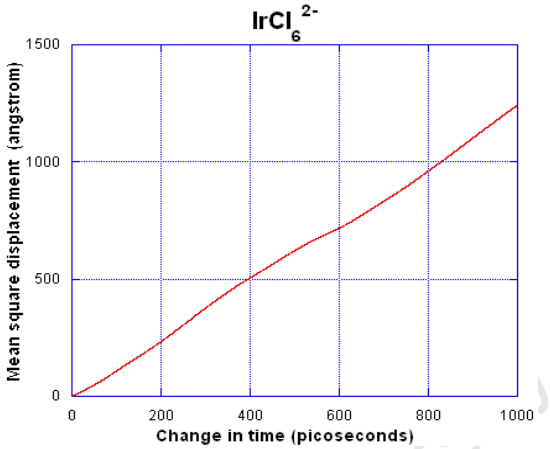

B

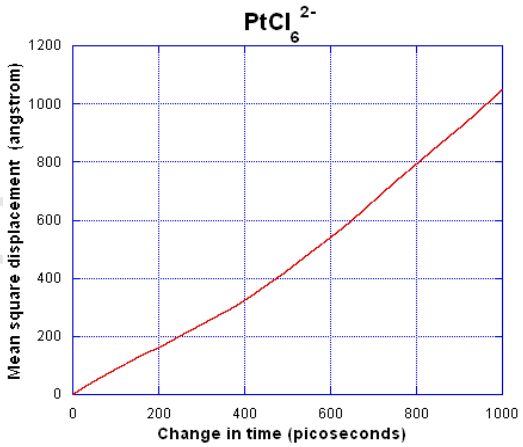

C

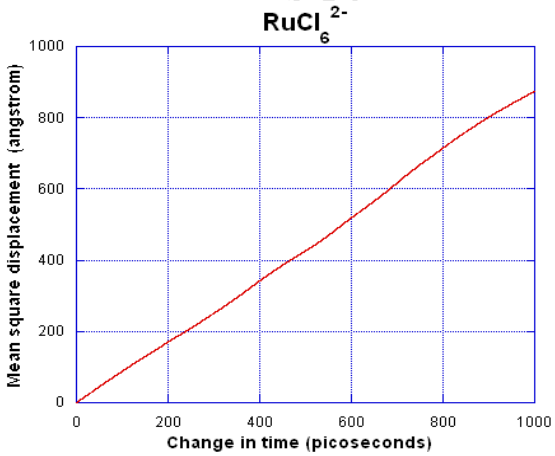

D

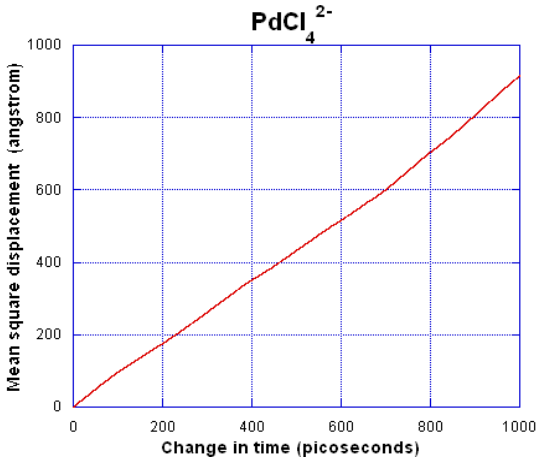

E

F

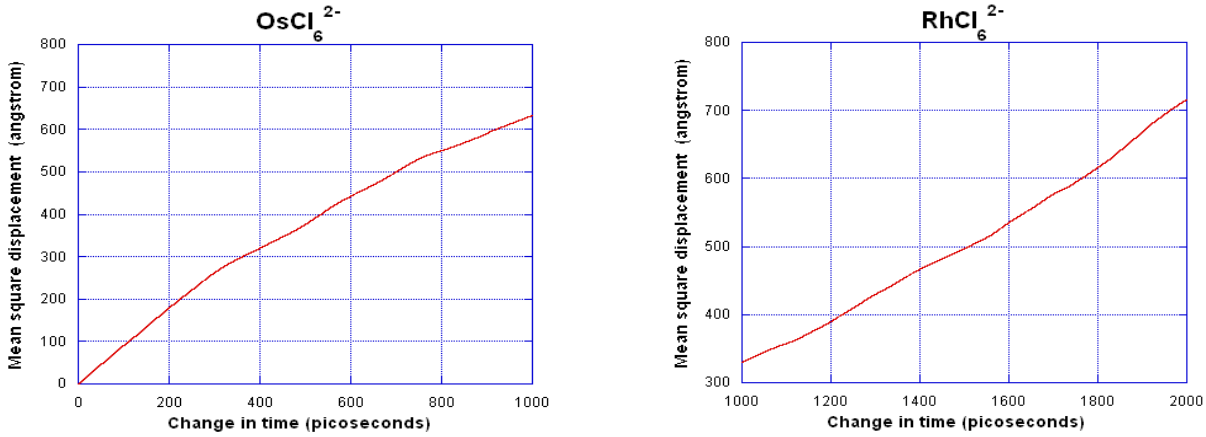

Figure 4.1.RMSD vs Δt plots for $RhCl_6^{3-}$, $PdCl_4^{2-}$, $PtCl_6^{2}$, $IrCl_6^{2-}$, $RuCl_6^{2-}$ and $OsCl_6^{2-}$ complexes in water given by plot A, B, C, D, E and F respectively. The simulation of 1.0 ns was used to approximate the linear plots.

Diffusion plots for $IrCl_6^{2-}$, $PtCl_6^{2}$, $RuCl_6^{2-}$, $PdCl_4^{2-}$, $OsCl_6^{2-}$ and $RhCl_6^{3-}$ in water solvent in the presence of polymer one

OsIV

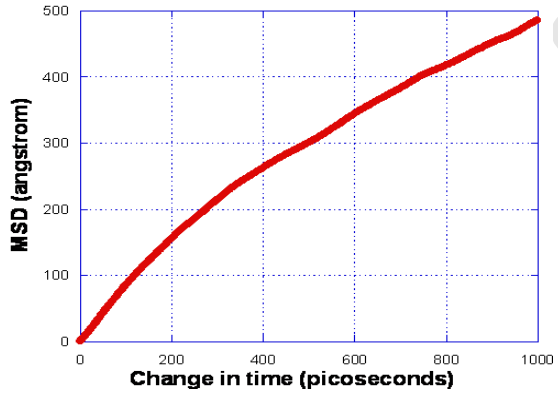

B. PtIV

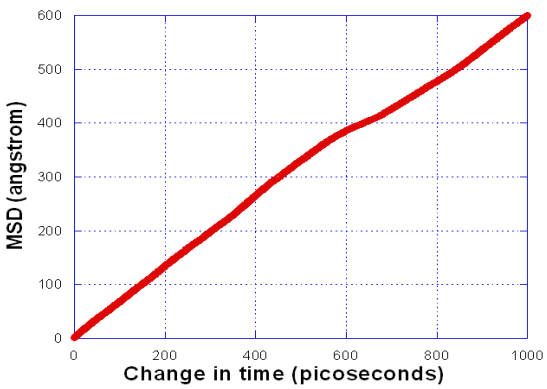

C. IrIV

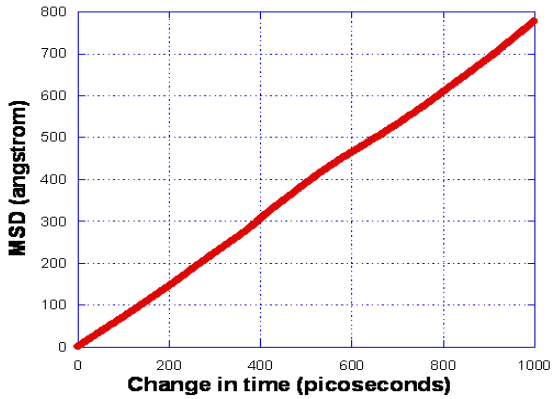

D. RuIV

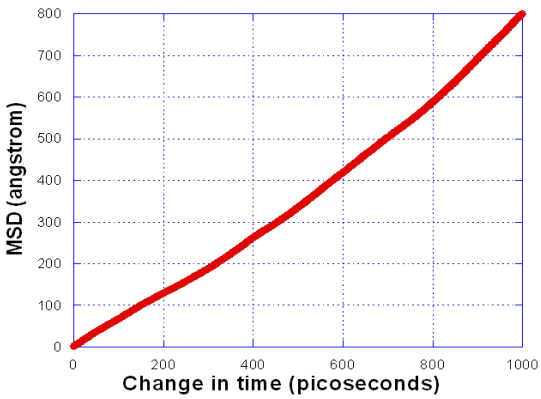

E. PdII

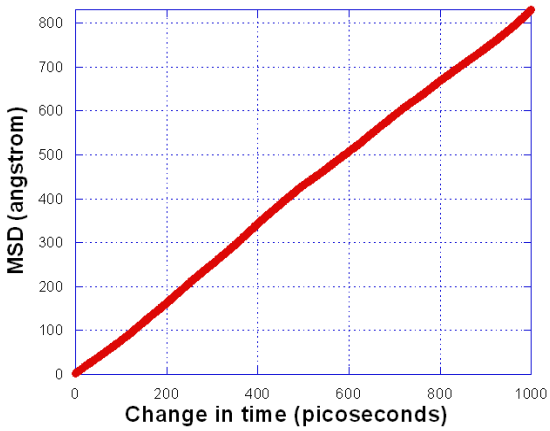

F. RhIII

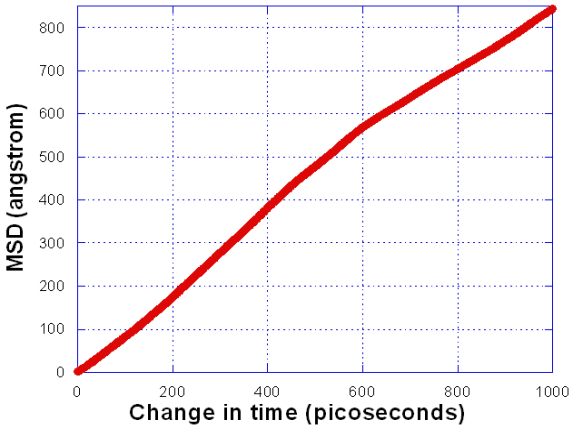

Figure 4.2.RMSD vs Δt plots for RhCl63-, PdCl42-, PtCl62, IrCl62-, RuCl62- and OsCl62- complexes in water solvent in the presence of polymer one. The diffusion coefficient values were estimated from 3.5 ns simulation date with only 1.0 ns of the data used to estimate the plots.

Diffusion plots for $IrCl_6^{2-}$, $PtCl_6^{2}$, $RuCl_6^{2-}$, $PdCl_4^{2-}$, $OsCl_6^{2-}$ and $RhCl_6^{3-}$ in water solvent in the presence of polymer two

A. OsIV

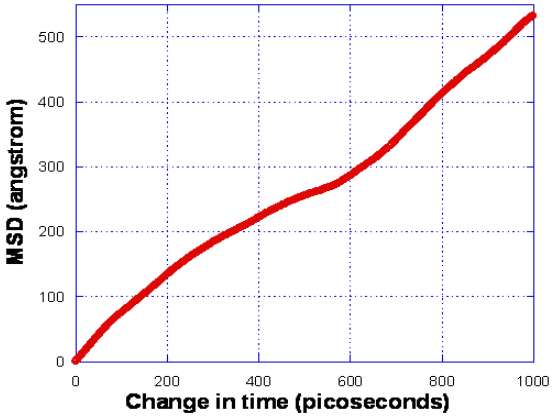

B. PtIV

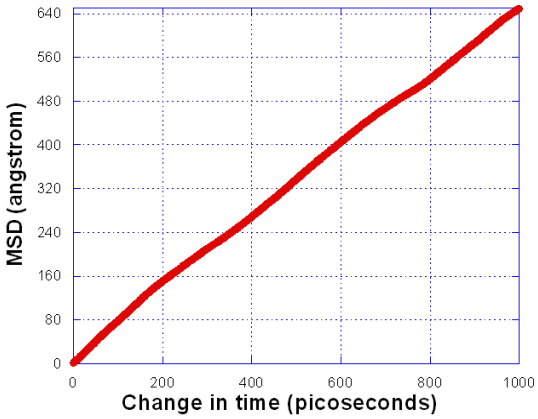

C. IrIV

D. RuIV

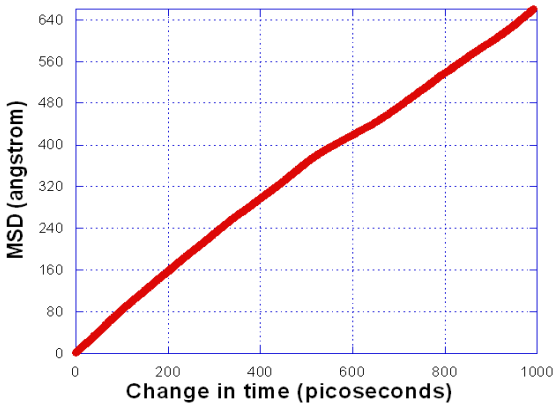

E. PdII

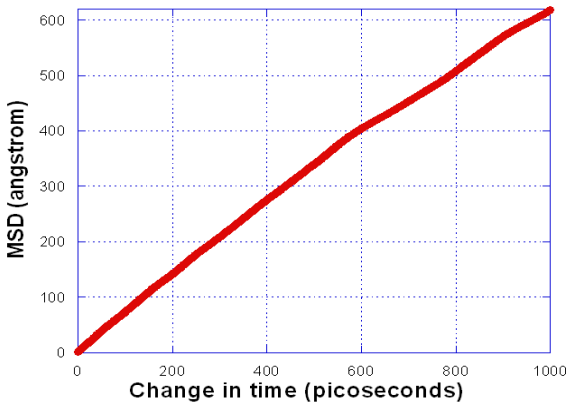

F. RhIII

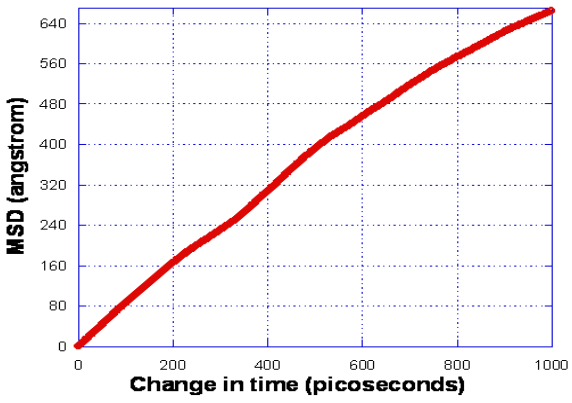

Figure 4.3. RMSD vs Δt plots for $RhCl_6^{3-}$, $PdCl_4^{2-}$, $PtCl_6^{2-}$, $IrCl_6^{2-}$, $RuCl_6^{2-}$ and $OsCl_6^{2-}$ complexes in water solvent in the presence of polymer two. The diffusion coefficient values were estimated from 3.5 ns simulation date with only 1.0 ns of the data used to estimate the plots.

B. Helmholtz Free Energy Differences, ΔA.

Table 4.1. Free energy difference values for some of the PMG chloro-complex anions in water. Energy parameters given on table are Helmholtz free energy difference ΔA. Free energy difference was calculated using FEP path based method with the dual topology scheme using thermodynamic simulation method (TSM) on CHARMM program and the simulation length was 130 ps. The values were given for both forward and backward simulations. 19 λ steps were used.

	ΔAkcal/mol	ΔAkcal/mol	ΔAkcal/mol	ΔΔAkcal/mol	ΔΔAkcal/mol
19 λ steps	*water*	*Organic solution*	*vacuum*	*Organic solution*	*Aqueous solution*

$PtCl_6^{2-} \rightarrow OsCl_6^{2-}$ $PtCl_6^{2-} \leftarrow OsCl_6^{2-}$	28.349 -24.989	23.640 -22.745	-15.800 15.846	-4.709 2.244	44.149 -40.835
$IrCl_6^{2-} \rightarrow OsCl_6^{2-}$ $IrCl_6^{2-} \leftarrow OsCl_6^{2-}$	18.210 -14.749	16.171 -12.996	16.283 -16.299	-2.039 1.753	1.927 1.549
$RuCl_6^{2-} \rightarrow OsCl_6^{2-}$ $RuCl_6^{2-} \leftarrow OsCl_6^{2-}$	-33.146 29.001	-37.481 34.159	-36.405 36.401	-4.334 5.157	3.258 -7.399

C. Interaction Energy Plots

A. OsIV

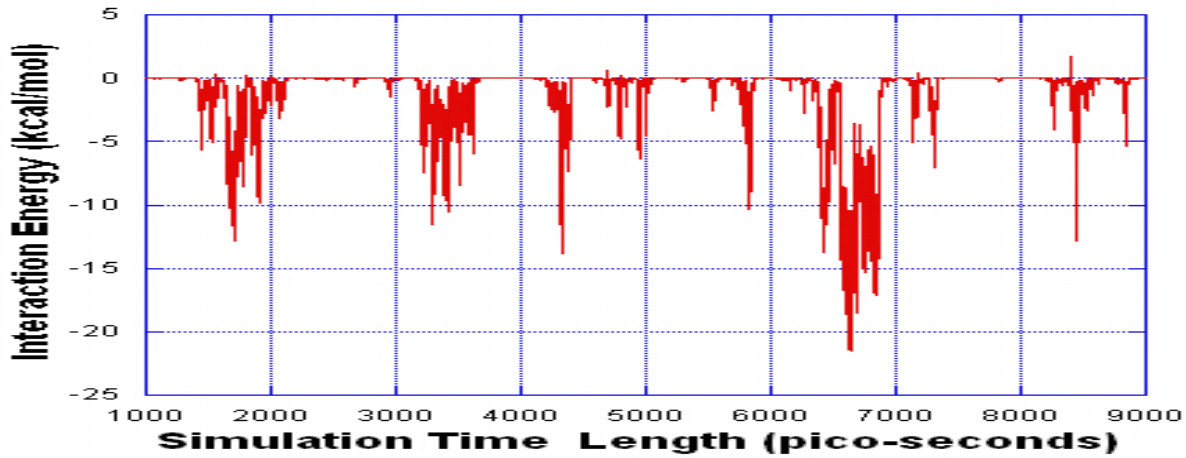

B. PtIV

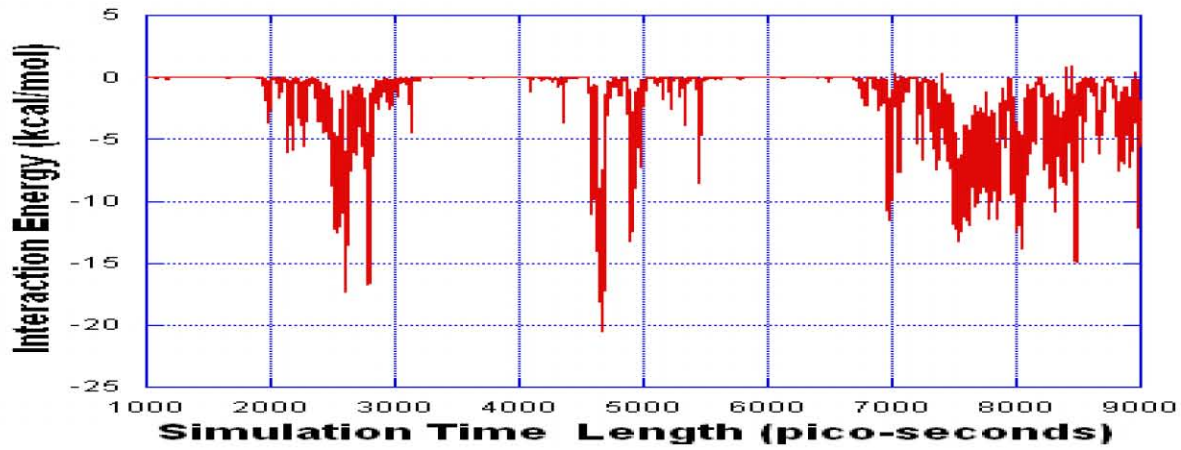

C. IrIV

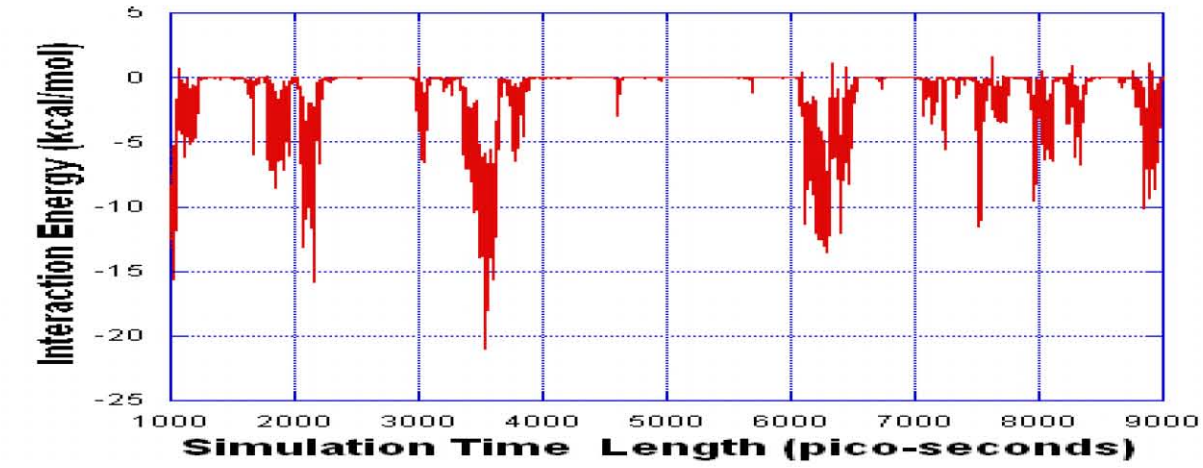

D. RuIV

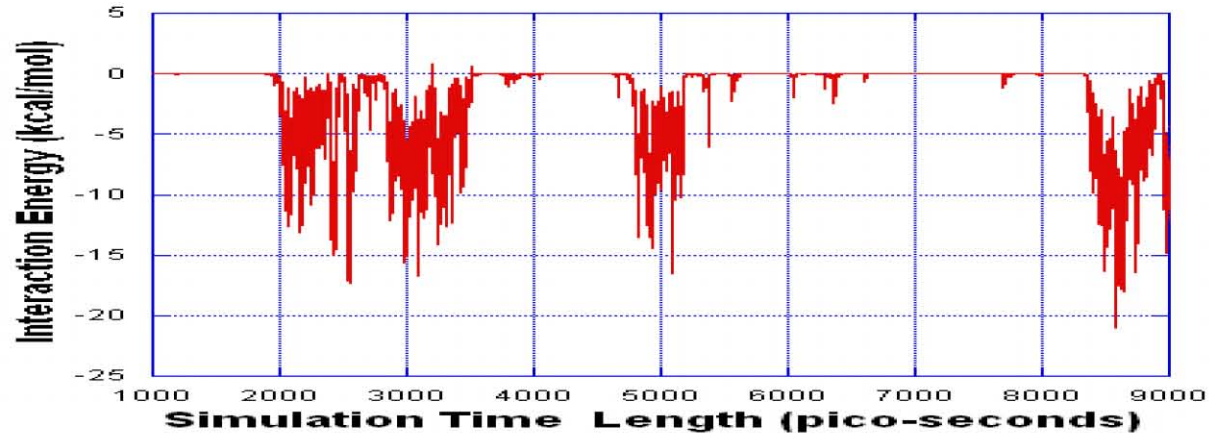

E. PdII

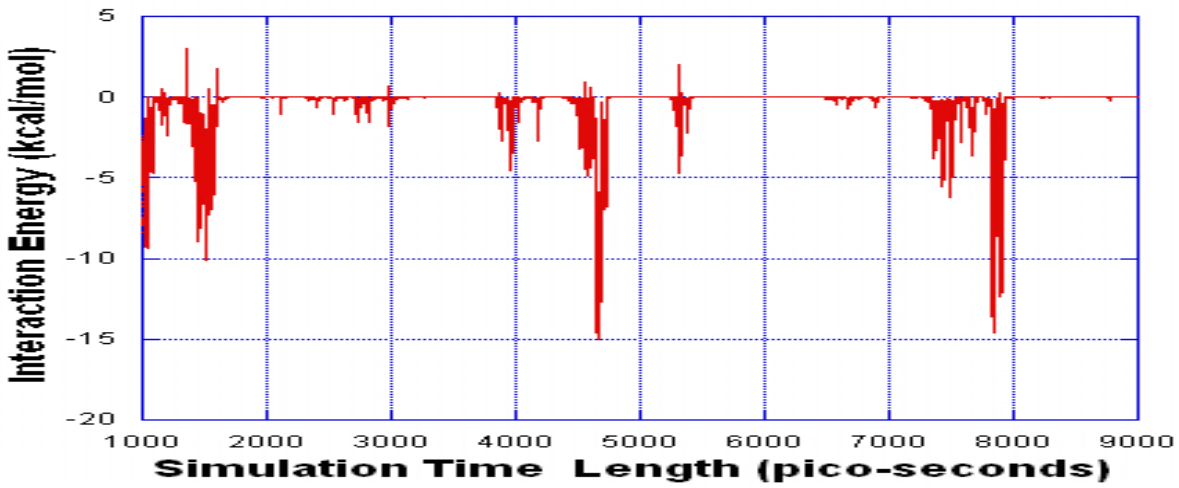

F. RhIII

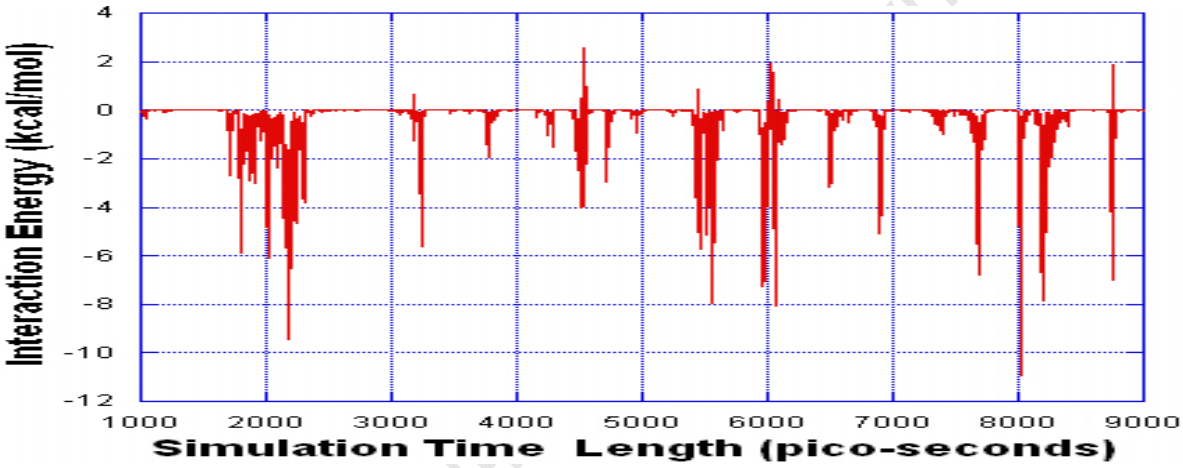

Figure 4.4. The interaction plots for $OsCl_6^{2-}$, $PtCl_6^{2-}$, $IrCl_6^{2-}$, $RuCl_6^{2-}$ $PdCl_4^{2-}$ and $RhCl_6^{3-}$complexes with polymer one given at letter A, B, C, D, E, and F respectively. The positive value gives the repulsive interaction strength and negative value gives attractive interaction strength.

A. OsIV

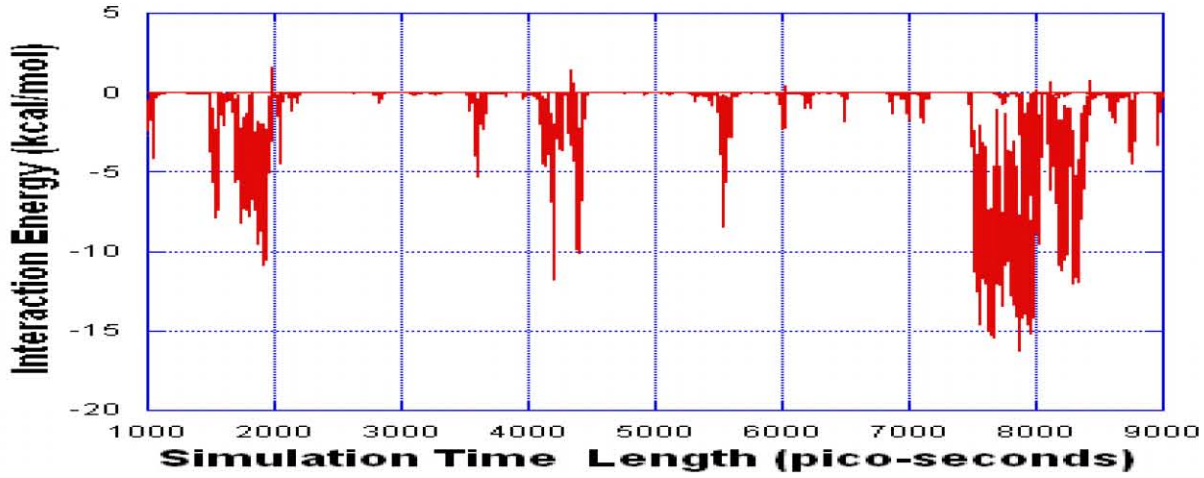

B. IrIV

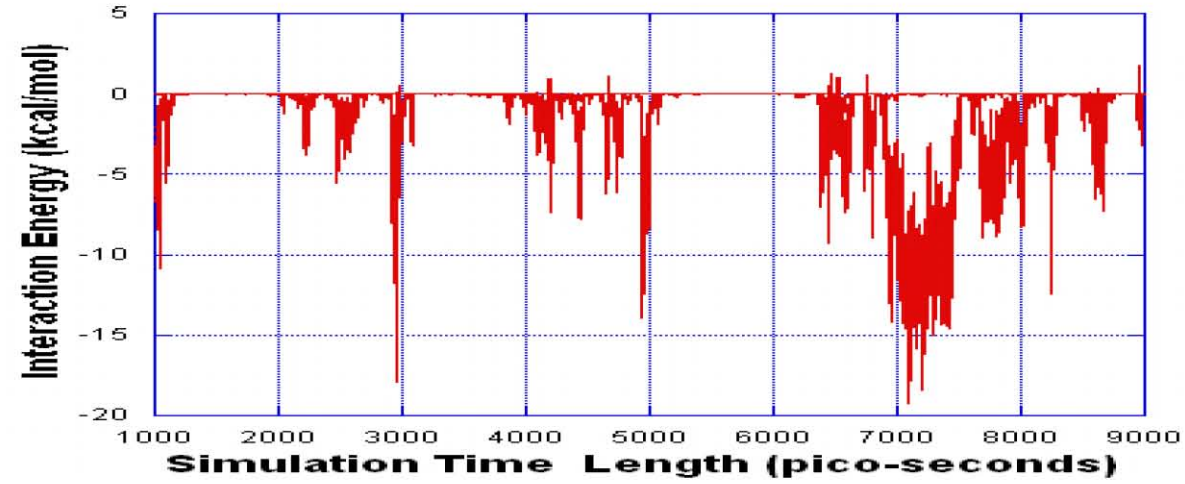

C. PtIV

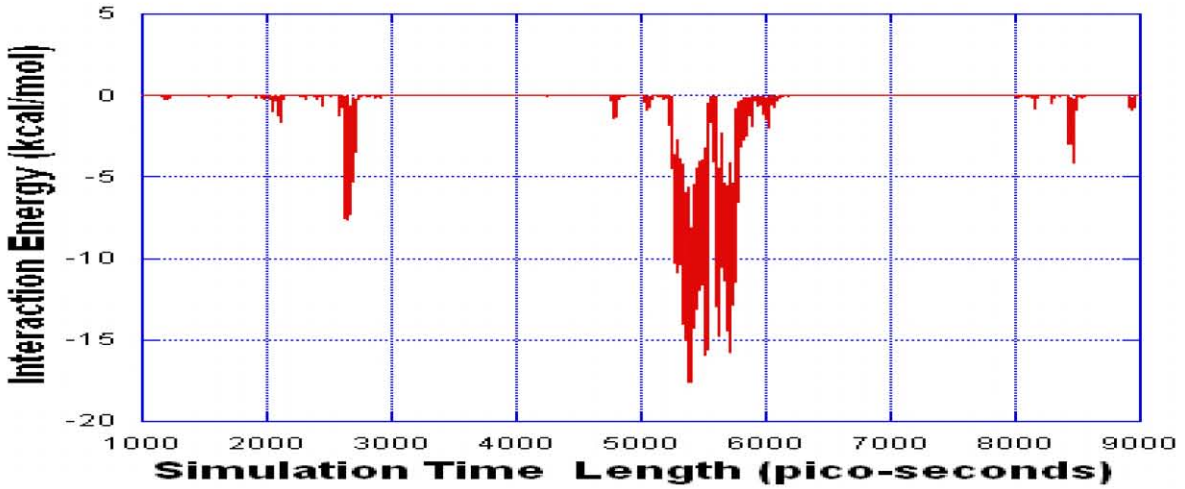

D. RuIV

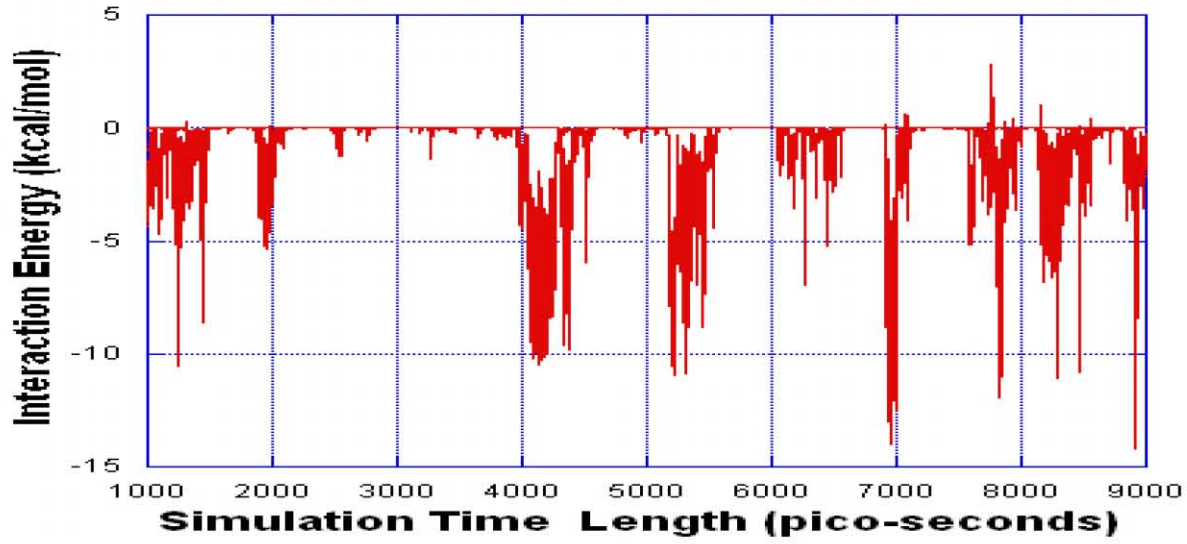
Interaction Energy (kcal/mol)
5
0
-5
-10
-15
1000
2000
3000
4000
5000
6000
7000
8000
9000
Simulation Time Length (pico-seconds)

E. PdII

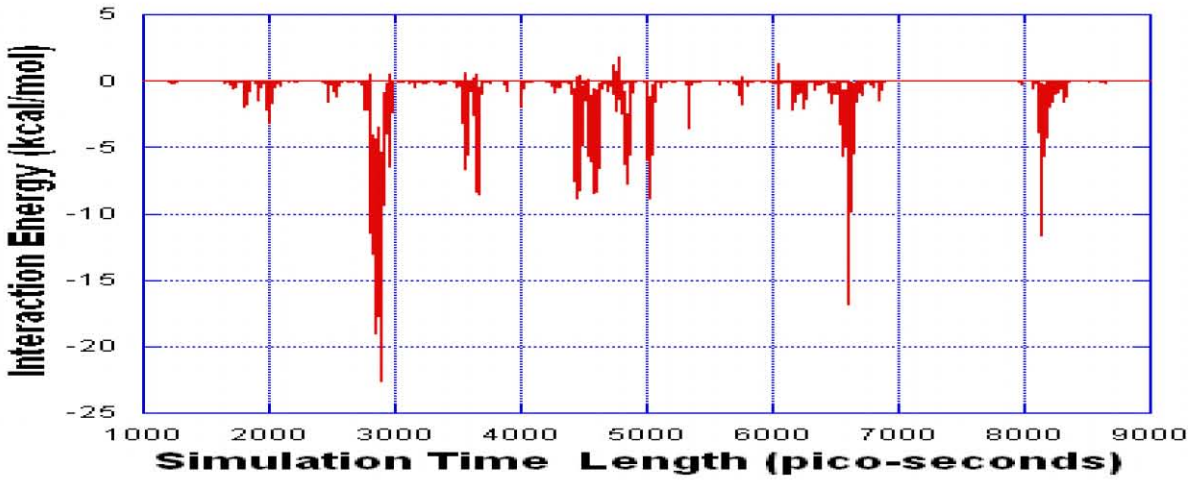
Interaction Energy (kcal/mol)
5
0
-5
-10
-15
-20
-25
1000
2000
3000
4000
5000
6000
7000
8000
9000
Simulation Time Length (pico-seconds)

F. RhIII

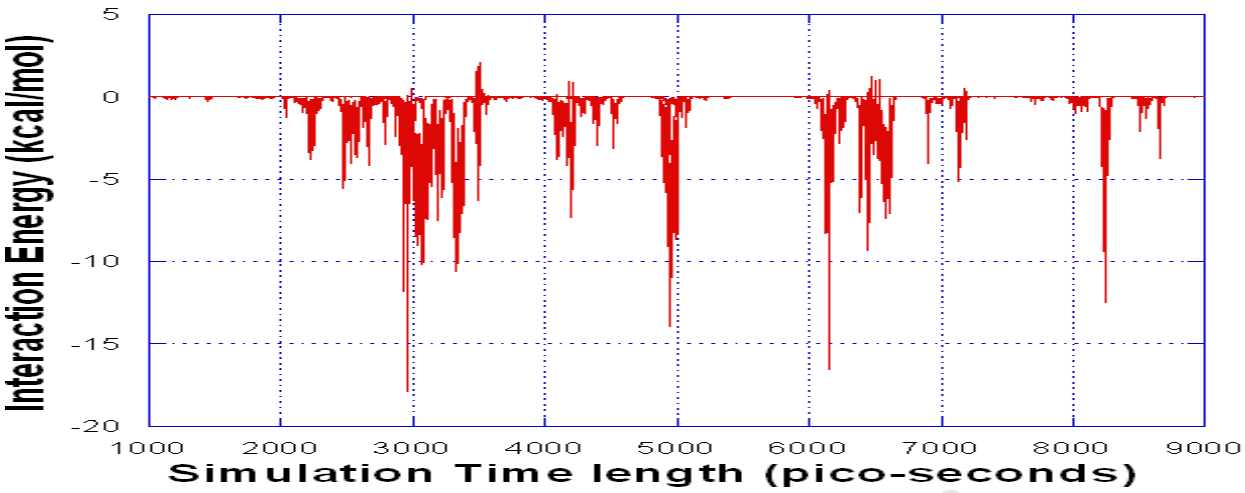

Figure 4.5. The interaction plots for $OsCl_6^{2-}$, $IrCl_6^{2-}$, $PtCl_6^{2-}$, $RuCl_6^{2-}$ $PdCl_4^{2-}$ and $RhCl_6^{3-}$complexes with polymer two given at letter A, B, C, D, E, and F respectively. The positive value gives the repulsive interaction strength and negative value gives attractive interaction strength.